OPTIMAL FORMATION FLIGHT CONTROL

THESIS

Shawn B. McCamish
Second Lieutenant, USAF

AFIT/GE/ENG/95D-16

DEPARTMENT OF THE AIR FORCE
AIR UNIVERSITY

AIR FORCE INSTITUTE OF TECHNOLOGY

Wright-Patterson Air Force Base, Ohio

OPTIMAL FORMATION FLIGHT CONTROL

THESIS
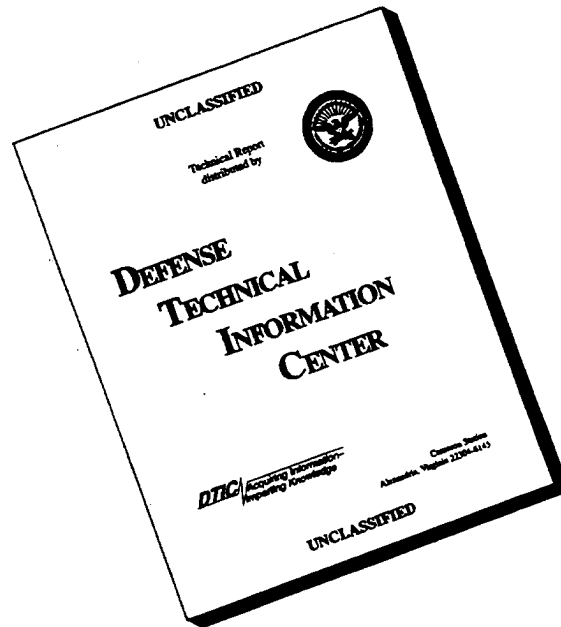
Shawn B. McCamish
Second Lieutenant, USAF

AFIT/GE/ENG/95D-16

19960617 009

Approved for public release; distribution unlimited

DISCLAIMER NOTICE

UNCLASSIFIED

Technical Report
distributed by

DEFENSE
TECHNICAL
INFORMATION
CENTER

DTIC Acquiring Information
Imparting Knowledge

Cameron Station
Alexandria, Virginia 22304-6145

UNCLASSIFIED

THIS DOCUMENT IS BEST
QUALITY AVAILABLE. THE
COPY FURNISHED TO DTIC
CONTAINED A SIGNIFICANT
NUMBER OF PAGES WHICH DO
NOT REPRODUCE LEGIBLY.

The views expressed in this thesis are those of the author and do not reflect the official policy or position of the Department of Defense or the U. S. Government.

OPTIMAL FORMATION FLIGHT CONTROL

THESIS

Presented to the Faculty of the Graduate School of Engineering

of the Air Force Institute of Technology

Air University

In Partial Fulfillment of the

Requirements for the Degree of

Master of Science in Electrical Engineering

Shawn B. McCamish, B.S. Electrical Engineering

Second Lieutenant, USAF

December 1995

Table of Contents

ix

xii

List of Tables

xiii

List of Symbols

xv

AFIT/GE/ENG/95D-16

Abstract

Automatic formation flight involves controlling multiple wing aircraft equipped with standard Mach-hold, altitude-hold, and heading-hold autopilots in order to maintain a desired position relative to a lead aircraft throughout formation maneuvers. Changes in the lead aircraft's states, including formation heading, velocity, altitude, and geometry changes, are treated as disturbance and are rejected by the formation flight control system. The work in this thesis is a continuation of five previous theses, dealing with the design of formation flight control systems. The goal of the optimal formation flight control design is to achieve robust formation maintenance in the face of formation maneuvers and the presence of full system nonlinearities. Second-order aircraft/autopilot models are included in the design and a new control law is employed. A constrained optimization for determining the optimal controller gains of fixed structure controllers is employed. The two controllers considered are a Proportional plus FeedForward (PFF) controller, previously developed at AFIT, and a new Proportional plus Integral and FeedForward (PIFF) controller, which uses less feedforward information. Finally, the constrained optimization is applied to a wide variety of formation maneuvers and geometry changes initiated from both the *tight*, closely spaced, and *loose*, more widely dispersed, types of formations.

OPTIMAL FORMATION FLIGHT CONTROL

I. Introduction to Optimal Formation Flight Control

1.1 Overview of Thesis

This thesis is concerned with the control of an aircraft formation. It is postulated that each aircraft is equipped with standard autopilots. The optimal gains in a fixed structure, proportional plus integral formation flight control system, are being sought.

In the first chapter, the formation flight control problem is introduced. The motivation, assumptions, research, and scope are addressed.

The second chapter reviews the current formation flight control literature. Related work is presented and its relative importance to this thesis is discussed.

The third chapter introduces the models and kinematic equations used in the thesis. The aircraft models are described in detail and the nonlinear kinematics governing the formation flight control problem are derived. In addition, the complete formation flight control system structure for nonlinear simulations is presented. This chapter provides the reader with enough information to be able to reproduce the results from this research.

The fourth chapter extends Lieutenant Veth's formation flight control work from December of 1994 [23]. The control law is modified such that integral action replaces lead heading information in the y-separation channel. The energy tracking control concept for energy swing minimization during formation changes is employed. A constrained optimization method is employed for determining feedback gains, which improve heading, velocity, and energy tracking. Second-order models developed by Captain Buzogany [2, Chapter 2] are incorporated into the design procedure and simulation. As in previous theses, lead heading, velocity, and altitude commands introduce disturbances into the system.

The fifth chapter presents the formation flight control system optimization for the *tight*, closely spaced, formation (see page 1-5). A Proportional plus FeedForward (PFF)

controller, developed by Veth [23, chapter 4], and the Proportional plus Integral and Feed-Forward (PIFF) controller, developed in Chapter IV, are optimized. The *tight* formation results allow for easy comparison with results from previous theses.

The sixth chapter presents the *loose*, more widely dispersed, formation optimization (see page 1-5); PFF and PIFF controllers are being optimized. The *loose* formation represents formation flight configurations used in C-130 aircraft operations.

The final chapter summarizes the findings of this research, provides conclusions, and makes recommendations for future research.

1.2 Motivation for Formation Flight Control

The diverse capability of modern Air Force aircraft comes at the cost of increased aircraft complexity and aircrew workload. A specific type of mission which has a great potential for aircrew saturation is conducted by the Air Force Special Operations Force (AFSOF). The AFSOF mission emphasizes concealment and secrecy and may require long range penetration behind enemy lines. To reduce the probability of detection, AFSOF missions are primarily flown at night, in close formation, and at very low altitudes [23, Chapter 1]. In addition, these formations may consist of like or dissimilar aircraft, depending on mission requirements. Hence, these formation flight conditions increase aircrew workload and reduce aircrew flight safety margins. As a result, current aircraft flight control technology needs to be applied to the demanding task of maintaining formation. In other words, automation of the formation flight control task is required. This control advancement will reduce aircrew workload, thereby increasing endurance and overall mission effectiveness [4, Chapter 1].

Formation flight control design work, however, differs from traditional flight control design. Traditional flight control is based on designing controllers which achieve the desired handling qualities over a range of aircraft model variations by manipulating the aircraft's control surfaces in response to pilot command inputs. In contrast, current formation flight control research at the Air Force Institute of Technology (AFIT) seeks to use the aircraft's existing inner loop flight control systems to maintain formation with other similarly

equipped aircraft. The main difference between the two types of control paradigms is that traditional flight control focuses on the dynamics associated with individual aircraft while the formation flight control system focuses on the dynamics associated with a number of aircraft. Conventional flight control is concerned with maneuvering flight which predicates inner loop control; whereas formations, which maneuver relatively slowly, predicate outer loop control. Strictly speaking, the time scale of interest in conventional flight control is relatively short, while the time scale in formation flight control is long. The resulting formation flight control problem is fairly rich and provides new insights into control system design.

1.3 Problem Description

The objective of this research is to optimize fixed structure formation flight control systems. First, the refinement of the formation-hold autopilot concept, previously addressed by Captains Rohs, Dargan, Buzogany, and Reyna, and Lieutenant Veth, is addressed. Particular attention is given to the following:

- Verification of previous research

- Incorporation of second-order C-130 aircraft/autopilot models

- Direct feedforward of the lead aircraft velocity, V_L, without heading information

- Employment of only V_L feedforward for wing aircraft energy swing minimization during formation maneuvers

- Alleviation of deleterious effects caused by rate saturation in the wing aircraft/autopilot model

- Investigation of the application of optimization design methods to formation flight control system design

In addition, C-130 aircraft/autopilot models are employed in this thesis for two reasons. First, C-130s are currently used by the Air Force Special Operations Force (AFSOF) which initiated the formation flight control research. Second, using the same C-130 aircraft/autopilot models allows for comparison with results from previous AFIT theses.

The two basic formation geometries investigated are the trail and diamond formations. Simple three ship examples of these formations are shown in Figures 1.1 and 1.2, respectively. These formations are commonly used in the AFSOF mission. The trail formation enables a minimum amount of area to be covered during penetration flights. In contrast, the diamond formation covers more area, but improves visibility between aircraft.

Formation flight control is concerned with both formation maneuvers and formation geometry changes. Formation maneuvers include changes in the formation's velocity, heading, and altitude. Examples of these maneuvers are shown in Figures 1.3 and 1.4. Formation geometry changes include changes in types of formations and in the separation distances between aircraft in the formation. An example of a formation geometry change is shown in Figure 1.5.
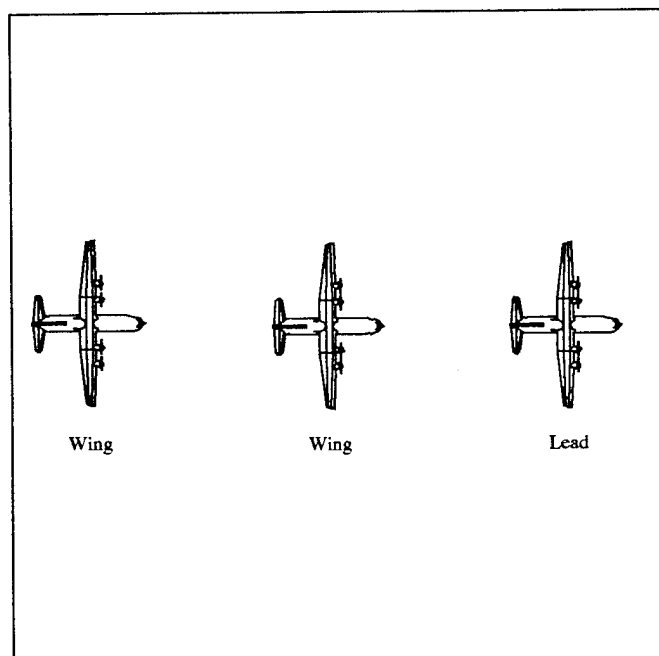
Figure 1.1   Trail Formation
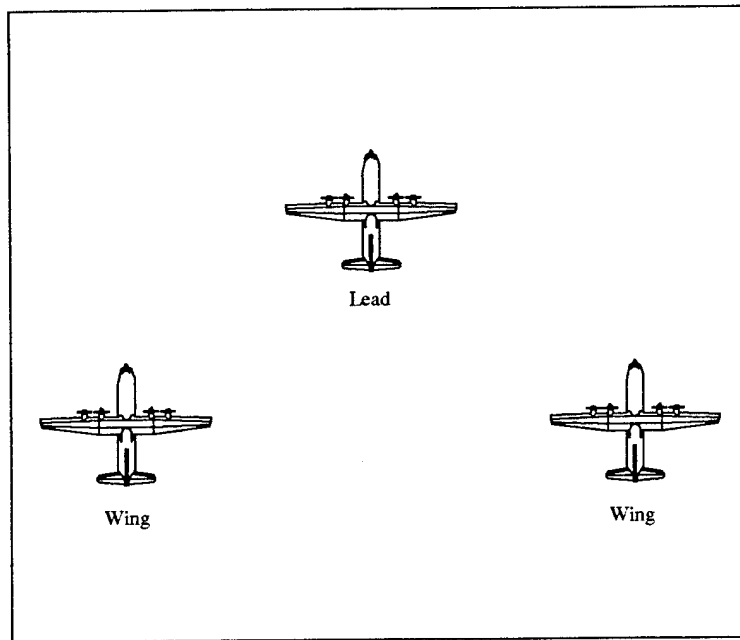
Figure 1.2   Diamond Formation
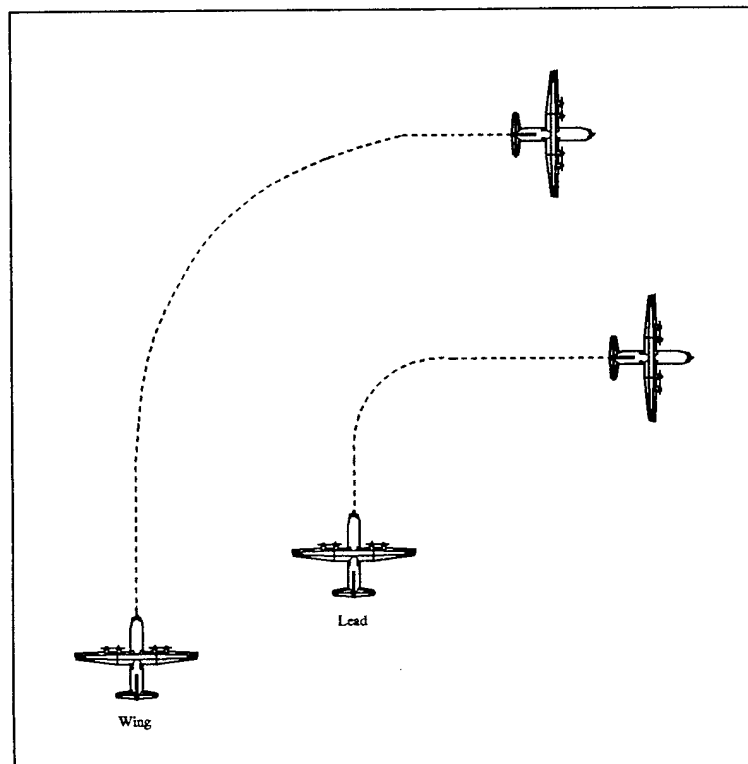
Figure 1.3   Diamond Formation Heading Change Maneuver
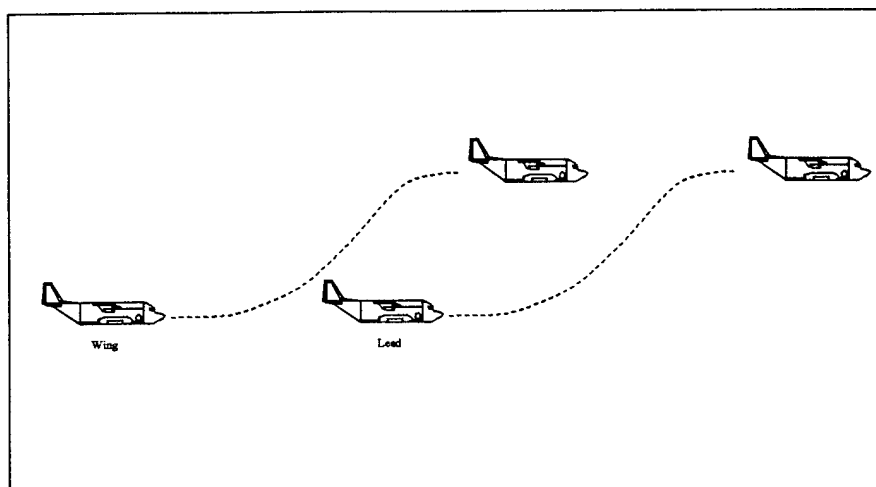
Figure 1.4   Trail Formation Altitude Change Maneuver
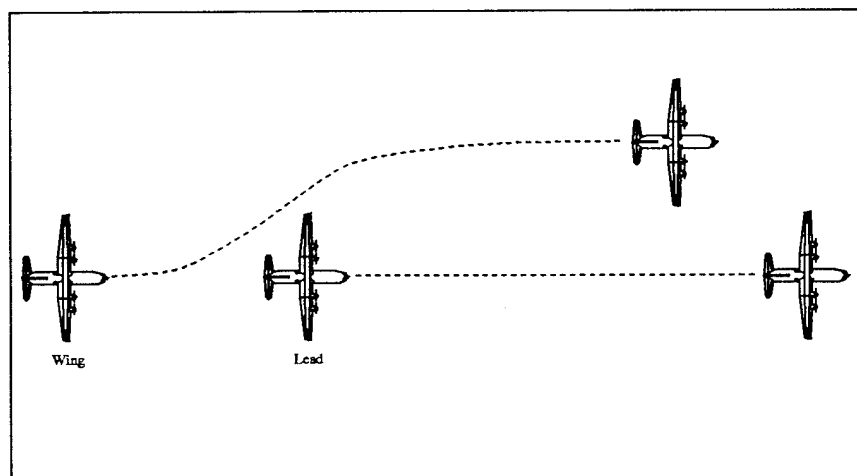
Figure 1.5   Trail To Diamond Formation Change Maneuver

The research reported in this thesis is primarily focused on aircraft in a generic diamond formation. Use of the diamond formation allows for comparison with Lt Veth's results [23] and offers more interesting dynamics than the symmetrical trail formation. Separation distances, like aircraft formations, are also dynamic and may depend on the type of aircraft, formation, and mission.

In traditional manual formation flight there is no attempt to accurately maintain established separation distances throughout the maneuver. During manual formation flight maneuvers, a wing aircraft may simply delay, by a predetermined amount of time (say 10 seconds), executing the formation heading change until a prearranged turn point is reached. When the wing aircraft reaches the turning point it simply performs the same heading change as the lead aircraft. However, in optimal formation flight control the wing aircraft attempts to maintain the formation throughout the maneuver, and no time delays are designed into the system. Either way the formation is maintained, the lead aircraft has to be considerate of the y-separation distance offset position of his wing aircraft in order to avoid "flying" the wing aircraft into topographical obstacles.

In order to investigate separation dynamics, two different initial nominal diamond formation separations are utilized. These separation distances are the "tight" and "loose" formations, defined below:

- The *tight* formation is a left diamond formation ($\overline{X} = 500$ ft, $\overline{Y} = 500$ ft)

- The *loose* formation is a left diamond formation ($\overline{X} = 3500$ ft, $\overline{Y} = 1000$ ft)

The *tight* formation allows for comparison with Lt Veth's results; whereas, the *loose* formation represents a common separation distance used in C-130 aircraft operations during some segments of the formation flight. Extensive nonlinear simulations are conducted on both formations in order to validate the design.

1.4 Procedure

The first step undertaken in this research entailed the verification of the previous AFIT results from the equations of motion, to the nonlinear SIMULINK simulations. By gaining full confidence in previous work, the foundation for further research is established.

Once verification is complete, the second-order models are incorporated into the simulation with only feedforward of the lead aircraft's velocity (V_L). The new controller does not employ feedforward of the lead aircraft's heading (Ψ_L). The resulting controller is evaluated in three-dimensional analyses using SIMULINK nonlinear simulations. Initially the controller uses a combination of Capt Buzogany's Proportional plus Integral (PI) controller gains [2] and Lt Veth's direct feedforward gains [23]. However, the nonlinear simulation results are used to further adjust and manually fine tune controller gains to improve formation responses.

Next, automated optimization methods are investigated in order to determine which set of gain values yield the best overall formation flight response. The gain values which were manually chosen to yield improved formation responses are used as the initial starting point for optimization. The gain values from optimization are a priori constrained in order to include rate saturation effects in the elementary aircraft/autopilot models. This research is then used to indicate the best possible performance which can be achieved at this level of controller and modeling complexity.

The final task is to apply optimization techniques to a number of controller designs. The optimal designs are evaluated using a wide range of test conditions which encompass the complete formation flight envelope of the C-130 aircraft. The design must demonstrate the ability to complete all standard formation flight phases without becoming unstable, colliding with other aircraft in formation, or colliding into the ground.

1.5 Assumptions

The primary goal of this thesis is the study of a unique flight control system application, viz., the design of a formation flight control system. Assumptions are made which make the formation flight control problem amenable to analysis and at the same

time address the most important real world considerations. This thesis is a continuation of previous work. The assumptions are:

- Each wing aircraft in the formation has the following autopilots in place:

  a) Mach-Hold Autopilot

  b) Heading-Hold Autopilot

  c) Altitude-Hold Autopilot

- Recall that all autopilots are, by definition, decoupled. In other words, heading changes can be made independently of velocity and altitude changes, etc.

- The controller has access to the following ideal measurements: lead aircraft's velocity heading, and altitude and the x- and y-separation distances measured relative to the wing aircraft.

- Initial conditions for all simulations are straight and level flight.

- Aircraft/autopilot models are considered to be time invariant over the simulation time period (150 or 300 seconds).

- The formation flight control system uses continuous time measurements. No digital implementations are considered.

1.6   Criteria for Success

In order to design a control system it is important to establish a standard by which desirable output responses can be gauged. However, there are no established flying qualities for formation flight control. Nevertheless, practicality and conventional control method specifications mandate that the formation flight control system must meet the following criteria:

- The control system must maintain commanded formation with zero steady-state error.

- Unnecessary and undesirable excursions by the wing aircraft must be eliminated.

- The system must be robust over a wide range of command inputs.

- Other aircraft and terrain obstacles must be avoided.

1.7 Materials and Equipment

All simulations are performed using the MATLAB 4.2c analysis package [12]. MATLAB 4.2c is sold by Mathworks and uses double precision arithmetic and standard command files to execute computations. It is available for a wide variety of computer platforms. A fifth-order Runge-Kutta differential equation solver with fourth-order step-size control is used in all nonlinear simulations, and a Sequential Quadratic Programming (SQP) method is used in all constrained optimization applications [6]. The equipment and software is provided by the Department of Electrical and Computer Engineering in the Navigation and Flight Control Lab (Room 133) of the Air Force Institute of Technology. In addition, the thesis document is written using LaTeX document preparation software.

1.8 Conclusion

This research begins by refining the formation autopilot controller. This refinement includes limiting the feedforward signal to only the lead aircraft's velocity (V_L) and adjusting the controller gains by using established optimization techniques. Next, optimization techniques are applied to fixed flight structure controllers designed to maintain formation throughout maneuvering tasks. Once the optimization of these controllers is complete, extensive simulations are performed in order to validate the design. These formation flight control algorithms are intended to provide an effective solution to the current problems encountered during formation flying tasks.

II. Literature and Concept Review

This chapter reviews the literature pertaining to formation flight control. The research and concepts which directly apply to this thesis effort are outlined.

2.1 Development of Formation Flight Control Systems

Research and development of the formation flight controller has been underway for many years and a variety of techniques have been used, each with its own merits. Initial formation flight techniques centered around controlling drone aircraft. Today the focus is on the dynamic and practical problem of maintaining formation with both piloted and drone aircraft. Recently the path has forked off into two very different directions. One path relies on making more accurate and complete situational information available to the pilot, thereby allowing the pilot to better fly in formation. The other path, in contrast, hinges on the development of a formation-hold autopilot. The emphasis of this thesis is on the latter.

2.2 Formation Flight Control Pioneers

The earliest formation flight control systems were used to control drone aircraft. These drones, in turn, were used to test the effectiveness of air-to-air weapons against enemy formations. The Navy used two separate controllers to fly formations of QF-9 drone aircraft as early as 1963. These controllers commanded the wing drone to maneuver itself to keep its view of the lead aircraft in the center of a TV screen [22]. Even though this system performed adequately for simple commands, it was limited to only a two ship formation because of difficulties with coordination and fine adjustment of the flight control system (FCS). A noteworthy system used to control drone aircraft was developed in the mid seventies by the Army and IBM. This system was able to control multiple QF-102 aircraft in take-off, missile attack evasion, and landing modes [22]. However, this system implementation required direct access to the aircraft's flight control system, and this access restriction made modification to other aircraft extremely difficult. Despite the fact that

both of these pioneer formation flight control systems performed adequately for drones, neither could be effectively adapted to piloted aircraft.

2.3 Pilot-In-The-Loop Approach

A current approach to flying multiple ship formations is being researched by Loral Federal System. Loral's approach is to augment the wing pilot's ability to locate other formation aircraft through enhanced situational awareness [9]. Recent reports by Loral show that its Intra-Formation Positioning System (IFPS) is successful in assisting aircrews which are flying formation tasks [10]. The IFPS combines Forward Looking Infrared (FLIR), Terrain Following (TF), a HAVE QUICK II data-link system, and improved GPS/INS relative positioning. The IFPS integrates all available formation flight information and simultaneously displays it on a situational awareness display, which shows where adjacent aircraft are located, and on a flight director display, which provides visual guidance as to where the aircraft should be in order to maintain formation. These visual enhancement systems help to increase mission capability by improving the aircrew's situational awareness, but still require the aircrew to manually fly the formation. In order to further alleviate the aircrew workload accrued in formation flight, a second approach to formation flight control is currently underway at AFIT.

2.4 Previous AFIT Research

The development of an automatic formation control system, acting as a formation hold autopilot, would relieve aircrews of additional pressure during formation flying tasks. The formation flight control system has been the focus of AFIT research for several years. The research has been well documented in five previous theses, and in conference and journal papers. Gradual improvements in both aircraft modeling and controller performance have been achieved.

2.4.1 Rohs: A Fully Coupled, Automated Formation Control System for Dissimilar Aircraft in Maneuvering, Formation Flight.
Initially, a simple planar control system for first-order C-130 aircraft models was studied by Rohs in March of 1991 [22]. As a

result, a control system capable of controlling a formation of similar, or dissimilar, aircraft through three separate maneuvers was developed. These maneuvers included a heading change, a terrain avoidance altitude change, and a formation change. Aircraft position was measured using a Cartesian reference frame, with rotations into inertial and wing aircraft frames being achieved by using the Equation of Coriolis, see Figure 2.1. In standard form, the Equation of Coriolis is

$$\dot{R}_i = \dot{R}_p + \omega_{ip} \times R_p \tag{2.1}$$

with

- $\dot{R}_i$ = the vector velocity of the point in the i reference frame

- $\dot{R}_p$ = the vector position of the point in question as seen from the p reference frame

- ω_{ip} = the vector angular velocity of the p reference frame with respect to the i reference frame

- R_p = the vector position of a point in the p frame
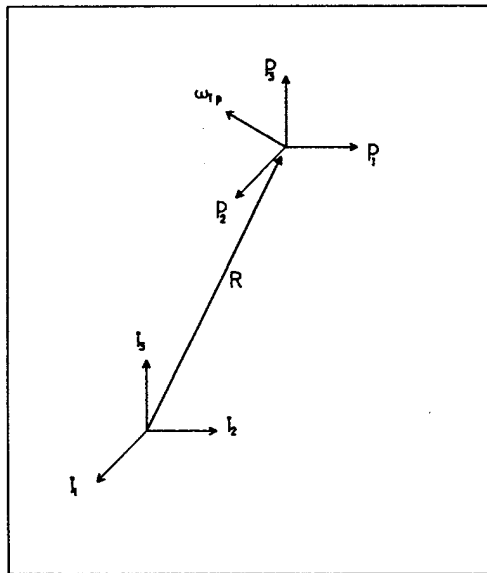
Figure 2.1   Inertial and Rotating Frames of Reference

Furthermore, it was assumed that perfect lead aircraft position information was available to each wing aircraft's control system. This was a fine start, but much more research was needed in both controller design and aircraft modeling.

2.4.2   Dargan: Proportional Plus Integral Control of Aircraft for Automated Maneuvering Formation Flight.   Next, the controller was improved by Dargan, in December of 1991 [4]. He designed a multi-variable controller which gave favorable results and proved the initial viability of the approach. The lead aircraft's velocity (V_L) and heading (Ψ_L)were used as feedback in order to maintain the commanded x- and y-separation distances between aircraft. The design was extended by using proportional plus integral (PI) control in conjunction with a linear mixer [4]. The PI system successfully controlled aircraft in planar movements, using refined first-order C-130 aircraft/autopilot models.

2.4.3   Buzogany: Automated Control of Aircraft in Formation Flight.   Further research focused on evaluating true three-dimensional maneuvers, see Figure 2.2. As a result, a controller which conserved wing aircraft energy level was implemented by Buzogany, in December of 1992 [2]. Throttle fluctuations were eliminated, minimizing fuel consumption, but preventing the aircraft from tracking changes in lead altitude or velocity [2]. In addition, more accurate second-order C-130 aircraft/autopilot models were developed.

2.4.4   Reyna: Automation of Formation Flight Control.   Reyna continued Buzogany's research of formation flight during three-dimensional maneuvers. In March of 1994 he developed a solution to the limitations of the energy conserving controller which allowed wing energy fluctuations, but made them as small as possible [20]. This energy minimizing technique demonstrated the ability to track lead altitude and velocity changes, while reducing fuel consumption and achieving adequate formation performance. However, Reyna's design was only applied to the first-order C-130 aircraft/autopilot models.

2.4.5   Veth: Advanced Formation Flight Control.   The most recent research, conducted by Veth and concluded in December of 1994 [23], extended both Reyna's formation flight control work and the energy minimizing concept pioneered by Buzogany and enhanced by Reyna. First, the formation flight control law was modified to improve per-

altitude

wing ——
lead — —

500

450

40000
35000
30000
25000
20000
15000
10000
5000
0

0   1000   2000   3000   4000   5000   6000   7000

X inertial

Y inertial
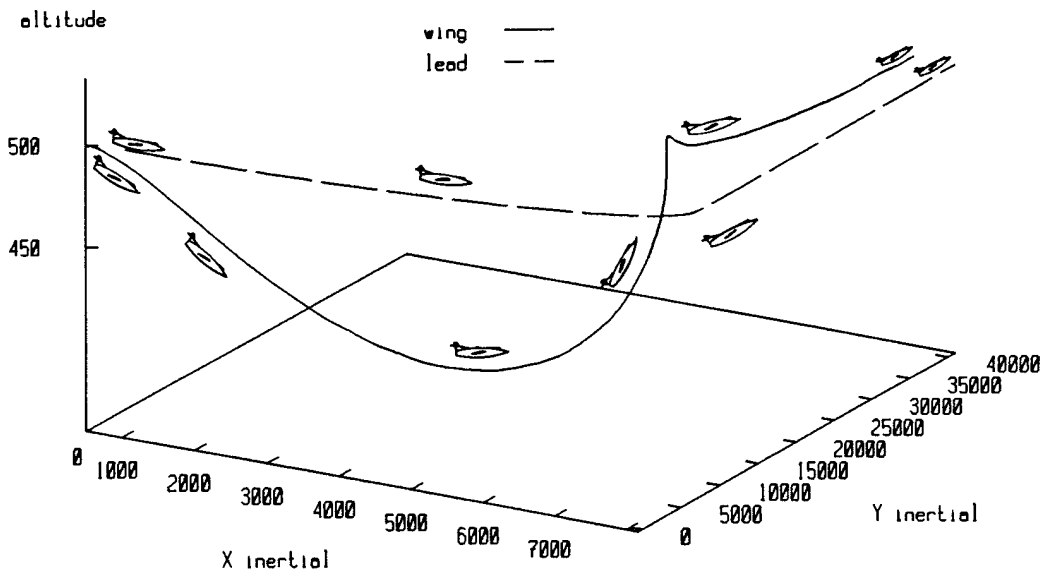
Figure 2.2 Three Dimensional Rendition of Aircraft in Formation Heading Change Maneuver

formance by changing the feedforward gains to provide lead heading and velocity tracking [23]. This law incorporated the second-order models, developed by Buzogany [2], into the design procedure and simulation. As in previous theses, lead heading and velocity commands were introduced as disturbances into the system. Second, the energy conservation and energy minimization concepts were combined into one controller. For planar maneuvers the controller incorporated the energy conserving technique developed by Buzogany. This algorithm enabled the wing aircraft to vary altitude as a means of eliminating energy excursions, but limited the wing aircraft's capability of tracking energy changes by the leader. In order to overcome this deficiency, the controller also incorporated Reyna's energy minimizing algorithm which enabled the wing aircraft to track energy changes and thereby reduce wing energy swings. By combining these concepts, Veth was able to develop an energy tracking system which responds well to both energy tracking and energy conserving aircraft/autopilot commands [23]. This composition allowed the design of a hybrid controller, improving performance and providing further insights into the energy tracking concept.

Additionally, Veth extended the formation flight control concept to automatically fly an aircraft about a fixed point on the earth. The autopilot for flying circular paths

was designed to track command changes in airspeed and in orbit radius. The leader is a computer-generated signal (or "rabbit") which follows the ideal orbit path [23]. The wing aircraft were able to track the leader with minimum overshoot. This development was an interesting extension of the formation flight control problem.

2.5 Conclusion

This thesis continues the AFIT research into a formation flight control autopilot which performs the demanding task of maintaining formation. This advancement shows great potential for reducing aircrew workload during formation flying tasks, thereby increasing endurance and overall mission effectiveness. In addition to its operational benefits, the formation flight controller research has provided new insights into both the dynamics associated with multiple aircraft formations and the related linear control system designs. From the first drone controllers to the current IFPS design by Loral, there has been constant progress toward the control of multiple aircraft formations. However, the formation flight controller developed at AFIT appears to be the only attempt to completely relieve aircrews of the additional stresses associated with formation flight.

The development of the AFIT formation flight controller has been underway for four years. The design started with the initial first order C-130 models and simple planar controllers developed by Rohs and has progressed to the point of using Buzogany's second-order C-130 aircraft/autopilots and Veth's energy tracking and energy conserving three-dimensional controllers. This thesis focuses the current research on optimizing the formation-hold autopilot controller gains and limiting the controller feedforward signal to include only lead aircraft velocity (V_L). With these advances, the AFIT formation flight controller should prove to be a vital technology in reducing aircrew workload and increasing overall mission effectiveness.

III. Model and Simulation Development

This chapter defines the models and kinematic equations used in the nonlinear simulation. Sufficient information is provided to enable the reader to reproduce the results of the research.

3.1 Aircraft/Autopilot Models

The development of the aircraft/autopilot models was accomplished by Rohs [22], Dargan [4] and Buzogany [2]. The aircraft/autopilot models were obtained by designing a custom autopilot system around C-130H aircraft models provided by Lockheed. The autopilot system includes Mach-hold, heading-hold, and altitude-hold autopilots. Due to the inherent properties of aircraft autopilots, the aircraft/autopilot models exhibit overdamped, decoupled responses. Using system identification techniques, first-order models were developed using rate limited, decoupled, first-order differential equations. The first-order aircraft/autopilot models are specified in equations (3.2) - (3.3).

$$\dot{V} = -\frac{1}{\tau_v}V + \frac{1}{\tau_v}V_{cmd} \tag{3.1}$$

$$\dot{\Psi} = -\frac{1}{\tau_\psi}\Psi + \frac{1}{\tau_\psi}\Psi_{cmd} \tag{3.2}$$

$$\dot{H} = -\frac{1}{\tau_h}H + \frac{1}{\tau_h}H_{cmd} \tag{3.3}$$

where,

V_{cmd} = commanded velocity τ_v = velocity time constant

Ψ_{cmd} = commanded heading τ_ψ = heading time constant

H_{cmd} = commanded altitude τ_h = altitude time constant

The most disturbing problem with the first-order models is the presence of instantaneous heading rate and vertical velocity changes. In order to more accurately represent a "true" aircraft/autopilot system, second-order aircraft/autopilot models were developed by Buzogany [2]. The second-order aircraft/autopilot models are better in that their re-
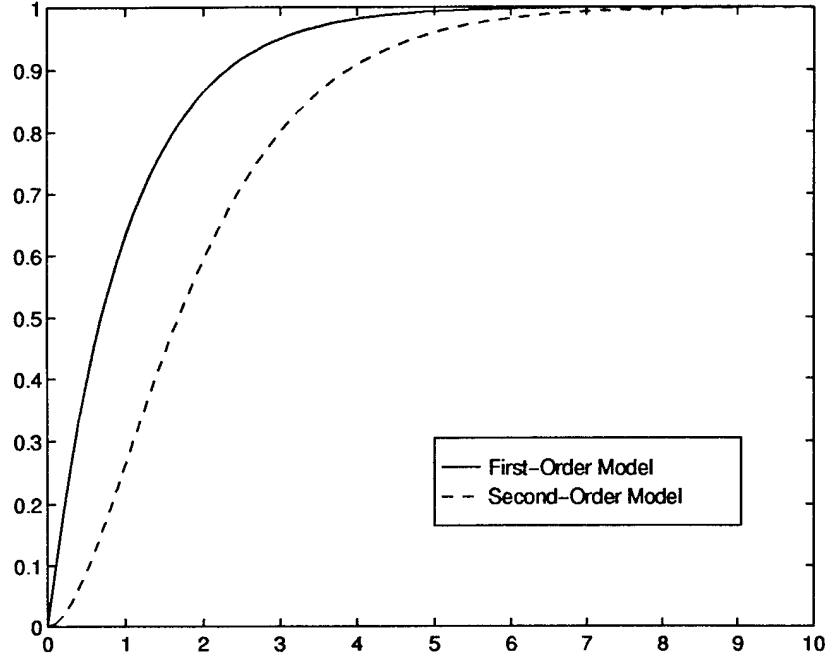
Figure 3.1   Comparison of First and Second-Order Responses

sponses do not exhibit instantaneous change. Figure 3.1 [8] compares an overdamped second-order response with a first-order response, and shows the difference in their initial rates. Consequently, heading and altitude responses are significantly improved using second-order models, even though the velocity response is modelled more precisely using a first-order model with a larger time constant. The resulting "second-order" models and time constants are specified in equations (3.5) - (3.6). The second-order models illustrated in Figure 3.2, include the inherent rate limited characteristics.

$$\dot{V} = -\frac{1}{\tau_v}V + \frac{1}{\tau_v}V_c \tag{3.4}$$

$$\ddot{\Psi} = -\left(\frac{1}{\tau_{\psi_a}} + \frac{1}{\tau_{\psi_b}}\right)\dot{\Psi} - \frac{1}{\tau_{\psi_a}\tau_{\psi_b}}\Psi + \frac{1}{\tau_{\psi_a}\tau_{\psi_b}}\Psi_c \tag{3.5}$$

$$\ddot{H} = -\left(\frac{1}{\tau_{h_a}} + \frac{1}{\tau_{h_b}}\right)\dot{H} - \frac{1}{\tau_{h_a}\tau_{h_b}}H + \frac{1}{\tau_{h_a}\tau_{h_b}}H_c \tag{3.6}$$

The time constants and nonlinear saturation values used in this thesis are specified in Table 3.1 [2] and 3.2 [20].

Parameter	Value
τ_{ψ_a}	1.838 sec
τ_{ψ_b}	1.838 sec
τ_v	10 sec
τ_{h_a}	0.615 sec
τ_{h_b}	7.692 sec

Table 3.1   Second-Order Aircraft/Autopilot Parameters

Parameter	Lower Limit	Upper Limit
Velocity	$304\frac{ft}{sec}$	$422\frac{ft}{sec}$
Acceleration	$-5\frac{ft}{sec^2}$	$2.5\frac{ft}{sec^2}$
Turn Rate	$-3\frac{deg}{sec}$	$3\frac{deg}{sec}$
Vertical Velocity	$-42\frac{ft}{sec}$	$8\frac{ft}{sec}$

Table 3.2   Aircraft/Autopilot Saturation Values
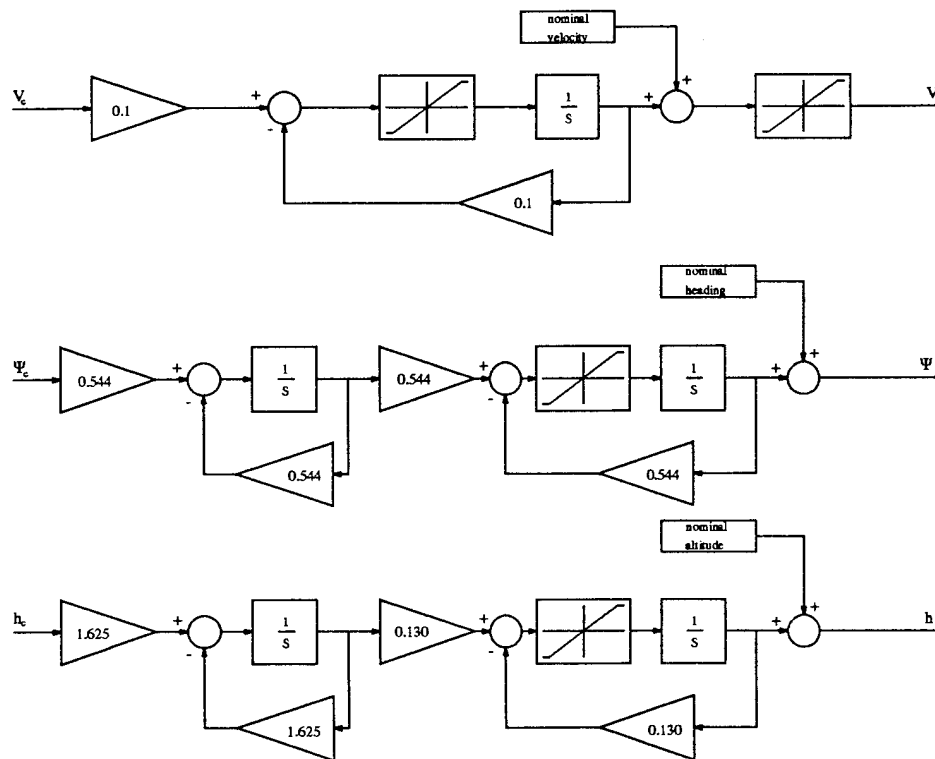
Figure 3.2   Second-Order Aircraft/Autopilot Models

3.2 Formation Coordinate System

The coordinate system used in this thesis is identical to the one used by Dargan [4], Buzogany [2], Reyna [20], and Veth [23]. The analysis of the system kinematics uses two coordinate frames:

- Inertial frame of reference

- Rotating reference frame centered on the wing aircraft

The base frame is an inertial North-East-Down system, with the earth considered to be flat and inertially fixed. The inertial reference frame and separation distances are shown in Figure 3.3.

The wing aircraft frame is centered on the wing aircraft. The x-axis is in the flight direction (i.e., aligned with the velocity vector), the y-axis points out the starboard wing, and the z-axis points toward the earth. The x- and y-separation distances are measured in the wing frame (Figure 3.4).
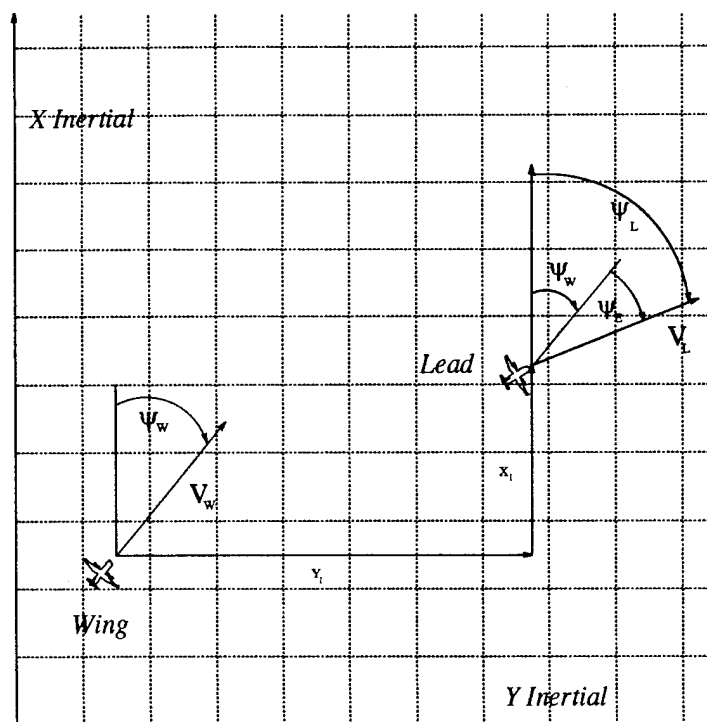
Figure 3.3   Inertial Reference Frame and Separation Distances

3-4
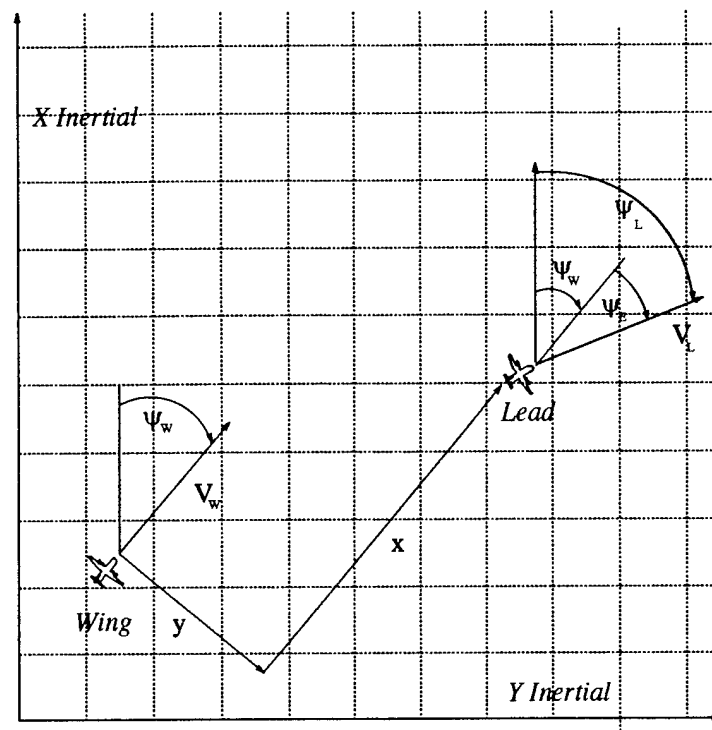
Figure 3.4   Wing's Rotating Reference Frame and Separation Distances

3.3 Kinematic Equations

In order to simulate the kinematics associated with the formation flight control model, kinematic equations must be derived. This derivation has already been performed by Dargan [4], Buzogany [2], and Reyna [20]. Reyna's derivation is repeated here to ensure clarity (from [20], pages 3:6-10).

Using the Equation of Coriolis (Chapter II), the velocity of the lead with respect to the wing has been found by Dargan as

$$V_{WL}^W = V_L^W - \omega_W^W \times R_{WL}^W - V_W^W + \omega_W^W \times R_W^W \tag{3.7}$$

with the following convention:

- The superscript indicates the reference frame.

- The subscript indicates the parameter described by the vector or a relation between two parameters.

For instance,

V_{WL}^W = velocity of lead aircraft with respect to wing, in the wing's reference frame

ω_W^W = angular velocity of wing aircraft in the wing reference frame

R_{WL}^W = position of lead aircraft with respect to wing, in the wing's reference frame

V_W^W = inertial velocity of wing aircraft in its own reference frame

V_L^W = inertial velocity of lead aircraft in the wing's reference frame

R_W^W = position of wing aircraft in its own reference frame

The development of the kinematic equations is based on the geometry displayed in Figure 3.5. The following relationships are defined:

$$\Psi_E = \Psi_L - \Psi_W \tag{3.8}$$
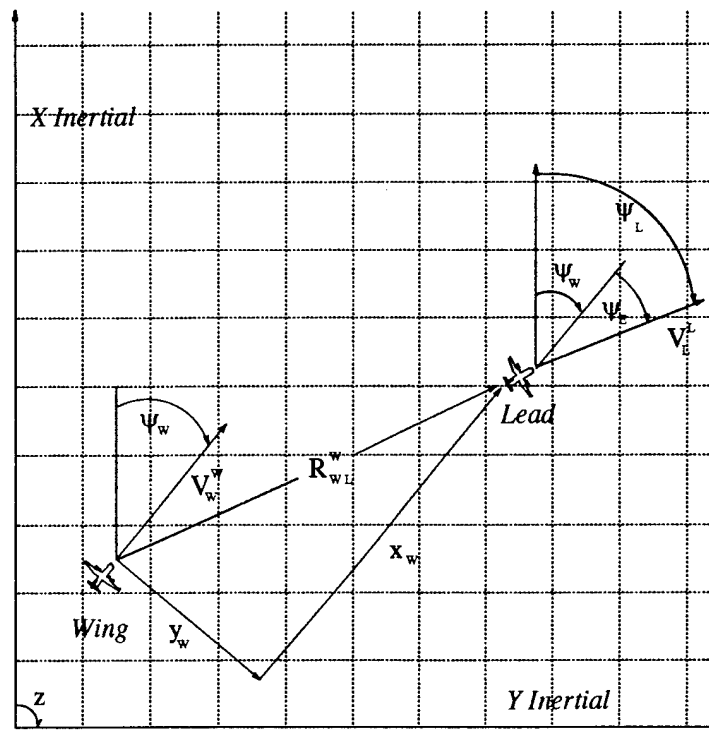
Figure 3.5 Relative Motion Diagram

$$\omega_W^W = \begin{bmatrix} 0 \\ 0 \\ \dot{\Psi}_W \end{bmatrix} \qquad (3.9)$$

$$R_{WL}^W = \begin{bmatrix} x^W \\ y^W \\ z^W \end{bmatrix} \qquad (3.10)$$

$$V_W^W = \begin{bmatrix} V_W \\ 0 \\ 0 \end{bmatrix} \qquad (3.11)$$

$$V_L^L = \begin{bmatrix} V_L \\ 0 \\ 0 \end{bmatrix} \qquad (3.12)$$

$$R_W^W = \begin{bmatrix} 0 \\ 0 \\ 0 \end{bmatrix} \qquad (3.13)$$

where,

Ψ_E = heading error

V_L^L = velocity of the lead aircraft in its own reference frame

In order to solve equation (3.7), V_L^L must be transformed into the wing reference frame. A Direction Cosine Matrix (DCM), developed by Dargan [4], is used to perform the rotation. Dargan found the necessary DCM to be

$$C_L^W = \begin{bmatrix} cos\Psi_E & -sin\Psi_E & 0 \\ sin\Psi_E & cos\Psi_E & 0 \\ 0 & 0 & 1 \end{bmatrix} \qquad (3.14)$$

V_L^W is found by substituting equations (3.12) and (3.14) into the following equation

$$V_L^W = C_L^W V_L^L = \begin{bmatrix} V_L cos\Psi_E \\ V_L sin\Psi_E \\ 0 \end{bmatrix} \qquad (3.15)$$

Substituting equations (3.9)-(3.11), (3.13), and (3.15) into equation (3.7) yields

$$V_{WL}^W = \begin{bmatrix} V_L cos\Psi_E \\ V_L sin\Psi_E \\ 0 \end{bmatrix} - \begin{bmatrix} 0 \\ 0 \\ \dot{\Psi}_W \end{bmatrix} \times \begin{bmatrix} x^W \\ y^W \\ z^W \end{bmatrix} - \begin{bmatrix} V_W \\ 0 \\ 0 \end{bmatrix} + \begin{bmatrix} 0 \\ 0 \\ \dot{\Psi}_W \end{bmatrix} \times \begin{bmatrix} 0 \\ 0 \\ 0 \end{bmatrix} \qquad (3.16)$$

$$V_{WL}^W = \begin{bmatrix} V_L cos\Psi_E \\ V_L sin\Psi_E \\ 0 \end{bmatrix} - \begin{bmatrix} -\dot{\Psi}_W y^W \\ \dot{\Psi}_W x^W \\ 0 \end{bmatrix} - \begin{bmatrix} V_W \\ 0 \\ 0 \end{bmatrix} \qquad (3.17)$$

Separating equation (3.17) into scalar components yields

$$\dot{x}^W = V_L cos\Psi_E + \dot{\Psi}_W y^W - V_W \tag{3.18}$$

$$\dot{y}^W = V_L sin\Psi_E - \dot{\Psi}_W x^W \tag{3.19}$$

$$\dot{z}^W = 0 \tag{3.20}$$

Equations (3.18) - (3.20) describe the kinematics of the formation's x- and y-separation distances in terms of the individual aircraft's heading and velocity. The formation's altitude separation (Z) is simply the difference between the aircraft altitudes.

3.4 Simulation Description

The nonlinear simulations are performed using SIMULINK dynamic simulation software from the MATLAB package. SIMULINK's intuitive interface and high quality nonlinear differential equation solver make it a useful research tool by which a modular description of the formation flight control problem is created. A simplified formation flight control system model is illustrated in Figure 3.6. This modular design allows for easy modification of the aircraft models or controller. The SIMULINK block diagram of the formation flight control system is shown in the Appendix A.1.

The formation flight control system allows for two tiers of simulation inputs. The lower tier consists of commands available to the pilot of the wing aircraft(s). These inputs dictate the formation geometry which is controlled by the separation distances. The upper tier consists of commands which are considered to reside on-board the lead aircraft. These upper tier commands control the entire formation's heading, speed and altitude. The combination of lower tier commands, which determine formation geometry changes, and upper tier commands, which determine formation maneuvers, allow for a wide range of command inputs.
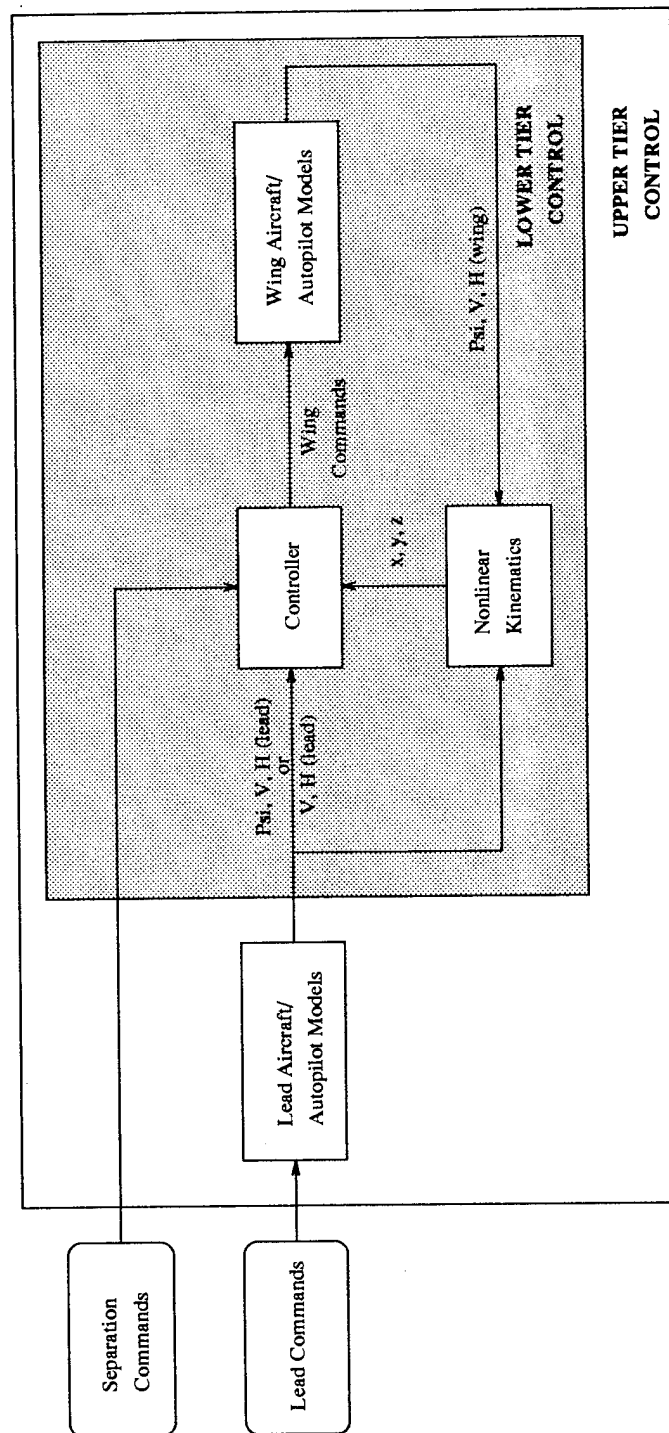
Figure 3.6 Formation Flight Control System Model

3.5 Explanation of Input Ramping

The broad range of command inputs into the formation flight control system determine the formation changes and maneuvers which are simulated. The command inputs can not be treated as simple step inputs from a nominal state to a desired state. These input commands must be ramped into the system in order to allow for more realistic responses by the formation. For example, if a formation is to perform a 45° turn, the pilot of the lead aircraft would not execute the turn at the limits of the aircraft's capability. This would put undue strain on the lead aircraft and make it even harder on the wing aircraft trying to maintain formation. Instead, formation changes and lead aircraft maneuvers are performed at more moderate rates.

The ramping in of commands, for formation changes and maneuvers, is initiated into the simulation with a step input of 0 to 1 at the 0 second. This step input is passed through a state-space block that has

$$A \;=\; 1 \tag{3.21}$$

$$B \;=\; 1 \tag{3.22}$$

$$C \;=\; [0;0] \tag{3.23}$$

$$D \;=\; [perturbation;(1 - perturbation)] \tag{3.24}$$

where *perturbation* is determined by the following calculations:

$$pert \;=\; command - nominal \tag{3.25}$$

$$perturb \;=\; \frac{sign(pert) + 1}{2} \tag{3.26}$$

$$perturbation \;=\; sign(perturb) \tag{3.27}$$

where *sign* is a MATLAB function which returns $+1$ if the number is positive, and -1 if the number is negative. So if the difference between the *commanded* and *nominal* values

is positive or zero then *perturbation* equals +1, however if the difference between the *commanded* and *nominal* values is negative then *perturbation* equals −1.

From the state-space block, mentioned above, the values of *perturbation* and $(1 - perturbation)$ are separated into two different paths. One path for positive changes from the *nominal* and one path for negative changes from the *nominal*. The two paths pass through integrators which have different slopes; the slopes are displayed in Table 3.3. These slopes are 3/4 of the maximum rate limits of the aircraft/autopilot models. The slopes are terminated when the difference value is reached. The difference is then added to the *nominal*, which gives the ramped input from *nominal* to the *commanded* value. If the *commanded* and *nominal* values are equal, then the positive path is taken. However, since the difference value is zero, the slope is immediately terminated and the *nominal* value is simply passed through.

Parameter	Lower Limit	Upper Limit
Acceleration	$-3.75\frac{ft}{sec^2}$	$1.875\frac{ft}{sec^2}$
Turn Rate	$-2.25\frac{deg}{sec}$	$2.25\frac{deg}{sec}$
Vertical Velocity	$-31.5\frac{ft}{sec}$	$8\frac{ft}{sec}$
X-Separation Change	$-50\frac{ft}{sec}$	$25\frac{ft}{sec}$
Y-Separation Change	$-35\frac{ft}{sec}$	$35\frac{ft}{sec}$

Table 3.3   Command Input Slopes

There are no "if" statements used and the paths allow for non-symmetric positive and negative rate limits. A sample SIMULINK diagram of the command inputs is illustrated in Figure 3.7.

This ramping of the input is conducted in the velocity, heading, and altitude channels to insure that the lead aircraft is not reaching saturation in its execution of commanded maneuvers.
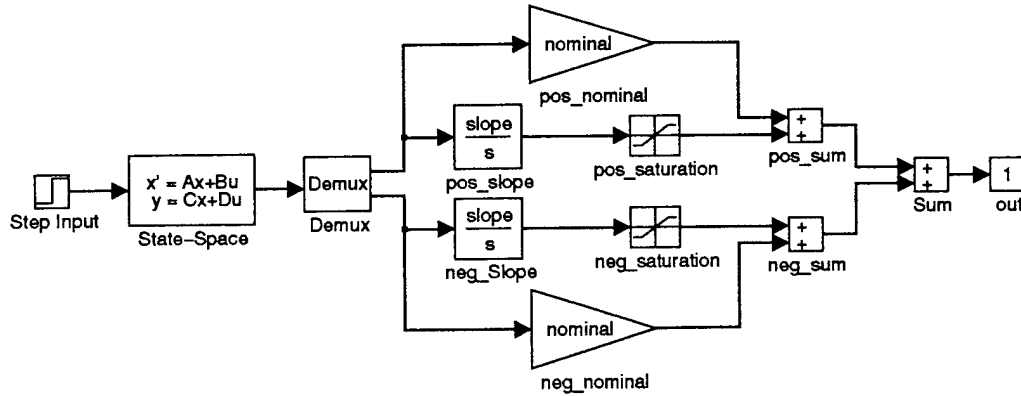
Figure 3.7   SIMULINK Velocity Command Input Diagram

3.6   Conclusion

The formation flight system model combines the second-order aircraft/autopilot models, formation coordinate system information, and the kinematic equations. The nonlinear simulation can be conducted for a broad range of command inputs into the formation flight control system. The commanded inputs for both the formation changes and maneuvers are ramped into the system. The only remaining piece of the model is the controller, which is discussed in Chapter 4.

IV. Optimization of the Formation-Hold Autopilot

The design of an optimal controller for the novel formation hold autopilots developed at AFIT is considered in this chapter. A fixed structure controller is stipulated. The considered controllers are a proportional plus feedforward controller, previously developed at AFIT, and a new proportional plus integral and feedforward type of controller, which uses less feedforward information. A constrained optimization technique for determining the optimal controller gains is employed. The evaluation uses second-order aircraft/autopilot models and nonlinear kinematics. This allows an objective comparison of the new control law with the previous design, experimentally developed by Veth in his M.S. Thesis [23]. The goal of the optimal design is to achieve robust formation maintenance in the face of formation maneuvers and the presence of full system nonlinearities.

4.1 Planar Control Laws

The new planar control law proposed in this thesis is a variation on the Proportional plus Integral (PI) control law developed by Reyna [20], and the Proportional plus FeedForward (PFF) control law developed by Veth [23].

The PI control law developed by Reyna [20] for wing velocity command (V_{wc}) and wing heading command (Ψ_{wc}) is represented by:

$$V_{wc} = k_{xp}e_x + k_{xi}\int_0^t e_x\, dt \qquad (4.1)$$

$$\Psi_{wc} = k_{yp}e_y + k_{yi}\int_0^t e_y\, dt \qquad (4.2)$$

The generalized error signals, e_x and e_y, are determined from:

$$e_x = k_x x + k_v(V_L - V_W)$$

$$e_y = k_y y + k_\psi(\Psi_L - \Psi_W)$$

where,

$$V_L = \text{lead velocity}$$

$$V_W = \text{wing velocity}$$

$$\Psi_L = \text{lead heading}$$

$$\Psi_W = \text{wing heading}$$

The proportional control design with state feedforward of V_L and Ψ_L developed by Veth [23] is represented by:

$$V_{wc} = V_L + K_{xp}(X - X_{cmd}) \tag{4.3}$$

$$\Psi_{wc} = \Psi_L + K_{yp}(Y - Y_{cmd}) \tag{4.4}$$

Note that in the control law, equations (4.3) and (4.4), full states, not perturbations, are used. The true x- and y-separation distances (X and Y) and the commanded x- and y-separation distances (X_{cmd} and Y_{cmd}) determine the planar position error (x and y).

The new Proportional plus Integral and FeedForward (PIFF) control law proposed and investigated in this thesis uses the proportional control and feedforward of V_L in the x-channel, and proportional plus integral control in the y-channel. The replacement of the Ψ_L information with integral action is intended to improve the performance of the controller during formation heading changes, especially heading changes of a trail formation [14]. Thus, consider the following argument: A wing aircraft in trail, which is receiving the leader's heading information during a turn, will have a tendency to execute the same turn and end up in echelon with the leader. Figure 4.1 demonstrates the potential trail to echelon geometry change resulting from unnecessary lead heading information. The x- and y-separation distance commands should avoid such unwanted geometry changes from actually occurring, but a conflict between the heading and separation information can adversely affect controller tracking.
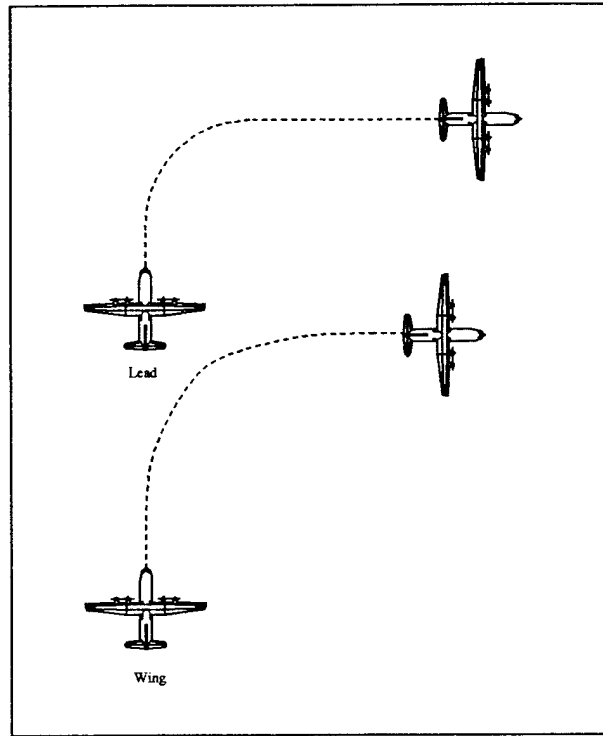
Figure 4.1   Potential Problem of Lead Aircraft Heading Information

As a result, the new y-channel design eliminates both "mixer" constants k_v and k_ψ and the state feedforward of Ψ_L. The PIFF control law is shown in equations (4.5) and (4.6).

$$V_{wc} = V_L + K_x(X - X_{cmd}) \qquad (4.5)$$

$$\Psi_{wc} = K_y(Y - Y_{cmd}) + K_{yi} \int_0^t (Y - Y_{cmd})\, dt \qquad (4.6)$$

4.2   Three-Dimensional Control Laws

The three-dimensional energy tracking controller design focuses on reducing energy swings of the wing aircraft during formation maneuvers, while maintaining the formation. Now, the specific energy state of the wing aircraft (E_W) is determined by total specific energy

$$E_W = \frac{1}{2}V_W^2 + gH_W \tag{4.7}$$

where g = gravitational acceleration and H_W = wing altitude. Differentiating equation (4.7) yields

$$\dot{E}_W = V_W\dot{V}_W + g\dot{H}_W \tag{4.8}$$

The energy rate is further defined by

$$\dot{E}_W = V_W\frac{T-D}{m} \tag{4.9}$$

where T = aircraft thrust, D = aircraft drag, and m = aircraft mass. It is readily observed from equation (4.9) that cycling engine thrust levels directly affects the aircraft's energy state. Conversely, changes in the aircraft specific energy requires thrust level adjustments which decrease efficiency, as well as increase engine wear. Therefore, reducing specific energy swings reduces throttle cycling. In addition, equation (4.7) shows that the energy level of the wing aircraft is determined exclusively by velocity (true speed) and altitude. Since the velocity command input is already being utilized in the planar controller, the altitude requirement can be relaxed, and the wing aircraft altitude can be controlled to minimize the wing aircraft's specific energy swings. Thus, the complete decoupling of the altitude aircraft/autopilot states from the planer control design law allows direct control of the aircraft specific energy, without altering the planar formation hold autopilot response.

In previous designs, energy conserving techniques were used which applied control inputs in order to regulate the perturbation in the wing aircraft energy level to zero. These energy conserving techniques restrict the wing aircraft to tracking only formation heading changes. Therefore, this concept is unsuitable if the leader changes the energy level of the formation, e.g., by changing the formation's velocity and/or altitude. In order to reduce energy swings and still maintain formation when the leader changes energy level, the wing aircraft must, in fact, track the lead aircraft energy level (E_L). Hence, it is stipulated that

$$E_W = E_L \tag{4.10}$$

This can be rewritten as,

$$\frac{1}{2}V_W^2 + gH_W = \frac{1}{2}V_L^2 + gH_L \tag{4.11}$$

where H_L = lead altitude. Solving equation (4.11) for H_W yields

$$H_W = H_L + \frac{1}{2g}\left(V_L^2 - V_W^2\right) \tag{4.12}$$

The second-order aircraft/altitude-hold autopilot model, as defined by Buzogany [2], is represented as follows,

$$\ddot{H} = -\left(\frac{1}{\tau_{ha} + \tau_{hb}}\right)\dot{H} - \left(\frac{1}{\tau_{ha}\tau_{hb}}\right)H + \left(\frac{1}{\tau_{ha}\tau_{hb}}\right)H_{cmd} \tag{4.13}$$

where, for the C-130 aircraft,

$$\tau_{ha} = 0.6154s^{-1}$$

$$\tau_{hb} = 7.6923s^{-1}$$

Differentiating equation (4.12) twice yields:

$$\ddot{H}_W = \ddot{H}_L + \frac{1}{g}\left(\dot{V}_L^2 + V_L\ddot{V}_L - \dot{V}_W^2 - V_W\ddot{V}_W\right) \tag{4.14}$$

Substituting equation (4.13) into equation (4.14) and solving for the wing altitude command (H_{wc}) yields the altitude control law

$$H_{wc} = H_W + \frac{\tau_{ha}\tau_{hb}}{\tau_{ha} + \tau_{hb}}\dot{H}_W + \frac{\tau_{ha}\tau_{hb}}{g}\left(\dot{V}_L^2 + V_L\ddot{V}_L - \dot{V}_W^2 - V_W\ddot{V}_W\right) \tag{4.15}$$

Since this control law requires access to unobservable states, an alternative solution is sought which ensures that an energy tracking path is determined by the controller. Reconsidering equation (4.11) and using wing commands instead of wing states in the right-hand side, yields:

$$\frac{1}{2}V_L^2 + gH_L = \frac{1}{2}V_{wc}^2 + gH_{wc} \tag{4.16}$$

$$H_{wc} = H_L + \frac{1}{2g}\left(V_L^2 - V_{wc}^2\right) \tag{4.17}$$

This altitude control analysis is not completely rigorous due to the fact that it fails to include the system dynamics. However, this approach allows for a relatively simple controller design which is effective over a wide range of command inputs. In addition, it is interesting to note the similarity between the velocity command control [equation (4.5)] and the new altitude command control [equation (4.17)]. The altitude control design consists of a base command which tracks the energy of the leader (H_L) and an energy conserving command to minimize energy swings. Likewise, the velocity control design consists of a base command which tracks the velocity of the leader (V_L) and an x-channel command to track x-separation changes. This similarity between the control designs is an intuitively satisfying state of affairs.

4.3 Controller Summary

The new PIFF control law proposed for the formation hold autopilot is summarized as,

$$V_{wc} = V_L + K_x(X - X_{cmd}) \tag{4.18}$$

$$\Psi_{wc} = K_y(Y - Y_{cmd}) + K_{yi}\int_0^t (Y - Y_{cmd})\,dt \tag{4.19}$$

$$H_{wc} = H_L + \frac{1}{2g}(V_L^2 - V_{wc}^2) \tag{4.20}$$

The controller block diagram is shown in Figure 4.2. The formation hold autopilot uses three-dimensional maneuvering to reduce wing aircraft energy excursions during formation maneuvers.
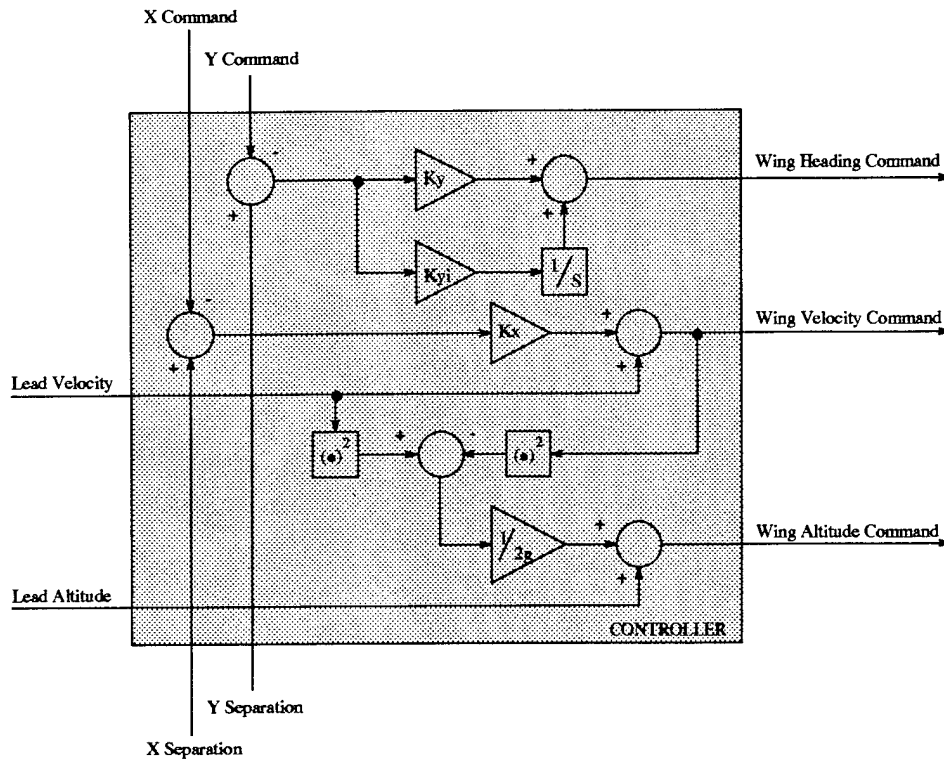
Figure 4.2   Proportional plus Integral and FeedForward (PIFF) Controller

4.4   Nonlinear

The formation flight control system is nonlinear due to two factors. First, the kinematics equations are nonlinear. Second, there are hard velocity, heading, and altitude rate/saturation limits in the aircraft/autopilot models. For illustration, the effect of imposing rate/saturation limits on wing aircraft/autopilot heading rate during a possible formation change is shown in Figure 4.3. The solid and dashed lines in Figure 4.3 represent the wing aircraft/autopilot heading rate with and without rate/saturation limits, respectively. Notice the clipping effect when rate/saturation limiting is applied. Finally, additional sources of difficulty are the commanded formation geometry and maneuver inputs which vary over a wide range. The commanded inputs are not simple linear scaled

step inputs into the control system, as would be the case if the dynamics were linear, which is indeed the case in Porter's research [15]. The difference between a 45° left turn and a 45° right turn, from a left echelon diamond formation, make the formation nonlinearities obvious. For the left hand turn, the lead aircraft encroaches on the wing aircraft by turning into the wing's flight path. For the right hand turn, the lead aircraft departs from the wing aircraft by turning away from the wing's flight path. Obviously, when the reference signals/commands are applied to a linear control system their amplitude and polarity can be simply disregarded, but this is not so in nonlinear control. Furthermore, it is readily verifiable that when the gains of a linear controller are optimized in a linear control system, the ensuing optimal gains will be independent of the amplitude and polarity of the reference signal; but this is not true when the same linear controller is used in a nonlinear control system.
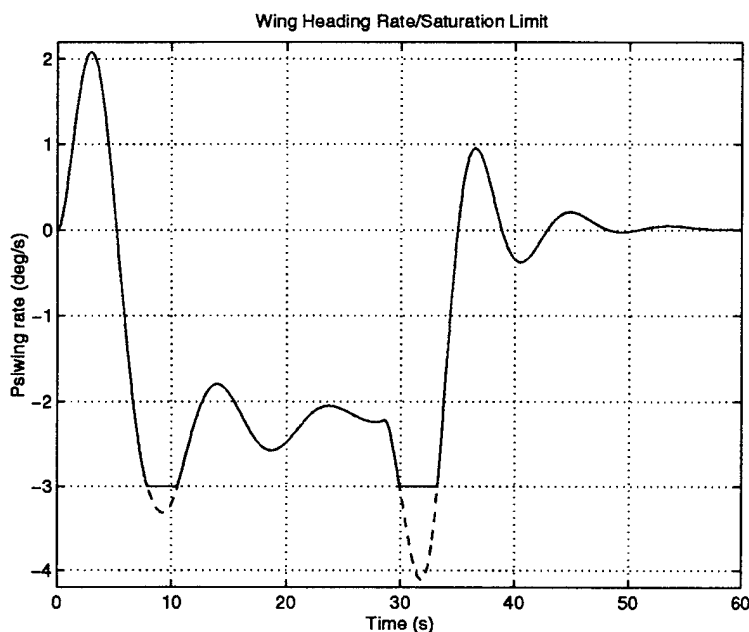
Figure 4.3   Effect of Rate/Saturation Limits

4.5 Integrator Windup

The ubiquitous presence of rate/saturation limits in the formation flight system may cause integrator windup. Windup is a problem associated with PI, or dynamic, controllers upstream of actuators which can saturate. Windup occurs when the linear PI controller saturates the system's actuators, and the integrator channel begins to integrate larger errors than otherwise occur without saturation. Once this takes place, the saturated integrator channel will not discharge its commanded control level even after the tracking error begins to decrease. This causes the total PI controller output to stay at or near the saturated value, even though the actual system might be very close to the desired value [13]. Thus, error adds up and continues to affect the integrator even after the tracking error signal decreases. This can cause very large and undesirable overshoots in observed system behavior. Hence, a serious mismatch occurs between the state of affairs as perceived during the linear design and the nonlinear reality. This can make system stability prediction invalid and render the saturating closed-loop control system unstable. For instance, the effect of integrator windup on wing aircraft/autopilot heading rate during a possible formation change is shown in Figure 4.4. The solid and dashed lines in Figure 4.4 represent the wing aircraft/autopilot heading rate with and without rate/saturation limits before the clipping effect, respectively. The integrator windup effect is also noticeable in wing aircraft/autopilot actual heading for the same maneuver, as shown in Figure 4.5. The solid and dashed lines in Figure 4.5 once again represents the wing aircraft/autopilot heading with and without rate/saturation limits, respectively.
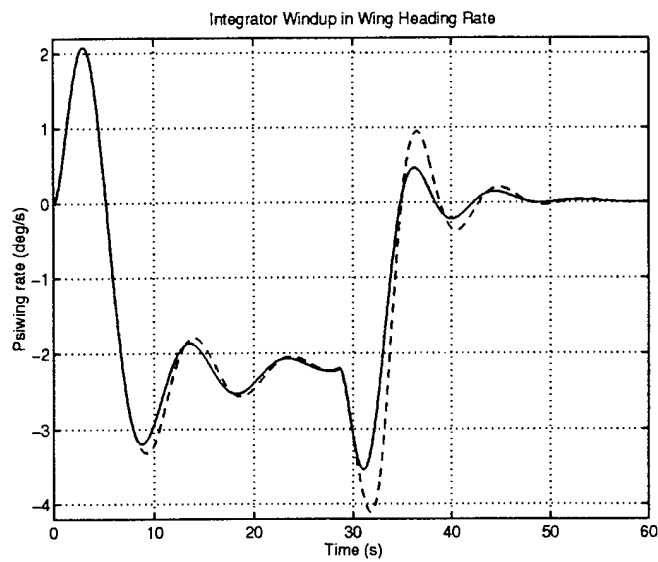
Figure 4.4   Integrator Windup in Wing Aircraft/Autopilot Heading Rate
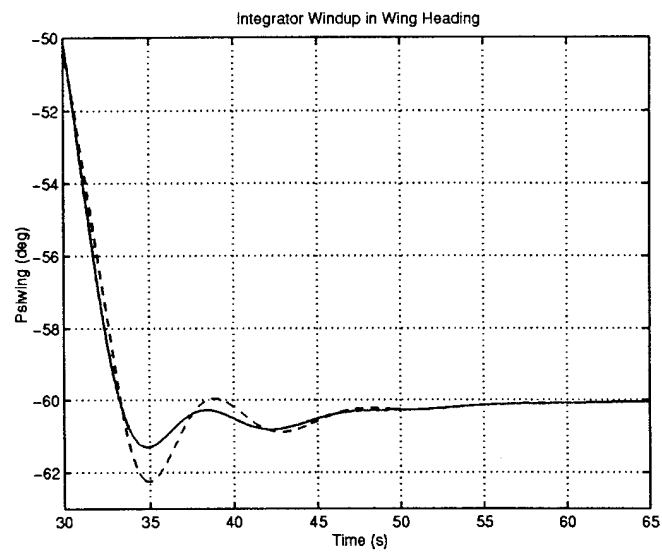
Figure 4.5   Integrator Windup in Wing Aircraft/Autopilot Heading

4.6 Optimization of Fixed Structure Controller Gains

The optimization of any controller design concerns the minimization of a utility function which represents the specifications of interest over the range for which the controller must perform. The "workable range" for a formation flight autopilot includes the following maneuvers and formation geometry changes:

- heading changes from 0 to $\pm 60°$ (right or left)

- velocity changes from 0 to $\pm 25 \frac{ft}{sec}$

- altitude changes from 0 to $\pm 200 ft$

- x-separation changes from 0 to $\pm 1500 ft$ (trail or lead)

- y-separation changes from 0 to $\pm 2000 ft$ (left or right)

The function to be minimized for the formation flight control problem consists of the tracking errors in the x- and y-separation distances and the total specific energy. A fixed structure controller is considered whose gains are to be optimized. A constrained optimization routine is selected so that the bounds on the gains are specified to be positive numbers less than ten ($0 < gains \leq 10$). The general mathematical programming problem can be stated as

$$minimizes \qquad f(\mathbf{x})$$

$$subject\ to \qquad G_i(\mathbf{x}) \leq 0, \qquad i = 1, 2, ..., m$$

where $\mathbf{x}$ is an n-dimensional vector of unknown gains, f is the objective function, and G are the constraints. The dimension of $\mathbf{x}$ is $n = 2$ for the PFF controller design and $n = 3$ for the PIFF controller design.

The constrained optimization routine which is available in MATLAB is used in this thesis, It is based on a Sequential Quadratic Programming (SQP) optimization method [6]. The SQP algorithm has proven to be highly efficient and accurate over a wide range of test problems. However, there is no way to insure that a *global* minimum is reached for a complex optimization problem [14]. MATLAB's SQP implementation consists of three main stages.

- First, at each major iteration a positive-definite quasi-Newton approximation of the Hessian matrix of the Lagrangian function is calculated.

- Second, at each major iteration a Quadratic programming (QP) problem is solved. The solution to the QP problem produces the search direction which will minimize the objective function.

- Third, a line search is conducted and a feasible optimal point is determined. Due to the quadratic nature of the objective function, there are only two choices for the length of the step in the search direction. Either the step is unity, or it is selected as close to unity as possible without violating any constraints. Feasibility is determined from the constraint boundaries.

The initial point given to the optimization should be feasible; but if it is not, a feasible point may be found by solving the QP problem [6]. It is always a good idea to have a firm starting point to verify the search direction of an optimization routine.

For the formation flight control problem, optimization is used to determine the gains for formation flight controllers. Trial and error analysis of a number of maneuvers yields a wide range of feasible guesses for the initial parameter gains. For this range of initial guesses, the optimization solution is independent of the specific initial condition used.

The saturation/rate limits on the C-130 aircraft/autopilot models are incorporated into the optimization as constraints. The rate/saturation limits act as hard limits for the operating range of aircraft models. These saturation/rate limits are specified in Table 3.2. Appendix A.2 shows the MATLAB code used to initialize the saturation/rate limits of the C-130 aircraft/autopilot models. The ramping in of the command inputs restricts the lead aircraft models from reaching the rate limits, but the wing aircraft models may reach these rate limits. Slight saturation of the wing aircraft/autopilot models is acceptable and ensures that the controller is being driven hard. However, the clipping effects on the wing aircraft's response due to imposing the saturation/rate limits is virtually unpredictable when combined with the formation flight system nonlinearities.

The cost function is based on the accrued weighted average of x-separation, y-separation, and energy fluctuations between the lead and the wing aircraft throughout a maneuver. The cost function is

$$f = \alpha \sum_{time=0}^{end} \left(\frac{|X_{cmd} - X|}{time} \right) + \beta \sum_{time=0}^{end} \left(\frac{|Y_{cmd} - Y|}{time} \right) + \delta \sum_{time=0}^{end} \left(\frac{|E_L - E_w|}{time} \right) \quad (4.21)$$

where $\alpha = 1$, $\beta = 1$, and $\delta = 32.2$. The weights for the x- and y-channels are set equal, but the energy fluctuation weighting is much higher. The energy weighting is determined by the altitude component of the energy, as shown in equation (4.7). The MATLAB code with the constrained optimization and optimization cost function are listed in Appendix A.4 and A.5, respectively.

4.7 Conclusion

The new PIFF control law proposed in this thesis uses proportional control and feedforward of V_L in the x-channel, proportional plus integral control in the y-channel, and feedforward of H_L in the altitude channel, for energy swings minimization. A constrained optimization procedure for determining the nonlinear formation flight control system's gains is selected. The rate/saturation limits are implemented as constraints; and the cost function is based on the weighted average of x-separation, y-separation, and energy fluctuations throughout the maneuvers. The results of utilizing the constrained optimization method for determining controller gains are presented in Chapters V and VI.

V. Tight *Formation*

The optimization and testing of the Proportional plus FeedForward (PFF) and the Proportional plus Integral and FeedForward (PIFF) controller designs during *tight* formations are considered in this chapter. Optimal gains for each controller are determined via constrained optimization. The constrained optimization algorithm is applied to a wide variety of formation maneuvers and geometry changes. The computer implementation of the constrained optimization technique is provided by a MATLAB routine. Comparisons of optimization costs and formation responses are made for each controller design. The PFF design, with Veth's gains which were determined via root locus analysis [23], is used as the baseline.

5.1 Formation Changes

In order to optimize controller gains which perform well over the entire operational range of a formation hold autopilot, a wide variety of formation maneuvers and geometry changes initiated from a nominal *tight* formation are considered. The nominal *tight* formation is a left diamond (echelon) formation ($\overline{X}$ = 500 ft, $\overline{Y}$ = 500 ft) at a velocity ($\overline{V}$) of 350$\frac{ft}{sec}$, an altitude ($\overline{H}$) of 5000ft, and without loss of generality, a heading ($\overline{\Psi}$) of 0°. In addition, some *tight* trail formation maneuvers ($\overline{X}$ = 500 ft, $\overline{Y}$ = 0 ft) are also investigated for completeness.

The formation maneuvers optimized are:

- 30° left turn

- 30° right turn

- 45° left turn

- 45° right turn

- 60° left turn

- 60° right turn

- altitude increase, or decrease, of 200ft (alt)

- velocity decrease of $25\frac{ft}{sec}$ (vel dn)

- velocity increase of $25\frac{ft}{sec}$ (vel up)

- 30° right turn, velocity increase of $25\frac{ft}{sec}$, and altitude decrease of $100ft$ (rvuphdn)

- 60° left, or right, turn from trail formation (trail_60)

Both left and right turns are simulated from a left diamond position, since the heading change maneuvers exhibit non-symmetric dynamics due to the obvious lack of symmetry in the formation's geometry. However, left and right turns simulated from a trail position are symmetric so heading changes of the same magnitude result in identical cost, regardless of the polarity. Altitude increases or decreases also result in identical costs due to the control law applied to the altitude channel. However, the velocity increases and decreases result in different costs due to the asymmetric non-linearity in the Mach-hold autopilot system. The relatively complex maneuver consisting of a 30° right turn, velocity increase of $25\frac{ft}{sec}$, and altitude decrease of $100ft$ (rvuphdn) gives insight about how the system responds during a three-dimensional maneuver.

The formation geometry change maneuvers optimized are:

- left diamond to trail (LD_trail)

- trail to left diamond (trail_LD)

- left diamond to right diamond (LD_RD) or right diamond to left diamond (RD_LD)

- decrease in x-separation from $1000ft$ to $500ft$ (x dec)

- increase in x-separation from $500ft$ to $1000ft$ (x inc)

- wing aircraft moves to a lead position, $500ft$ to $-500ft$ (wing_lead)

The formation geometry change maneuvers, which entail x- and y-separation increases and decreases, result in different costs due to the nonlinearities in the system dynamics. Also, the wing aircraft changing to a lead position is included for completeness.

The composite formation maneuvers and geometry changes optimized are:

- left diamond to right diamond with a 30° left turn (LD_RD_30L)

- left diamond to right diamond with a 30° right turn (LD_RD_30R)

- left diamond to right diamond with a 45° left turn (LD_RD_45L)

- left diamond to right diamond with a 45° right turn (LD_RD_45R)

- left diamond to right diamond with a 60° left turn (LD_RD_60L)

- left diamond to right diamond with a 60° right turn (LD_RD_60R)

- left diamond to right diamond, lead change, and a 30° left turn (LD_RD_ld_30L)

- left diamond to right diamond, lead change, and a 45° left turn (LD_RD_ld_45L)

- left diamond to right diamond, lead change, and a 60° left turn (LD_RD_ld_60L)

The most common of the composite maneuvers and geometry changes is the left diamond to right diamond during a left turn. This type of formation change allows the left echelon wing aircraft to save energy during turns.

Each single simulation is run for 150 seconds and the minimum and maximum step sizes of the fifth-order Runge-Kutta integration scheme are set equal to avoid inconsistency in the optimization routine. An example of the MATLAB code used to optimize the above maneuvers is listed in Appendix A.3.1.

In addition to single formation changes, formation maneuvers and geometry changes are combined into extended 300 second duration dual maneuvers that return the aircraft to the original state. These dual formation changes address the control system nonlinearities. For instance, the 45° left turn is paired with the 45° right turn to conduct a more complex maneuver. The objective is to find optimal controller gains which are independent of the turn maneuver's polarity. The maneuvers are input from a predetermined matrix of time, position, and velocity which starts ramping in the first maneuver, or geometry change, at $time = 0$ seconds and the second maneuver at $time = 150$ seconds, after the transients from the first maneuver have died out. The order of the first and second maneuver, or geometry change, is interchanged for a more complete look at the nonlinearities of the

dual maneuvers. See Appendix A.3.2 for an example of the MATLAB code used for dual formation maneuvers. Controllers are optimized for dual formation changes involving right and left heading changes, altitude increases and decreases, velocity increases and decreases, y-separation distance increases and decreases, and x-separation distance increases and decreases. However, the composite formation maneuvers which entail formation geometry changes and heading change maneuvers cannot be combined into dual maneuvers which return to the original state without the addition of extra heading or geometry changes. Hence, the composite formation maneuvers were not combined in order to make dual formation maneuvers and geometry changes. The optimization of dual formation change maneuvers result in narrowing the range of gains for a robust optimal controller.

5.2 PFF Design Baseline

The baseline controller used in this thesis is the Proportional plus FeedForward controller (PFF) design with Veth's experimentally determined gains. These gains are listed in Table 5.1.

Parameter	Value
K_{xp}	0.0250
K_{yp}	0.0187

Table 5.1   Veth's Gains For PFF

The controller gains, K_{xp} and K_{yp}, were determined by Veth, using successive loop closures and root-locus analysis to determine gains which give the desired response with the least amount of overshoot ($\zeta \cong 1$) [23]. This ensures that maneuvers are accomplished in "minimum" time without excessive excitation of the aircraft. Due to the rate limit nonlinearities in the system, it is inherently beneficial to choose relatively low controller gains. This helps to avoid forcing the system against its rate limits which could result in uncontrollability.

Furthermore, the baseline's PFF controller gains are designed specifically about the nominal *tight* left diamond formation ($\overline{X} = 500$ ft, $\overline{Y} = 500$ ft) at a nominal velocity ($\overline{V}$) of $350\frac{ft}{sec}$, nominal altitude ($\overline{H}$) of $5000 ft$, and a nominal heading ($\overline{\Psi}$) of $0°$.

The baseline results for single formation changes are listed in Table 5.2, and the baselines results for dual formation changes are listed in Table 5.3. The dual formation changes are listed according to the first maneuver, or geometry change, executed. The second, *opposite*, formation change maneuver is not listed but is initiated at time = 150 seconds. The achieved optimal costs, in Table 5.2 and 5.3, are listed in units of *feet* for the x-separation, y-separation, energy fluctuation, and total [see Chapter IV, equation (4.21)]. The Saturation (Sat) results are listed as "L=NL" if the rate limits are not encountered during the maneuver. Otherwise, saturation can occur and the rate limits are either not imposed (L) or imposed (NL) during the simulation. The imposing of rate limits on a saturating system results in clipping of the rate signal which, in turn, affects the optimization costs.

For dual maneuvers, the cost for an altitude increase and then a decrease is identical to the cost for an altitude decrease and then an increase. Similarly, for two dual formation geometry changes, the left diamond to right diamond and then a right diamond to left diamond formation maneuver yields identical costs to the right diamond to left diamond and then a left diamond to right diamond formation maneuver. In order to avoid redundancy, these duplicate formation change costs are not included in Table 5.3. As expected, the differences between the costs of complementary dual formation changes are small.

The PFF controller design is fairly robust over a wide variety of formation maneuvers and geometry changes. The aircraft/autopilot model rate limits are not encountered for any of the formation changes in the operational range.

Tight Formation Single Maneuver Results					
Maneuver	X Cost	Y Cost	Energy Cost	Total Cost	Saturation
30° left	50.89	27.37	26.49	104.75	L=NL
30° right	82.04	19.57	41.92	143.53	L=NL
45° left	65.49	42.61	33.50	141.59	L=NL
45° right	125.86	26.03	62.67	214.56	L=NL
60° left	77.23	58.24	38.29	173.77	L=NL
60° right	167.43	30.70	80.64	278.77	L=NL
alt	0	0	356.56	356.56	L=NL
vel dn	66.00	0	570.16	636.16	L=NL
vel up	65.90	0	626.78	692.68	L=NL
rvuphdn	121.30	18.87	233.16	373.32	L=NL
trail_60	44.68	44.23	21.63	110.54	L=NL
LD_trail	3.77	53.05	2.94	59.75	L=NL
trail_LD	5.64	53.08	3.27	61.99	L=NL
LD_RD	10.17	153.73	4.88	168.77	L=NL
x dec	149.59	0	68.64	218.24	L=NL
x inc	166.13	0	62.86	228.99	L=NL
wing_lead	332.26	0	134.45	466.71	L=NL
LD_RD_30L	24.23	127.57	15.02	166.81	L=NL
LD_RD_30R	72.89	173.54	32.62	279.06	L=NL
LD_RD_45L	14.38	114.47	12.50	141.35	L=NL
LD_RD_45R	87.53	181.68	39.40	308.61	L=NL
LD_RD_60L	40.52	114.46	25.73	180.71	L=NL
LD_RD_60R	86.68	189.77	40.13	316.58	L=NL
LD_RD_ld_30L	309.00	125.59	118.83	553.42	L=NL
LD_RD_ld_45L	324.50	110.42	125.99	560.91	L=NL
LD_RD_ld_60L	359.83	117.82	138.78	616.43	L=NL

Table 5.2   Costs Due to Single Maneuvers of the *Tight* Formation Using Veth's Gains (Baseline)

Tight Formation Dual Maneuver Results					
Maneuver	X Cost	Y Cost	Energy Cost	Total Cost	Saturation
30° left	66.41	23.49	34.29	124.19	L=NL
30° right	66.36	23.45	34.37	124.18	L=NL
45° left	95.61	34.34	48.23	178.19	L=NL
45° right	95.51	34.27	48.51	178.29	L=NL
60° left	122.26	44.51	59.69	226.46	L=NL
60° right	122.10	44.39	60.24	226.73	L=NL
alt	0	0	356.62	356.62	L=NL
vel dn	65.74	0	577.71	643.45	L=NL
vel up	65.68	0	620.57	686.26	L=NL
LD_trail	4.71	29.18	3.10	36.99	L=NL
trail_LD	11.40	29.18	8.47	49.06	L=NL
LD_RD	10.22	58.36	4.87	73.45	L=NL
x dec	132.59	0	65.92	198.51	L=NL
x inc	132.53	0	65.92	198.45	L=NL

Table 5.3 Costs Due to Dual Maneuvers of the *Tight* Formation Using Veth's Gains (Baseline)

5.3 PFF Design Optimization

This section displays the performance of the Proportional plus FeedForward controller (PFF) design with optimal gains, K_x^* and K_y^*. The optimal gains are determined using MATLAB constrained optimization on all of the formation maneuvers and geometry changes, which represent the formation flight autopilot's operational range. Each optimization of a specific maneuver yields a set of *optimal* gains, K_x and K_y, for that formation flight condition. The gains of each channel are averaged over the entire nonlinear operating range in order to get a feel for what the overall optimal formation flight controller's gains should be. Next, the averaged optimal gains are manually refined, still taking the aircraft/autopilot saturation limits and costs due to formation change maneuvers into account, to determine the optimal formation flight controller's gains, K_x^* and K_y^*. These optimal gains are listed in Table 5.4. The optimal gains are larger than the baseline gains and tend to drive the formation flight controller harder.

Parameter	Value
K_x^*	0.038
K_y^*	0.034

Table 5.4   Optimal Gains For PFF

The optimal gains, unlike Veth's experimentally determined gains, are not designed to give the response with the least amount of overshoot ($\zeta \cong 1$). So, although slightly higher energy fluctuations may occur, the optimal gains usually yield quicker settling times and less x- and y-separation variation. As a result, the optimal PFF controller gains result in lower cost for almost all the tested formation changes. The altitude maneuver costs remain the same, since the altitude channel controller is unchanged.

The results for single formation changes are listed in Table 5.5, and the results for dual formation changes are listed in Table 5.6. The same cost and saturation classifications, as in the previous section, are used so that comparisons can be made with the PFF baseline results. The comparison of total results (Compare) are qualitatively evaluated and listed as "better", "worse", or "close"; where "better" means that the total cost of the formation change is less than the baseline's, "worse" means that the total cost of the formation

change is more than the baseline's, and "close" means that the total costs being compared are within $1 ft$.

In conclusion, the optimal PFF controller design remains fairly robust over a wide variety of formation maneuvers and geometry changes. The aircraft/autopilot model rate limits are still not encountered for any of the formation changes in the performance range.

Tight Formation Single Maneuver Results						
Maneuver	X Cost	Y Cost	Energy Cost	Total Cost	Sat	Compare
30° left	37.92	15.91	39.43	93.26	L=NL	better
30° right	53.68	10.91	55.65	120.25	L=NL	better
45° left	52.79	24.59	53.26	130.63	L=NL	better
45° right	80.61	14.77	80.98	176.36	L=NL	better
60° left	67.16	33.54	64.83	165.53	L=NL	better
60° right	106.15	17.93	102.24	226.33	L=NL	better
alt	0	0	356.56	356.56	L=NL	same
vel dn	44.53	0	571.17	615.71	L=NL	better
vel up	44.50	0	629.37	673.87	L=NL	better
rvuphdn	79.54	10.56	241.83	331.94	L=NL	better
trail_60	19.45	25.22	18.95	63.62	L=NL	better
LD_trail	3.71	40.77	4.98	49.45	L=NL	better
trail_LD	6.01	40.83	6.80	53.64	L=NL	better
LD_RD	8.67	128.27	8.90	145.84	L=NL	better
x dec	107.69	0	96.86	204.56	L=NL	better
x inc	124.19	0	86.56	210.75	L=NL	better
wing_lead	248.38	0	187.28	435.66	L=NL	better
LD_RD_30L	14.91	114.19	18.86	147.96	L=NL	better
LD_RD_30R	41.98	139.10	36.68	217.76	L=NL	better
LD_RD_45L	14.30	106.81	18.71	139.82	L=NL	better
LD_RD_45R	43.81	144.24	39.03	227.08	L=NL	better
LD_RD_60L	34.12	106.43	39.34	179.89	L=NL	close
LD_RD_60R	34.65	149.57	38.84	223.05	L=NL	better
LD_RD_ld_30L	237.14	115.36	169.61	522.12	L=NL	better
LD_RD_ld_45L	248.53	104.52	180.48	533.54	L=NL	better
LD_RD_ld_60L	272.88	109.16	183.19	565.23	L=NL	better

Table 5.5   Costs Due to Single Maneuvers of the *Tight* Formation Using Optimal Gains (PFF)

Tight Formation Dual Maneuver Results						
Maneuver	X Cost	Y Cost	Energy Cost	Total Cost	Sat	Compare
30° left	45.81	13.41	47.54	106.76	L=NL	better
30° right	45.81	13.41	47.53	106.76	L=NL	better
45° left	66.71	19.68	67.10	153.50	L=NL	better
45° right	66.72	19.68	67.09	153.49	L=NL	better
60° left	86.68	25.74	83.50	195.92	L=NL	better
60° right	86.70	25.74	83.46	195.90	L=NL	better
alt	0	0	356.62	356.62	L=NL	same
vel dn	44.56	0	578.87	623.43	L=NL	better
vel up	44.57	0	621.79	666.36	L=NL	better
LD_trail	4.86	16.92	5.89	27.67	L=NL	better
trail_LD	12.35	16.92	15.83	45.09	L=NL	better
LD_RD	8.67	32.90	8.91	50.48	L=NL	better
x dec	90.88	0	91.67	182.55	L=NL	better
x inc	90.88	0	91.66	182.54	L=NL	better

Table 5.6   Costs Due to Dual Maneuvers of the *Tight* Formation Using Optimal Gains (PFF)

5.4 PIFF Design Optimization

This section displays the performance of the PIFF controller with optimized gains. The PIFF controller entails proportional control with direct disturbance feedforward of the lead aircraft/autopilot velocity (v_L) signal in the x-channel, and proportional plus integral control in the y-channel. The respective optimal gains, K_x^*, K_y^*, and K_{yi}^*, are listed in Table 5.7. These optimal gains for the PIFF controller are determined in the same manner as for the PFF controller, see Section 5.3. The optimal x-channel PIFF gain is the same as in the PFF optimization since no changes occur in the x-channel.

Parameter	Value
K_x^*	0.038
K_y^*	0.18
K_{yi}^*	0.02

Table 5.7   Optimal Gains For PIFF

The results for single formation changes are listed in Table 5.8, and the results for dual formation changes are listed in Table 5.9. The same cost and saturation classifications, as in the previous two sections, are used so that comparisons can be made with both the PFF baseline and PFF optimal gain results. The comparison of total results, under the "Compare" heading, are listed as two separate "better", "worse", or "close" comparisons. The first column shows the optimized PIFF controller comparison with the PFF baseline controller, and the second column shows the optimal PIFF controller comparison with the optimized PFF controller.

The optimized PIFF controller is slightly less robust than the PFF controller. This is evident due to the fact that the PIFF controller reaches the saturation limits during left diamond to right diamond geometry changes with left turns. Additionally, the left diamond to right diamond with a lead change and left turn maneuver was outside the performance range of the PIFF controller. The amplitudes of the rate limits caused the system to go unstable due to nonlinearities. However for all other formation changes considered, the PIFF performs very well. The PIFF controller out performs the optimal PFF controller except for formation changes involving relatively large left turns. The only single formation change for which the optimal PIFF performs *worse* than the PFF

baseline is the left diamond to right diamond with a 60° left turn (LD_RD_60L). The PIFF controller design shows the most improvement, over the PFF design, in heading changes from the trail formation. This is expected due to the replacement of Ψ_L information with integral action in the y-channel. As expected, the altitude maneuver cost still remains the same, since the altitude channel control remains unaltered.

In conclusion, the optimized PIFF formation flight controller design is able to perform well despite using less feedforward information than the PFF formation flight controller.

Tight Formation Single Maneuver Results					
Maneuver	X Cost	Y Cost	Energy Cost	Total Cost	Sat	Compare
30° left	41.96	10.00	42.14	94.10	L=NL	better/close
30° right	51.75	10.00	53.22	114.96	L=NL	better/better
45° left	60.86	15.00	59.29	135.14	L=NL	better/worse
45° right	78.38	15.00	78.22	171.59	L=NL	better/better
60° left	79.31	20.05	74.14	173.50	L=NL	close/worse
60° right	104.81	20.00	100.48	225.29	L=NL	better/better
alt	0	0	356.56	356.56	L=NL	same/same
vel dn	44.53	0	571.17	615.71	L=NL	better/same
vel up	44.50	0	629.87	673.87	L=NL	better/same
rvuphdn	77.69	10.00	240.10	327.79	L=NL	better/better
trail_60	13.09	20.00	12.65	45.74	L=NL	better/better
LD_trail	5.19	27.60	6.11	38.91	L=NL	better/better
trail_LD	8.04	27.63	9.11	44.78	L=NL	better/better
LD_RD	10.65	99.25	11.37	121.27	L=NL	better/better
x dec	107.69	0	96.86	204.56	L=NL	better/same
x inc	124.19	0	86.56	210.75	L=NL	better/same
wing_lead	248.38	0	187.28	435.66	L=NL	better/same
LD_RD_30L	11.55	91.15	14.14	116.84	L	better/better
	11.55	91.15	14.13	116.83	NL	
LD_RD_30R	27.32	107.54	22.94	157.79	L=NL	better/better
LD_RD_45L	21.74	89.62	24.45	135.81	L	better/better
	21.74	89.62	24.44	135.80	NL	
LD_RD_45R	20.78	111.03	21.24	153.05	L=NL	better/better
LD_RD_60L	46.69	93.56	50.82	191.07	L	worse/worse
	46.86	93.55	50.99	191.41	NL	
LD_RD_60R	22.29	115.37	28.26	165.92	L=NL	better/better

Table 5.8   Costs Due to Single Maneuvers of the *Tight* Formation Using Optimal Gains (PIFF)

Tight Formation Dual Maneuver Results						
Maneuver	X Cost	Y Cost	Energy Cost	Total Cost	Sat	Compare
30° left	46.86	10.00	47.68	104.53	L=NL	better/better
30° right	46.86	10.00	47.67	104.54	L=NL	better/better
45° left	69.63	15.00	68.73	153.36	L=NL	better/close
45° right	69.64	15.00	68.73	153.37	L=NL	better/close
60° left	92.10	20.03	87.26	199.38	L=NL	better/worse
60° right	92.11	20.03	87.24	199.38	L=NL	better/worse
alt	0	0	356.62	356.62	L=NL	same/same
vel dn	44.56	0	578.87	623.43	L=NL	better/same
vel up	44.57	0	621.79	666.36	L=NL	better/same
LD_trail	6.62	3.90	7.61	18.13	L=NL	better/better
trail_LD	13.99	3.92	18.60	36.51	L=NL	better/better
LD_RD	10.64	4.00	11.38	26.02	L=NL	better/better
x dec	90.88	0	91.67	182.55	L=NL	better/same
x inc	90.88	0	91.66	182.54	L=NL	better/same

Table 5.9   Costs Due to Dual Maneuvers of the *Tight* Formation Using Optimal Gains (PIFF)

5.5 Formation Changes/Maneuvers Optimization

Additional insight is gained by comparing nonlinear simulation responses during *tight* formations for the PFF baseline, optimized PFF, and optimized PIFF controllers. For selected formation changes, the wing aircraft/autopilot responses, wing aircraft/autopilot rates, and lead aircraft/autopilot responses are plotted. Lissajous figures, that show the variation in both x and y-separation distances during formation maneuvers, are also included. For all nonlinear simulation responses, the following legend is used:

PFF (Baseline):   "___"

PFF (Optimal):   "_ _ _"

PIFF (Optimal):   ". . ."

The units for each formation change response plot remains consistent; where heading change angles are in units of *degrees* (*deg*), altitude and separation distances are in units of *feet* (*ft*), and velocities and rates are in units of *feet per second* (*fps*). The lead aircraft/autopilot is not effected by changes in the formation autopilot residing on the wing aircraft, so only one lead aircraft/autopilot response appears in each nonlinear simulations. For the wing aircraft/autopilot rate, the plotted data is sampled before the limits are imposed to show how heavy into saturation the rates would go if clipping does not occur.

5.5.1 Formation Maneuvers. Six different *tight* formation maneuvers are presented, including left and right heading changes, a velocity increase, an altitude increase, a heading change from trail, and a 3-D maneuver. The responses due to a 45° left turn maneuver are displayed in Figures (5.1) - (5.4).

Figure 5.1 Wing Aircraft Responses for a 45° Left Turn (45° left) of the *Tight* Formation
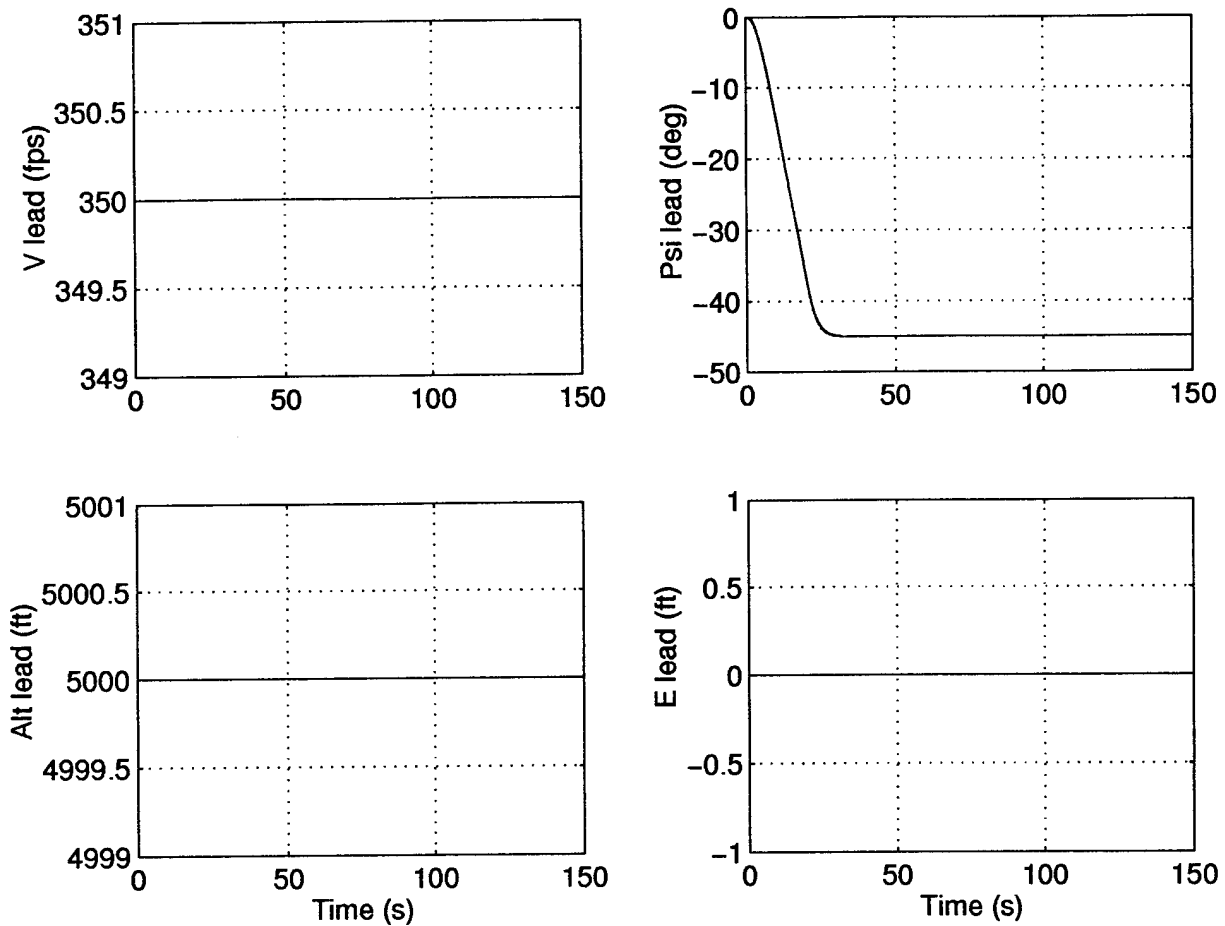
Figure 5.2   Lead Aircraft Responses for a 45° Left Turn (45° left) of the *Tight* Formation
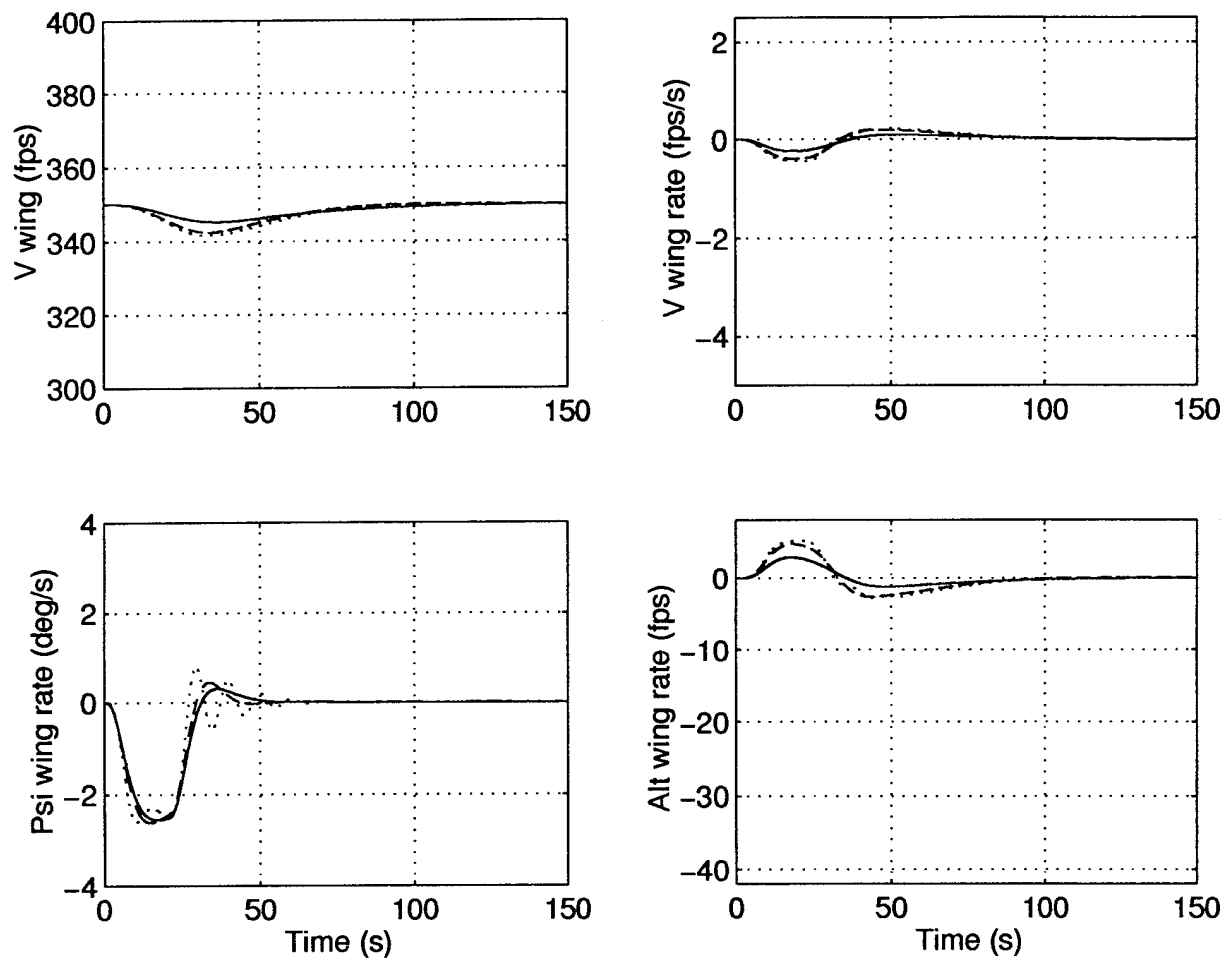
Figure 5.3 Rates of Wing Aircraft Responses for a 45° Left Turn (45° left) of the *Tight* Formation
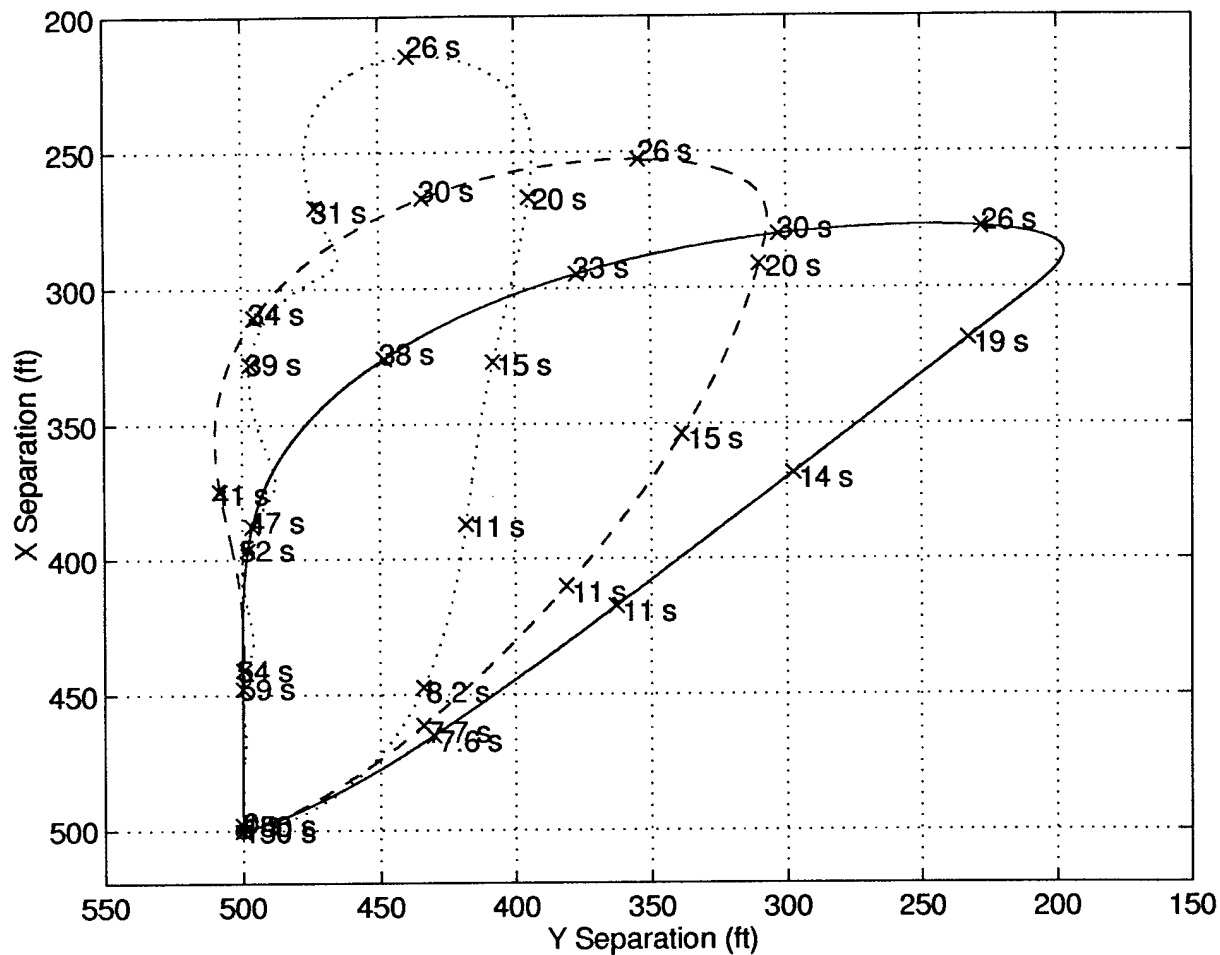
Figure 5.4 Lissajous Plots of Wing Aircraft Responses for a 45° Left Turn (45° left) of the *Tight* Formation

The responses due to a 45° right turn maneuver are displayed in Figures (5.5) - (5.8).

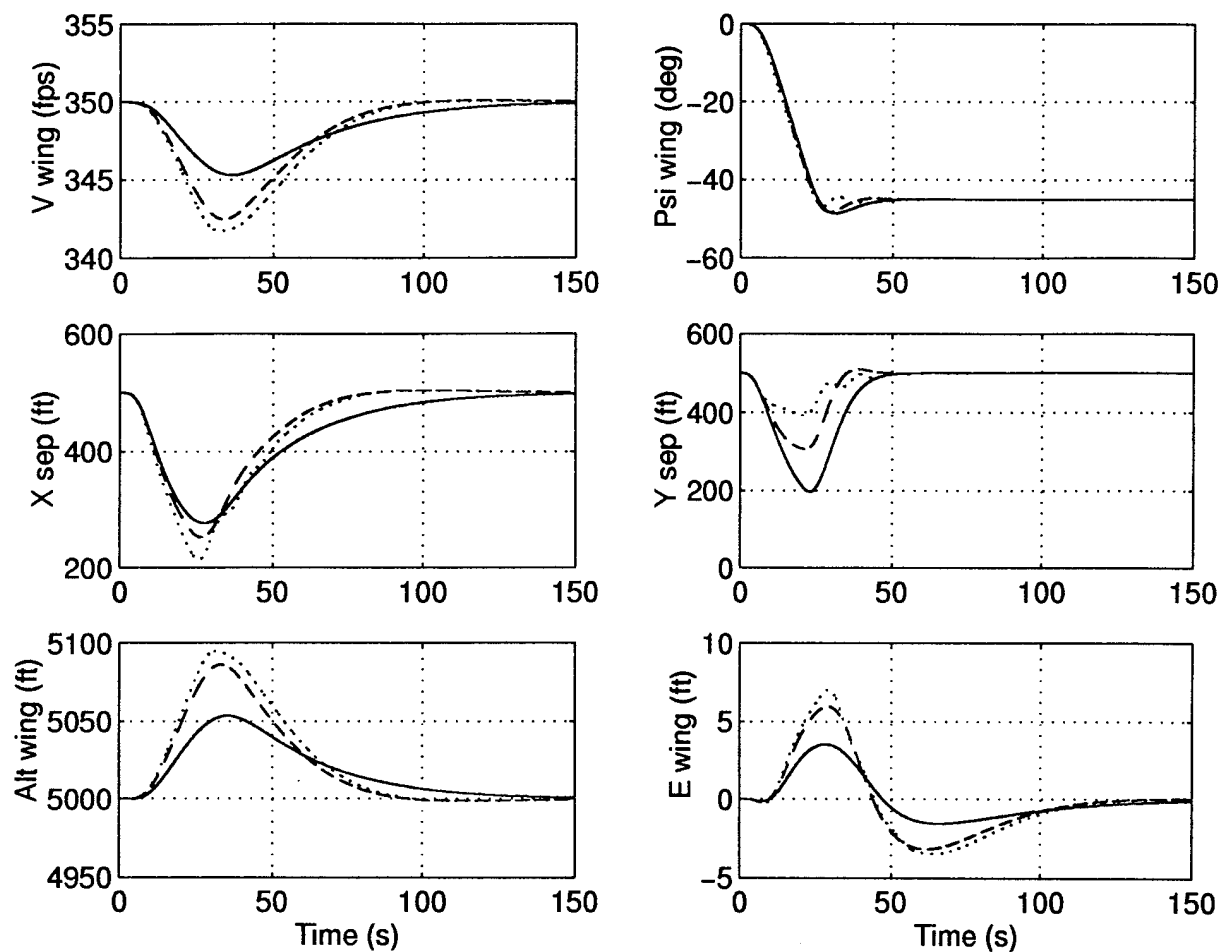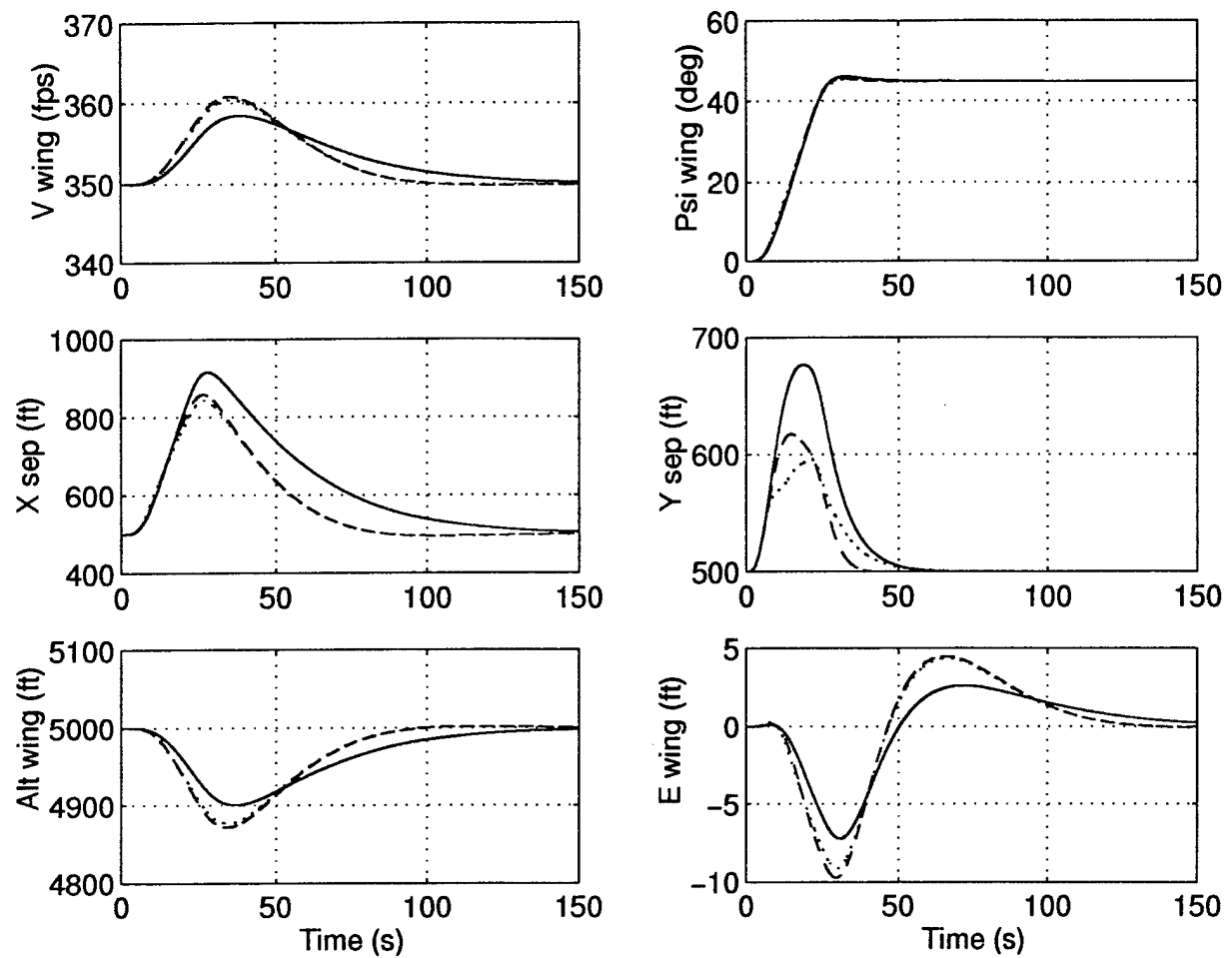Figure 5.5   Wing Aircraft Responses for a 45° Right Turn (45° right) of the *Tight* Formation
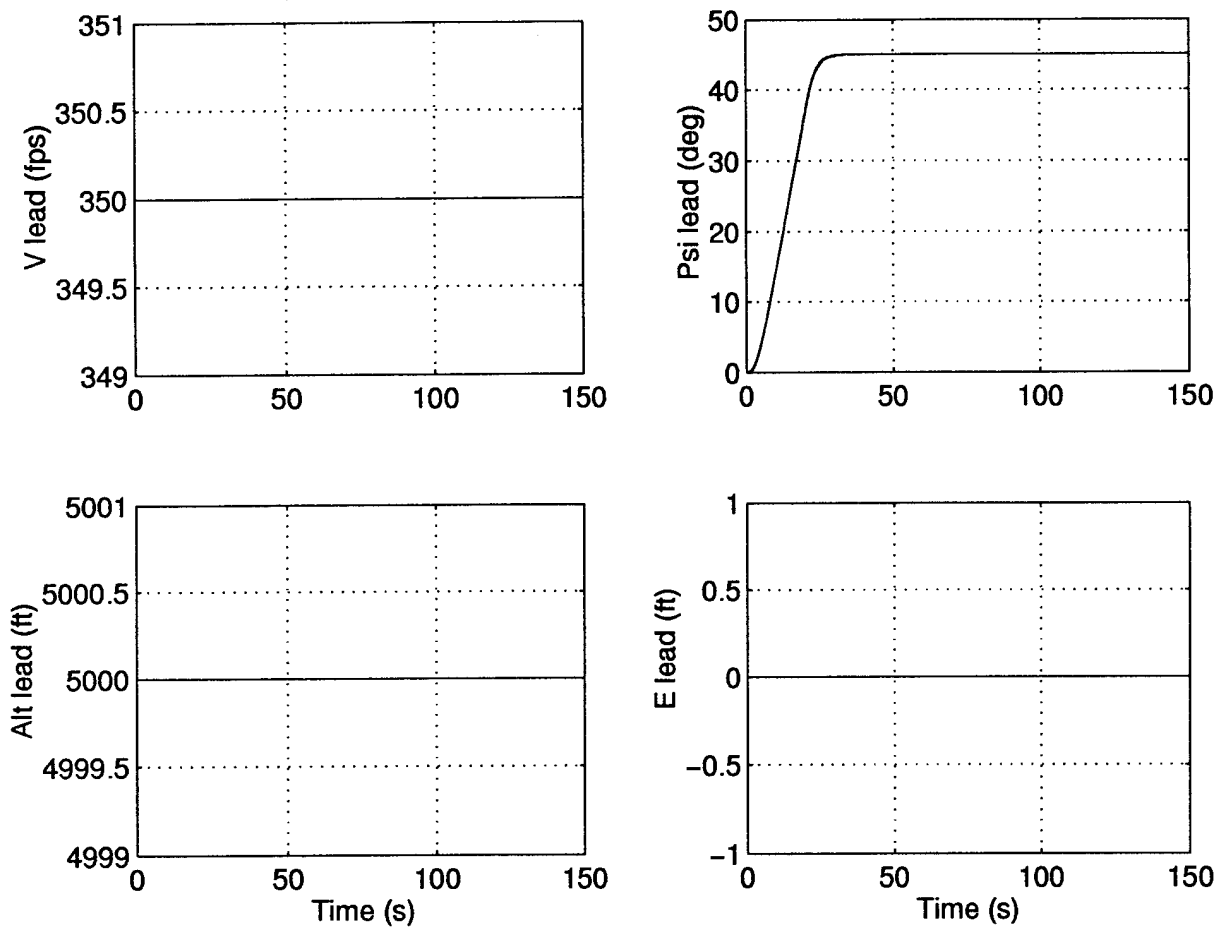
Figure 5.6   Lead Aircraft Responses for a 45° Right Turn (45° right) of the *Tight* Formation
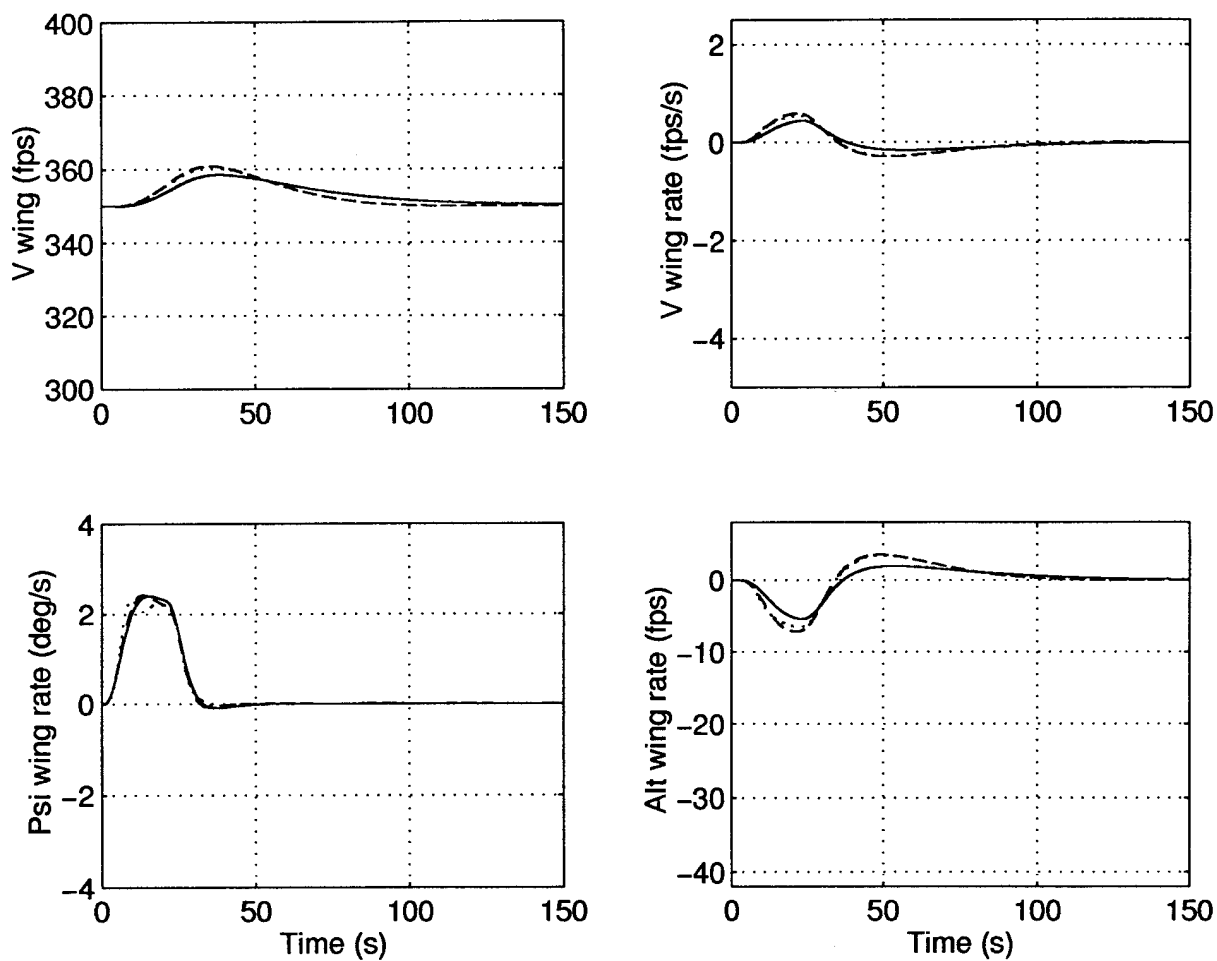
Figure 5.7   Rates of Wing Aircraft Responses for a 45° Right Turn (45° right) of the *Tight* Formation
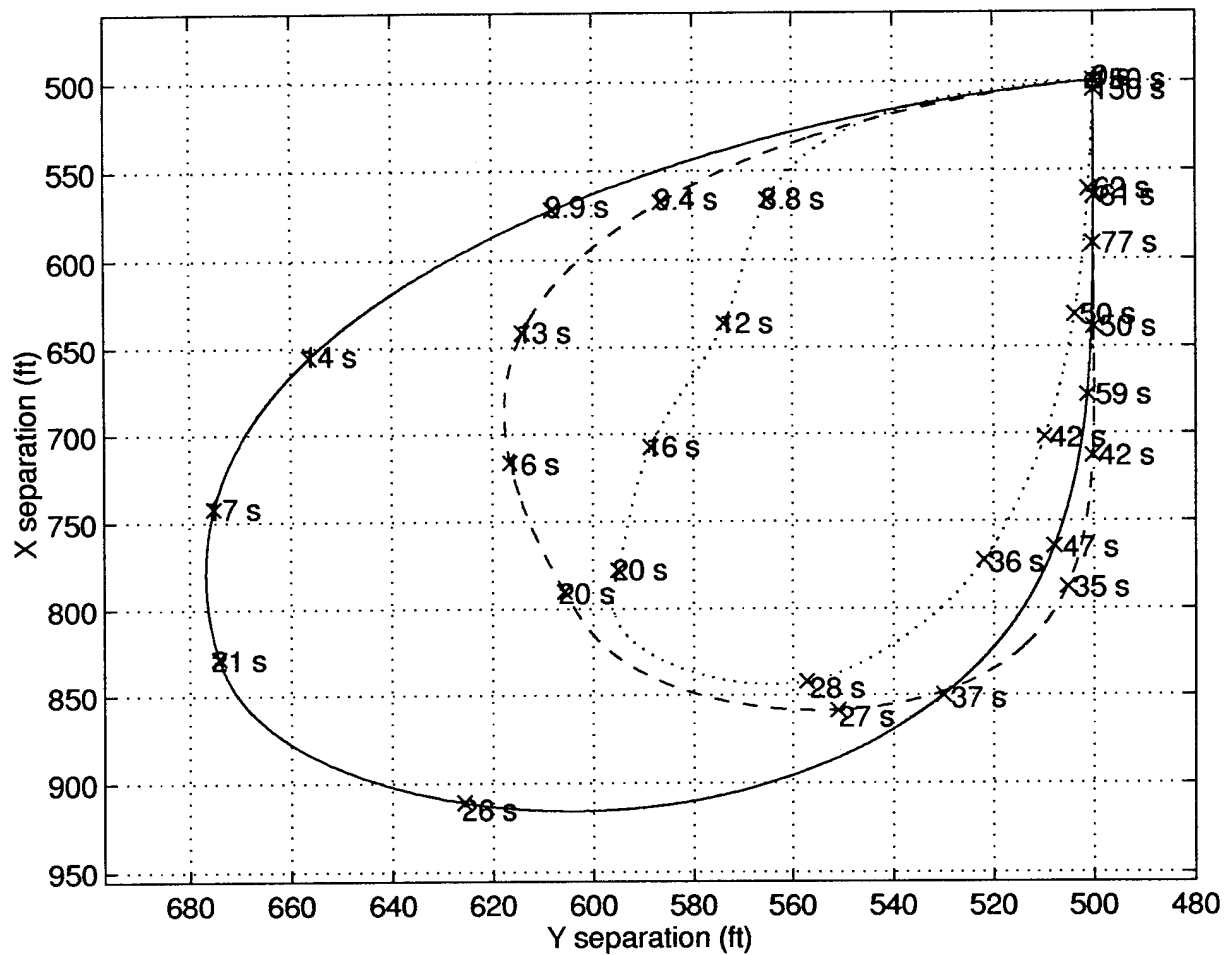
Figure 5.8   Lissajous Plots of Wing Aircraft Responses for a 45° Right Turn (45° right) of the *Tight* Formation

The responses due to a formation velocity increase of $25\frac{ft}{sec}$ (vel up) maneuver are displayed in Figures (5.9) - (5.11). The optimized PFF and PIFF formation flight controller responses coincide, since the x-channel characteristics of the two controllers are identical.
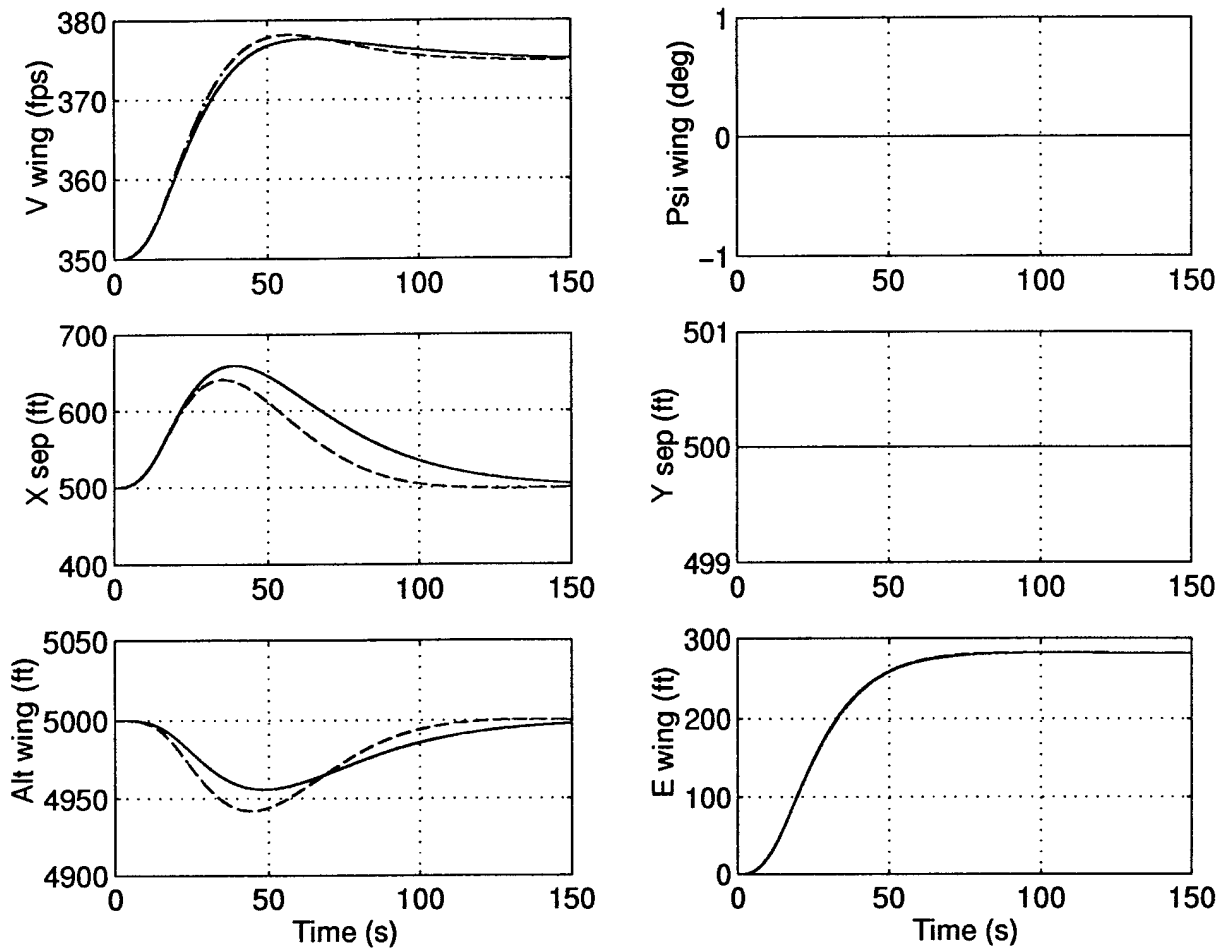
Figure 5.9   Wing Aircraft Responses for a $25\frac{ft}{sec}$ Velocity Increase (vel up) of the *Tight* Formation
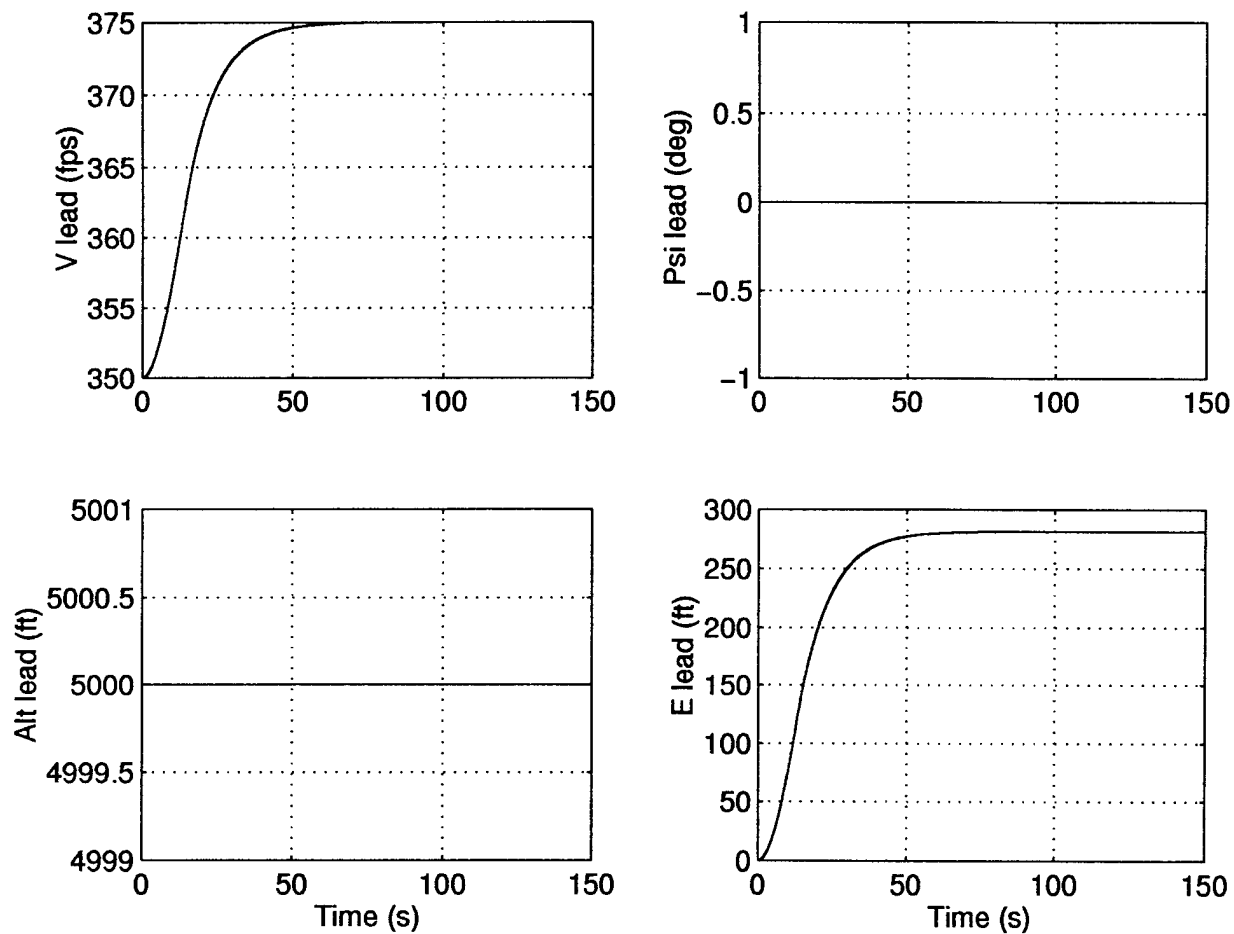
Figure 5.10   Lead Aircraft Responses for a $25\frac{ft}{sec}$ Velocity Increase (vel up) of the *Tight* Formation
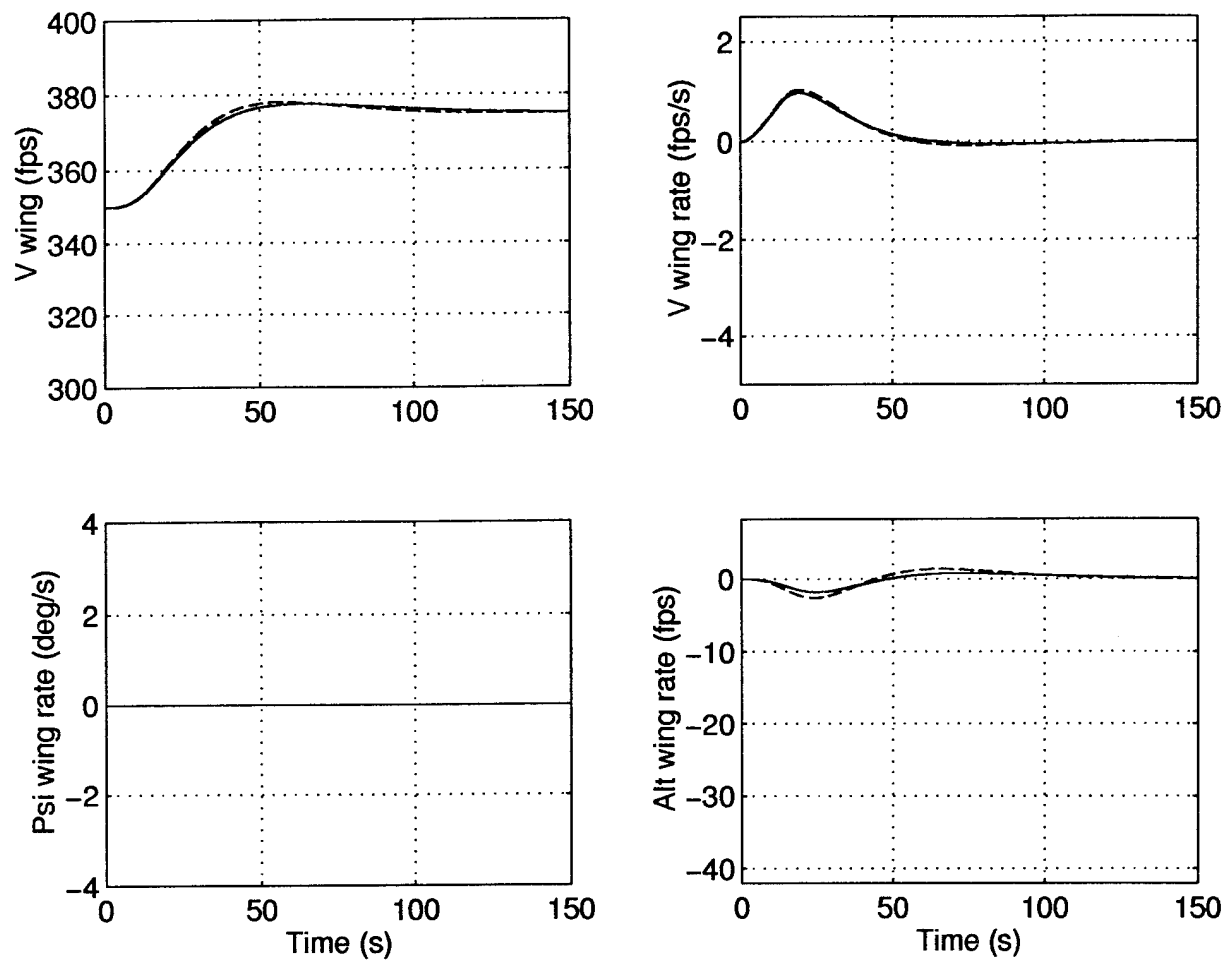
Figure 5.11   Rates of Wing Aircraft Responses for a $25\frac{ft}{sec}$ Velocity Increase (vel up) of the *Tight* Formation

The responses due to a altitude increase maneuver of 200ft (alt) are displayed in Figures (5.12) - (5.14). The optimized PFF and PIFF formation flight controller responses coincide, since the x-channel characteristics of the two controllers are identical.
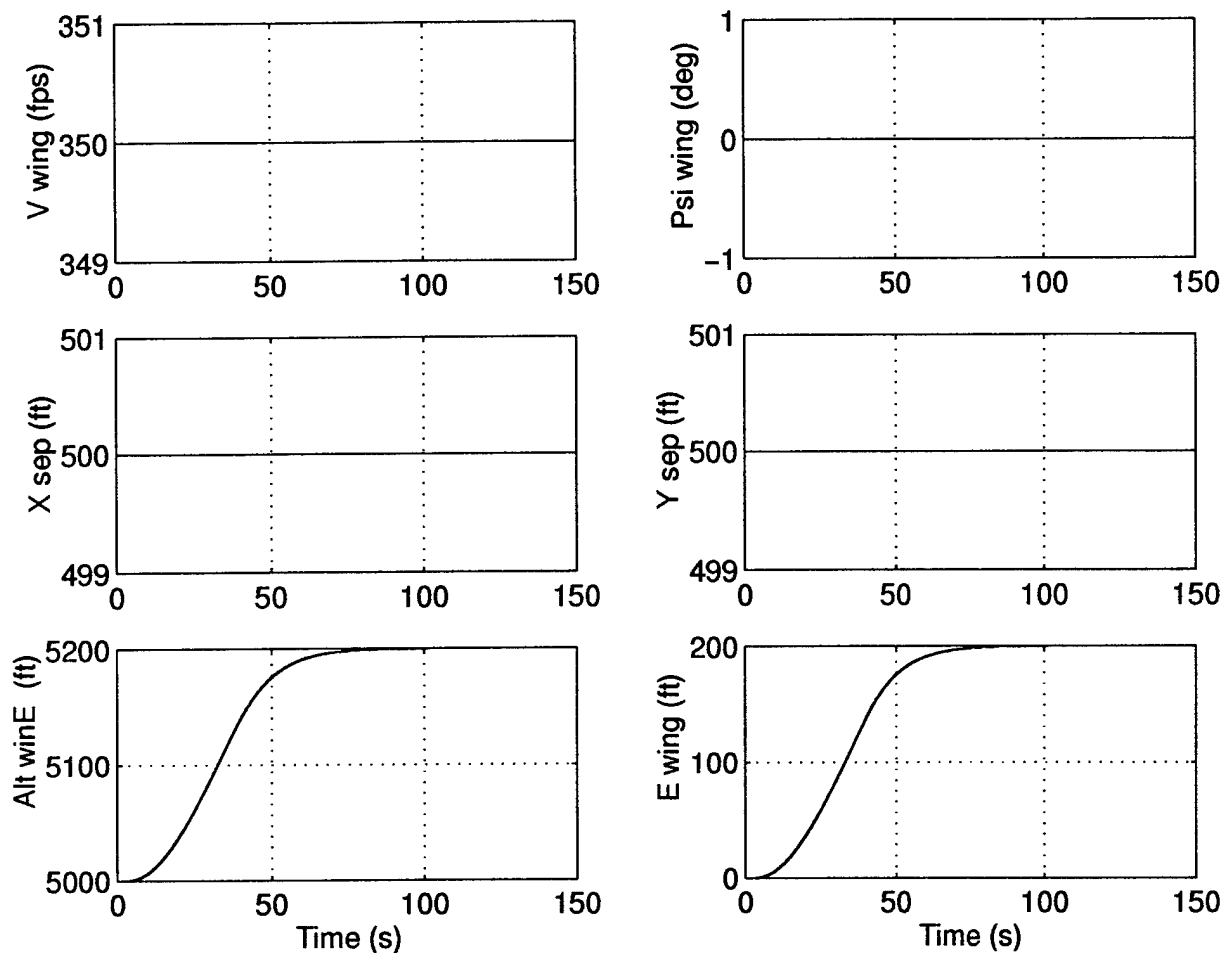
Figure 5.12   Wing Aircraft Responses for a 200ft Altitude Increase (alt) of the *Tight* Formation
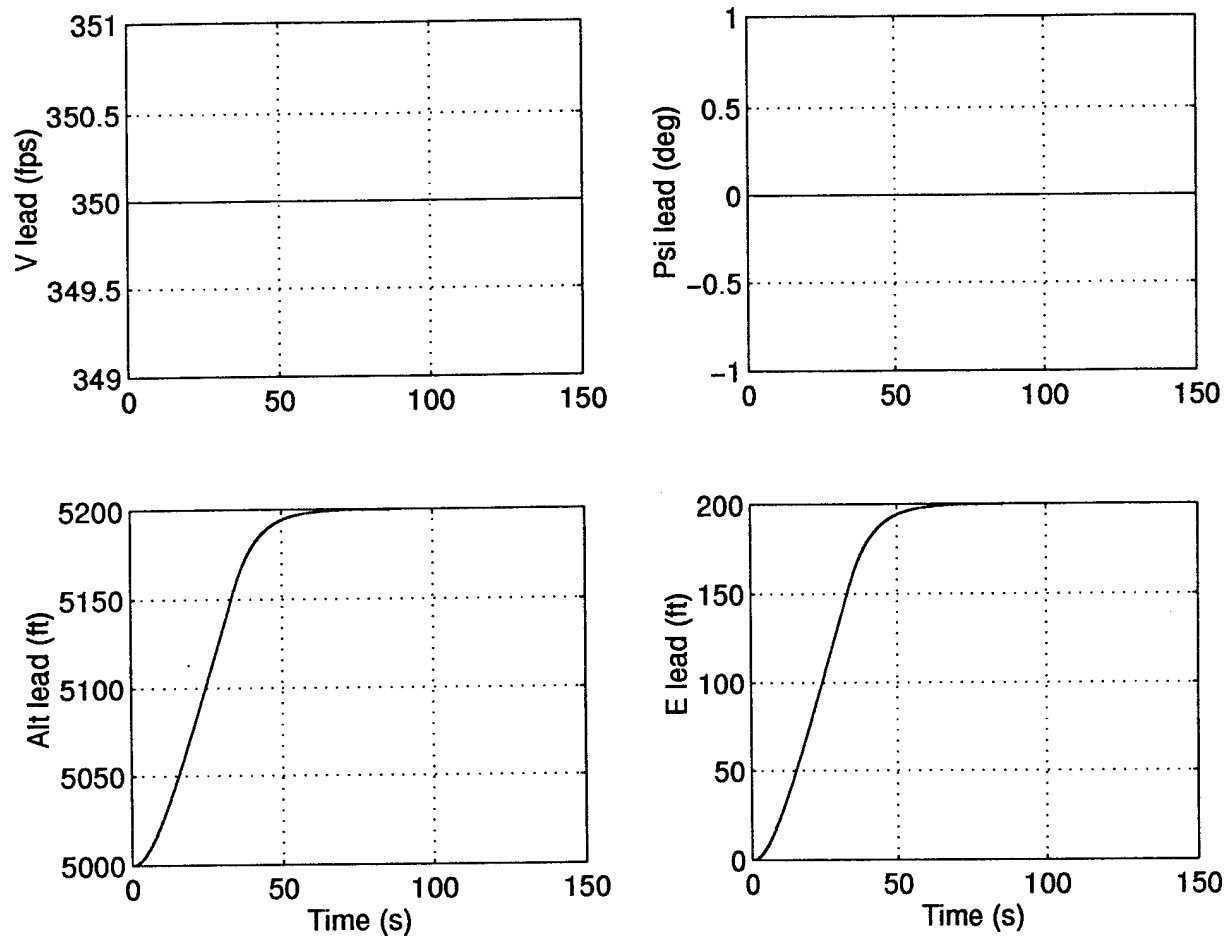
Figure 5.13   Lead Aircraft Responses for a 200*ft* Altitude Increase (alt) of the *Tight* Formation
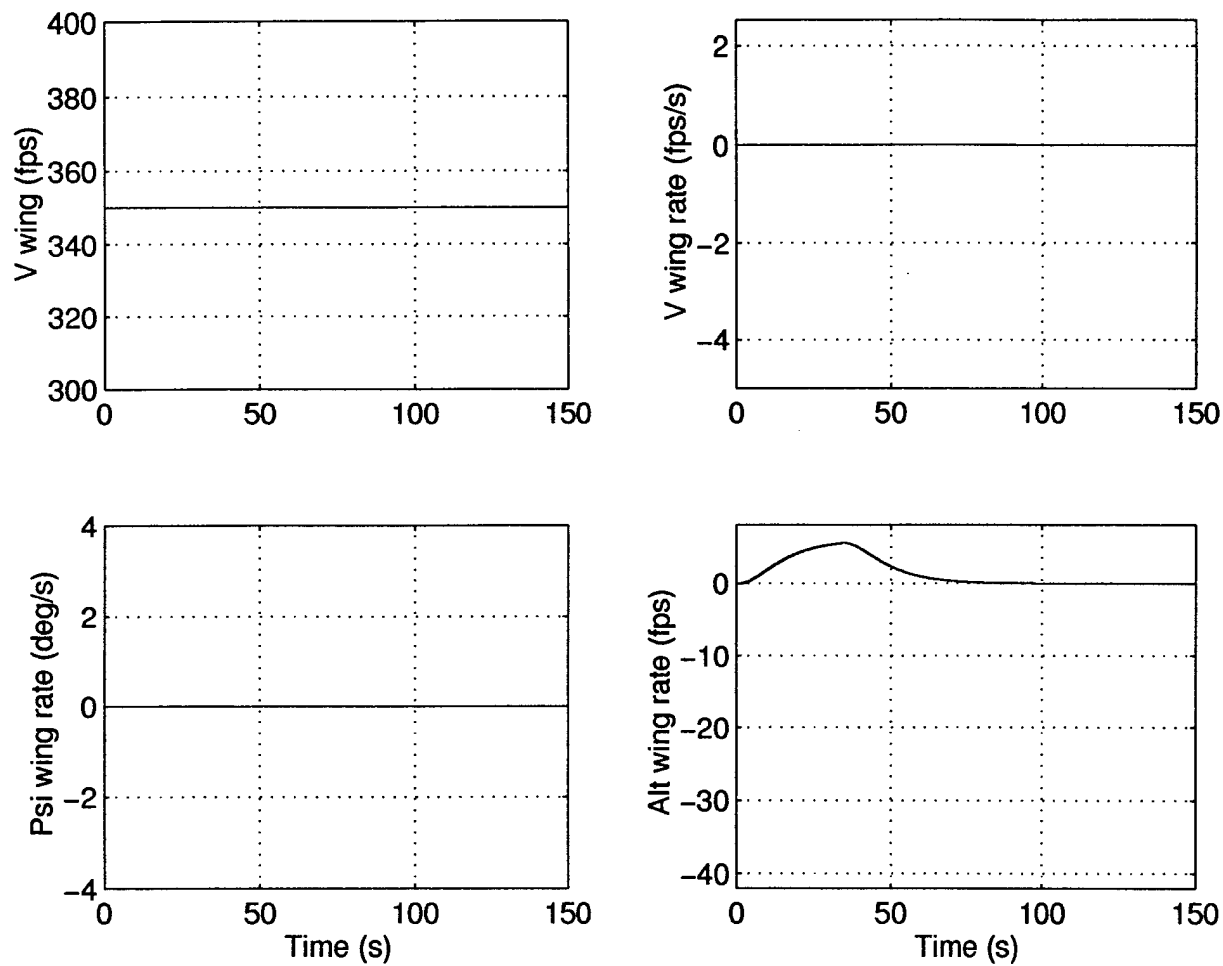
Figure 5.14　Rates of Wing Aircraft Responses for a $200ft$ Altitude Increase (alt) of the *Tight* Formation

The responses due to a 60° left turn maneuver from a trail formation (trail_60) are displayed in Figures (5.15) - (5.18). By symmetry, a right turn maneuver of a trail formation is simply a mirror image of these responses and is not shown. The Lissajous Figure 5.18 shows that the PIFF controller design's largest improvement, over the PFF design, is for heading change maneuvers of the trail formation.
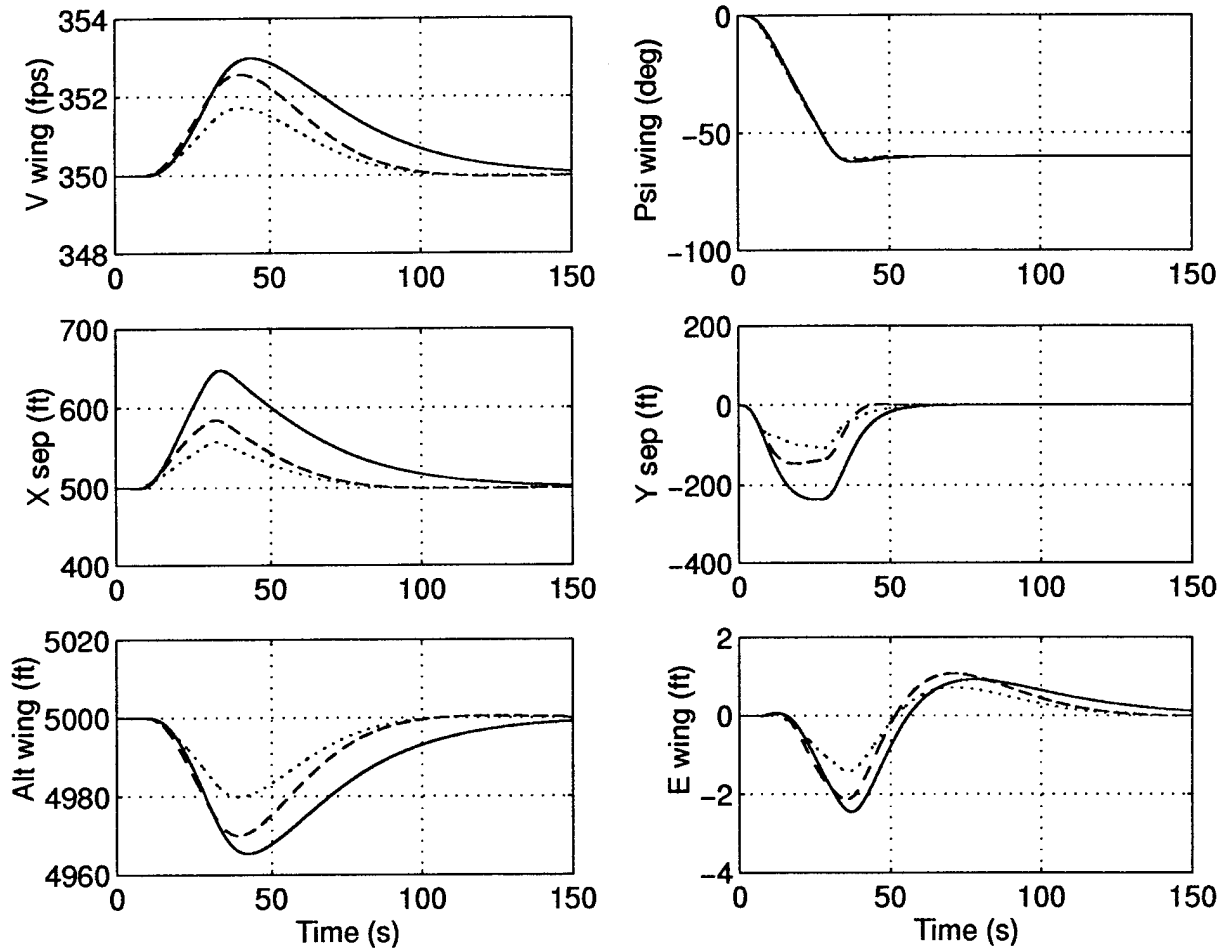
Figure 5.15   Wing Aircraft Responses for a 60° Left Turn of the *Tight* Trail Formation (trail_60)
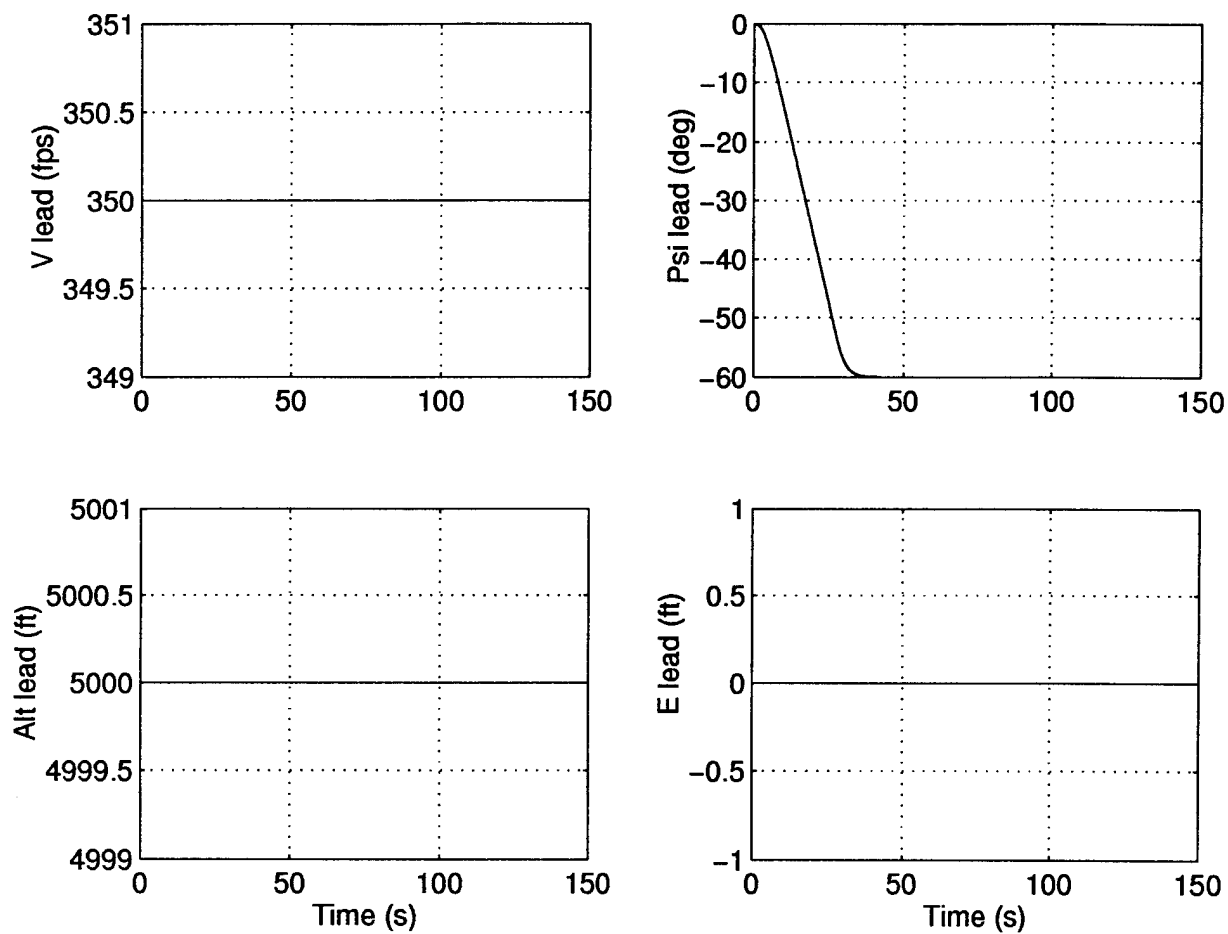
Figure 5.16   Lead Aircraft Responses for a 60° Left Turn of the *Tight* Trail Formation (trail_60)
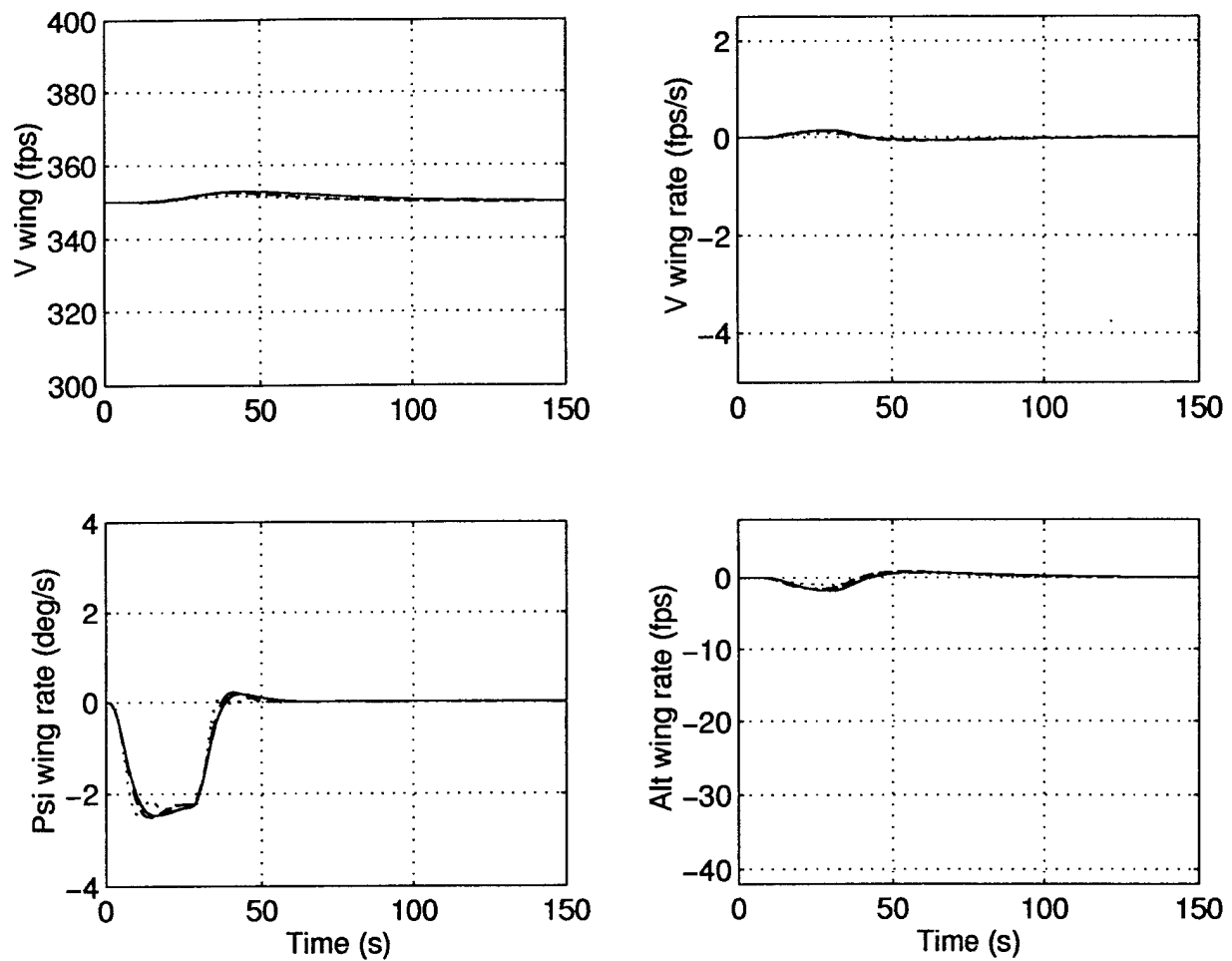
Figure 5.17   Rates of Wing Aircraft Responses for a 60° Left Turn of the *Tight* Trail
Formation (trail_60)
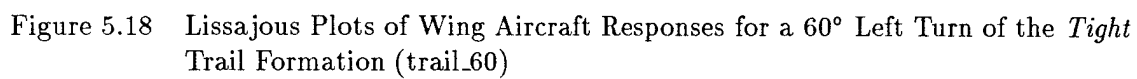
Figure 5.18   Lissajous Plots of Wing Aircraft Responses for a 60° Left Turn of the *Tight* Trail Formation (trail_60)

The responses due to a combined 30° right turn, velocity increase of $25\frac{ft}{sec}$, and altitude decrease of $100ft$ (rvuphdn) formation maneuver are displayed in Figures (5.19) - (5.22).
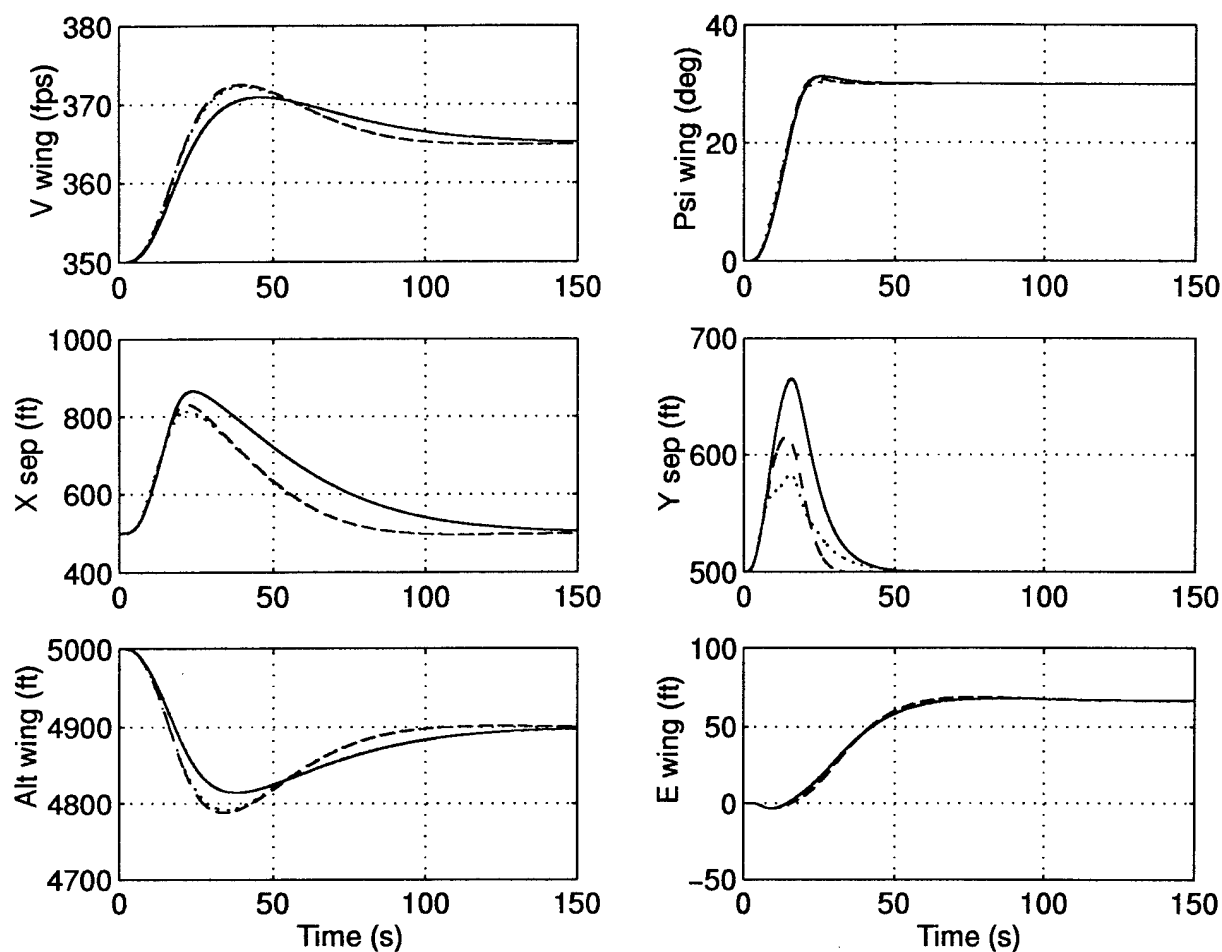
Figure 5.19   Wing Aircraft Responses for a 30° Right Turn, $25\frac{ft}{sec}$ Velocity Increase, and $100ft$ Altitude Decrease (rvuphdn) of the *Tight* Formation
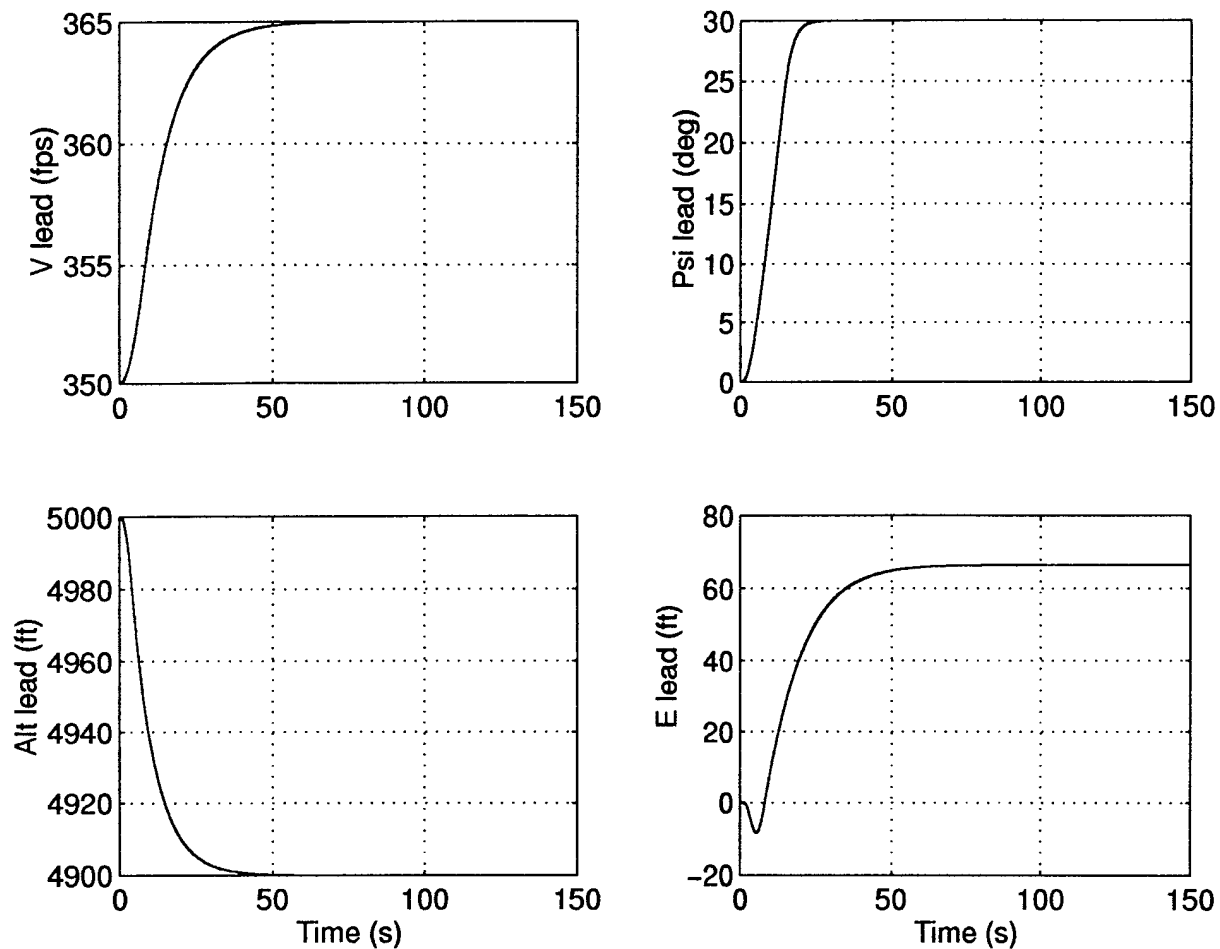
Figure 5.20   Lead Aircraft Responses for a 30° Right Turn, $25\frac{ft}{sec}$ Velocity Increase, and 100ft Altitude Decrease (rvuphdn) of the *Tight* Formation
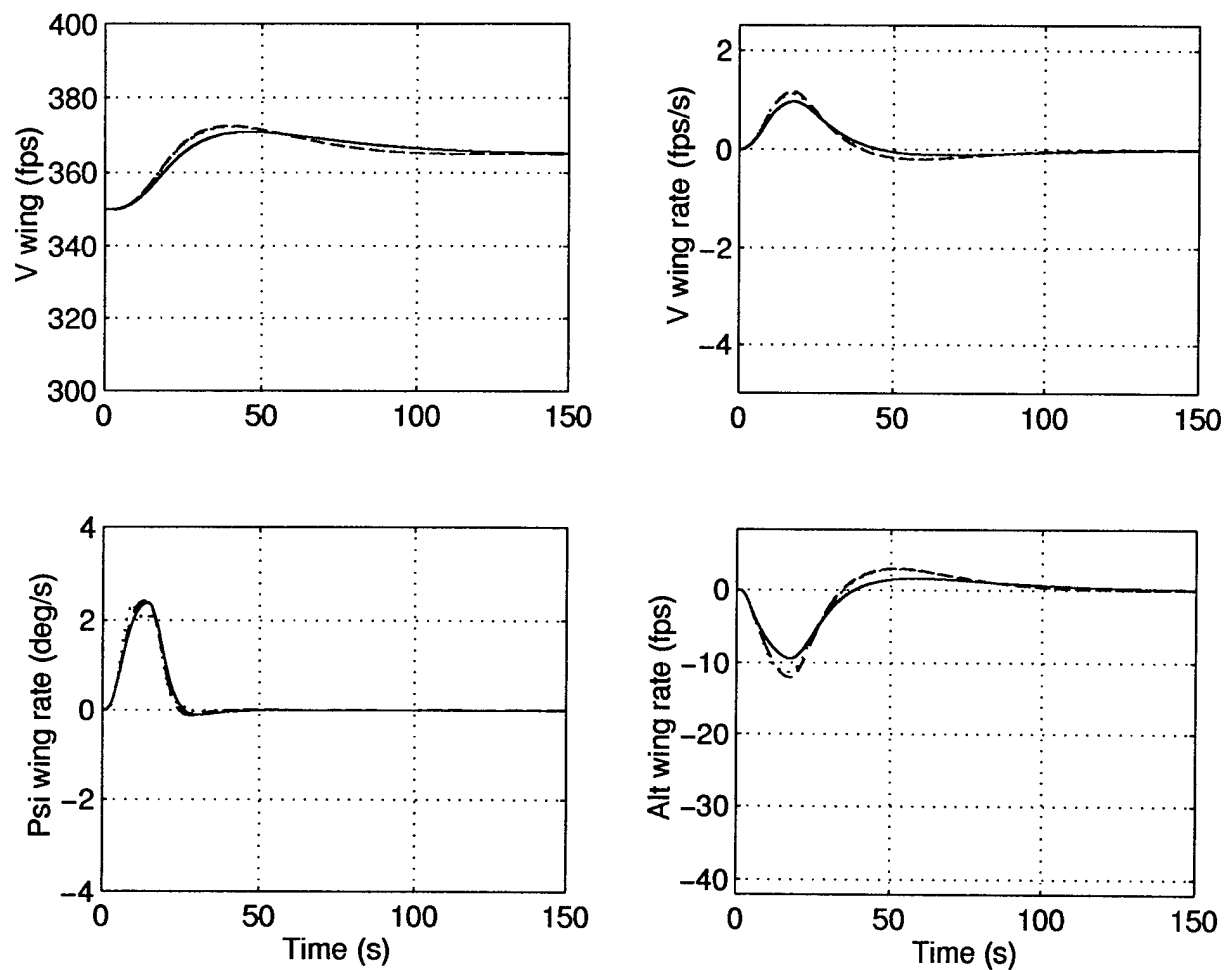
Figure 5.21   Rates of Wing Aircraft Responses for a 30° Right Turn, $25\frac{ft}{sec}$ Velocity Increase, and $100ft$ Altitude Decrease (rvuphdn) of the *Tight* Formation
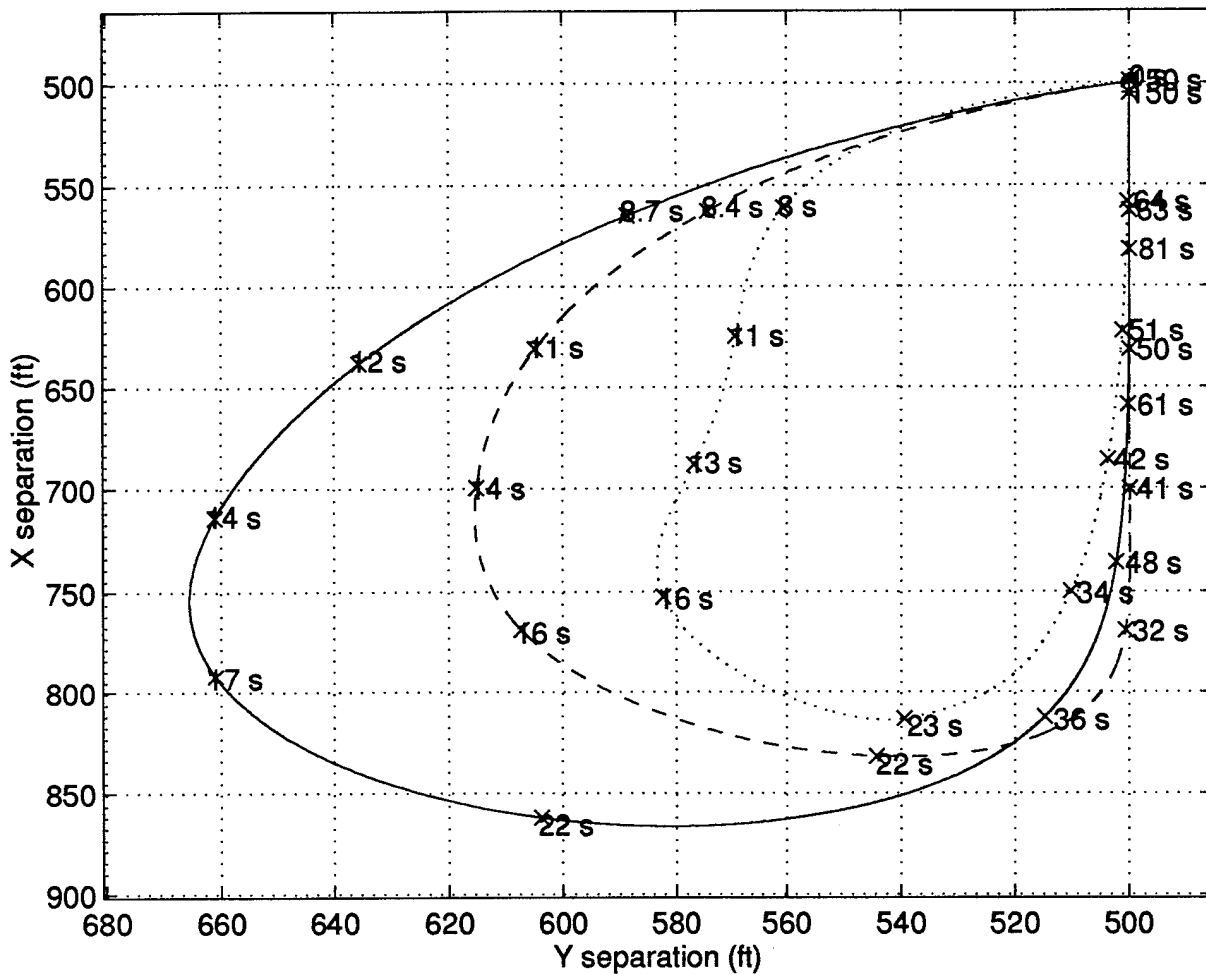
Figure 5.22 Lissajous Plots of Wing Aircraft Responses for a 30° Right Turn, $25\frac{ft}{sec}$ Velocity Increase, and $100\,ft$ Altitude Decrease (rvuphdn) of the *Tight* Formation

5.5.2 Formation Geometry Changes.   The two different *tight* formation changes presented are a left diamond to trail and an increase in x-separation formation geometry change. The responses due to a left diamond to trail (LD_trail) geometry change are displayed in Figures (5.23) - (5.26). There is no change in the lead aircraft's heading, altitude, velocity, or energy, since the change in geometry is performed by the wing aircraft.
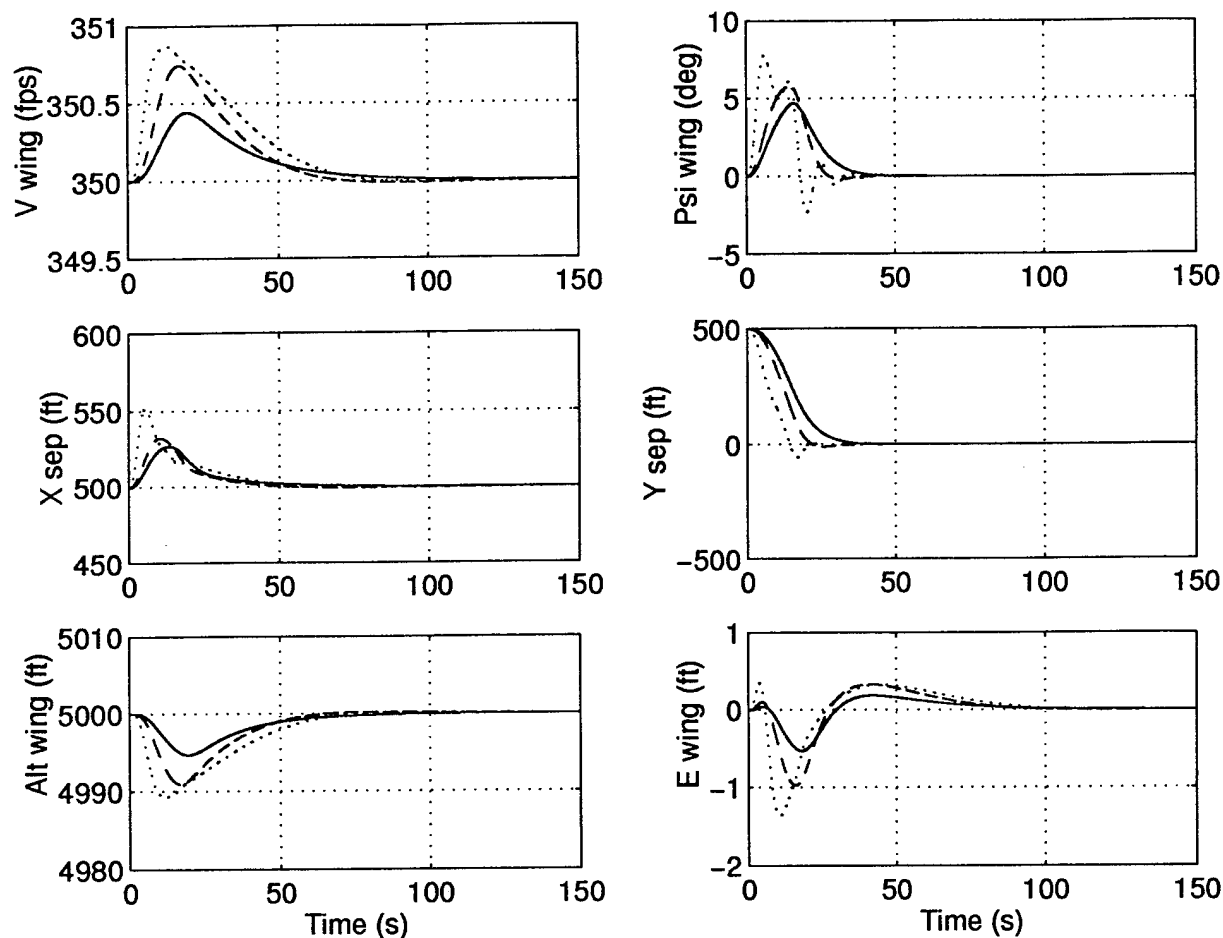
Figure 5.23   Wing Aircraft Responses for a Left Diamond to Trail Formation Geometry Change (LD_trail) of the *Tight* Formation
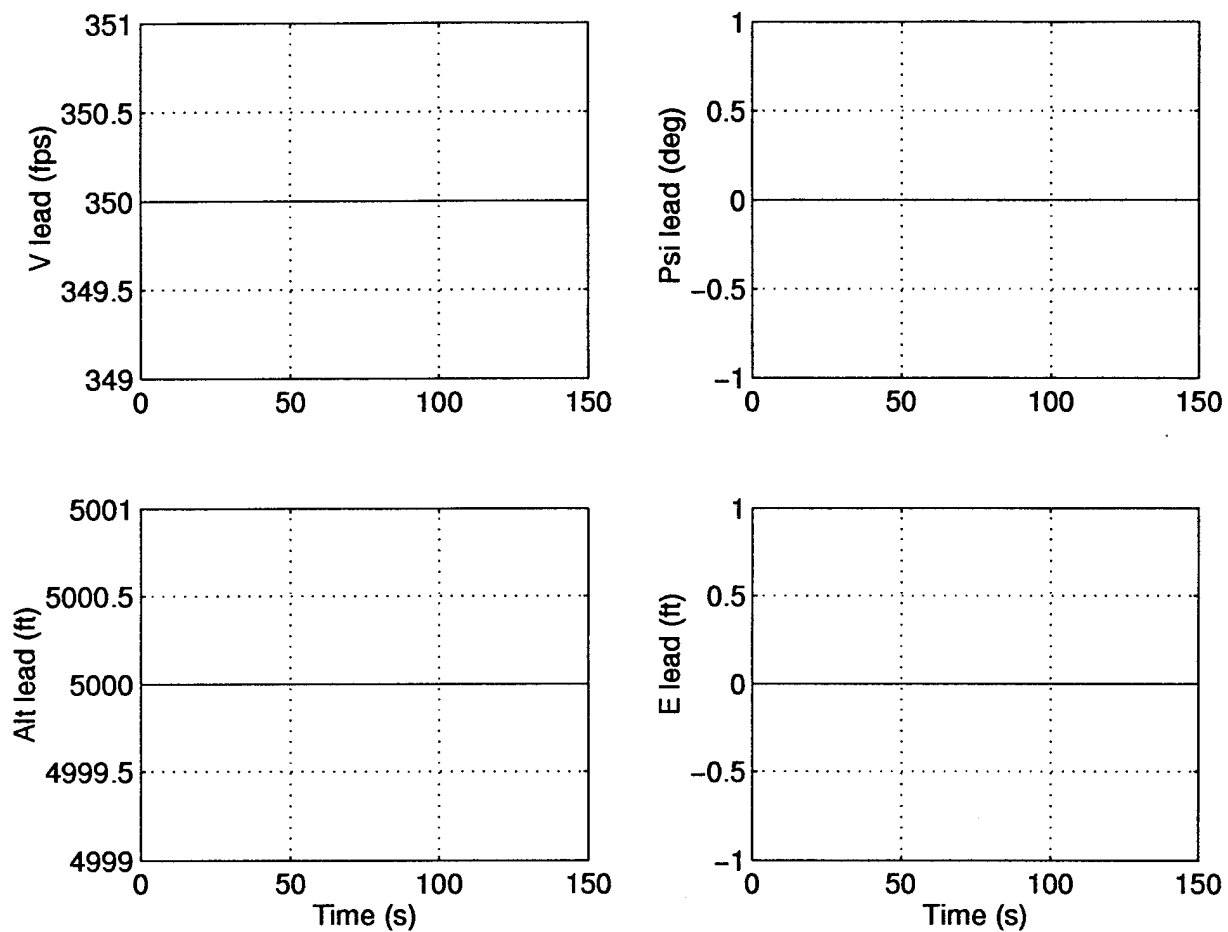
Figure 5.24   Lead Aircraft Responses for a Left Diamond to Trail Formation Geometry
Change (LD_trail) of the *Tight* Formation
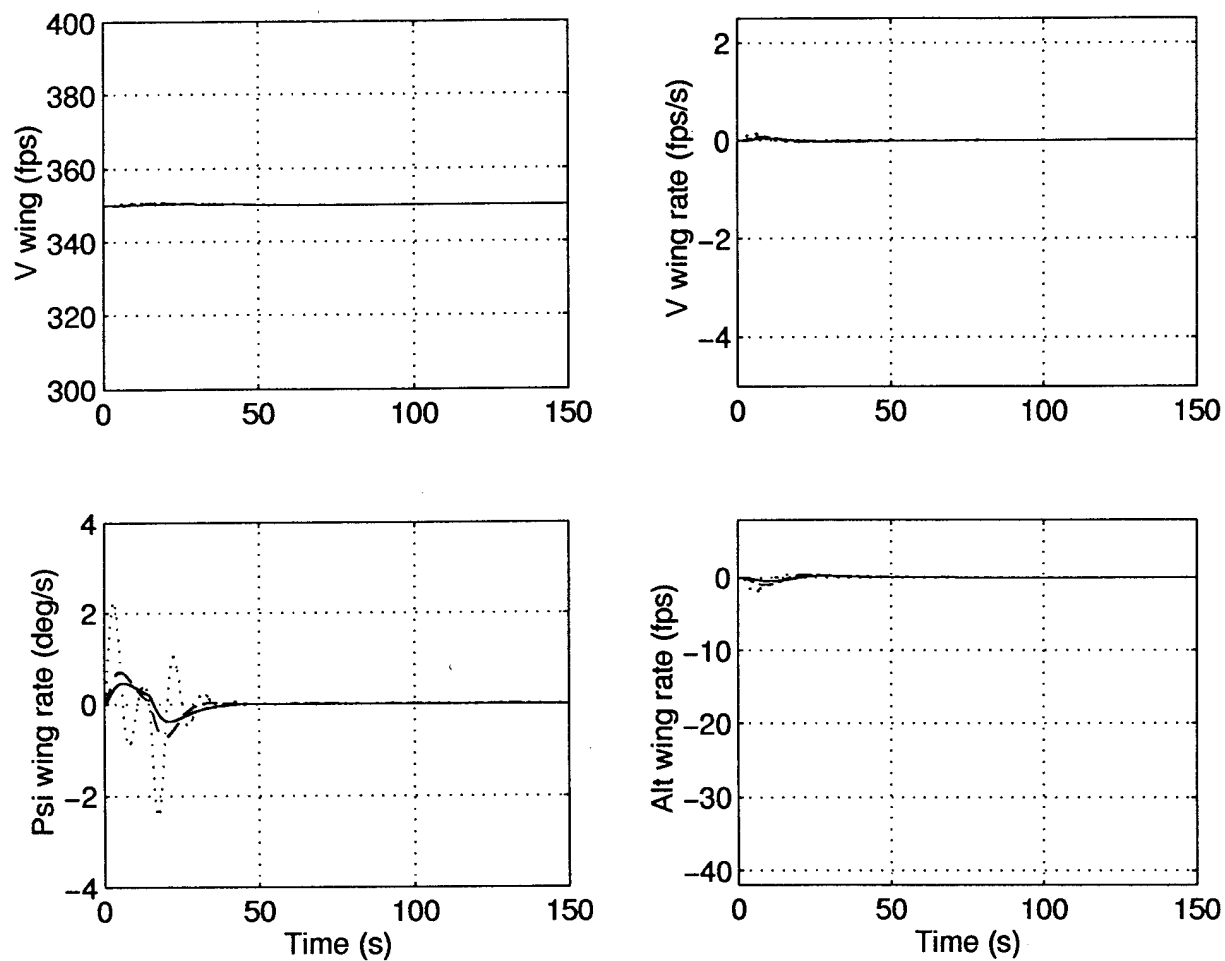
Figure 5.25 Rates of Wing Aircraft Responses for a Left Diamond to Trail Formation
Geometry Change (LD_trail) of the *Tight* Formation
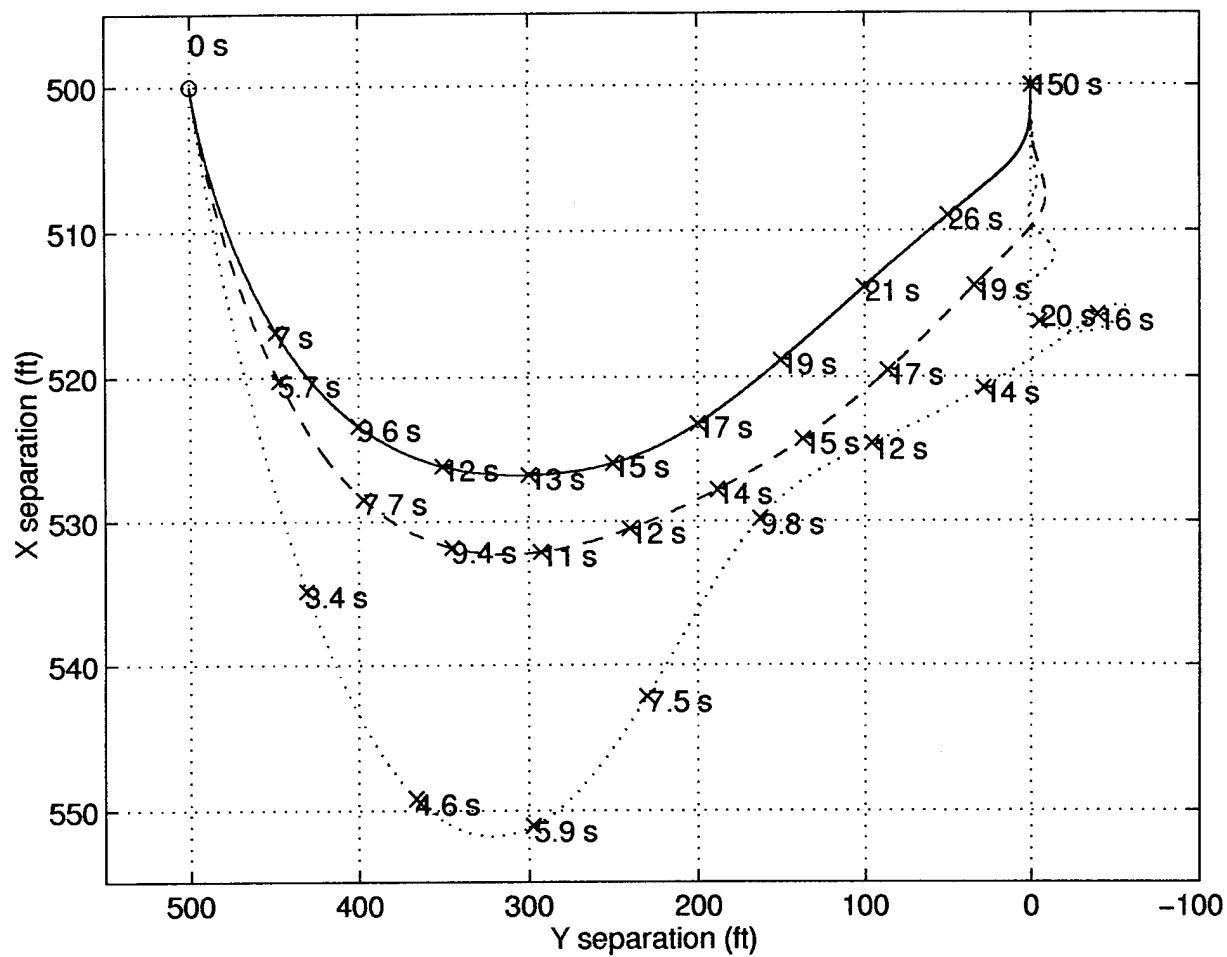
Figure 5.26   Lissajous Plots of Wing Aircraft Responses for a Left Diamond to Trail
Formation Geometry Change (LD_trail) of the *Tight* Formation

The responses due to an increase in x-separation, from $500ft$ to $1000ft$ (x inc), formation geometry change are displayed in Figures (5.27) - (5.29). There is no change in the lead aircraft's heading, altitude, velocity, or energy, since the change in geometry is performed by the wing aircraft. The optimized PFF and PIFF formation flight controller responses coincide, since the x-channel characteristics of the two controllers are identical.
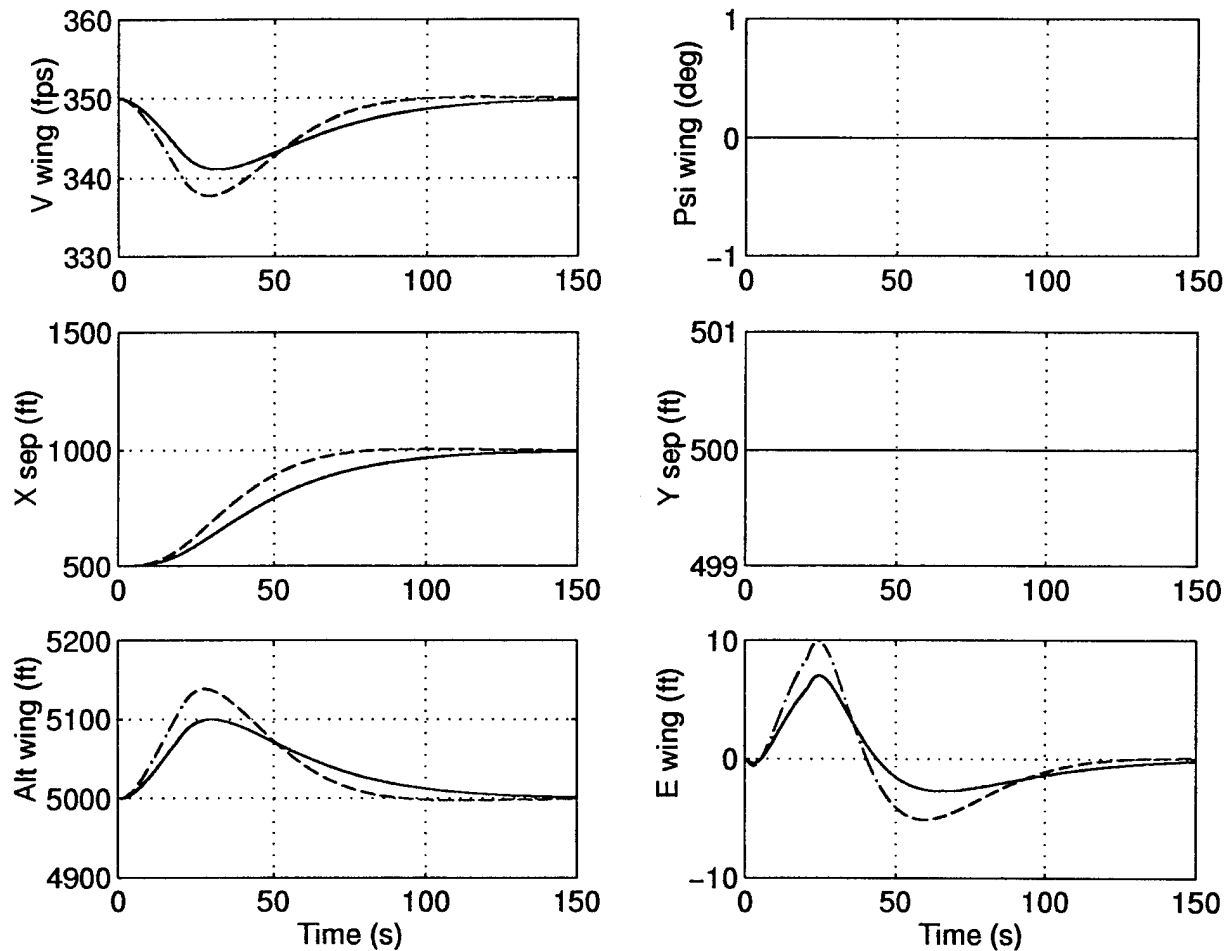
Figure 5.27   Wing Aircraft Responses for an Increase in X-Separation from $500ft$ to $1000ft$ (x inc) of the *Tight* Formation
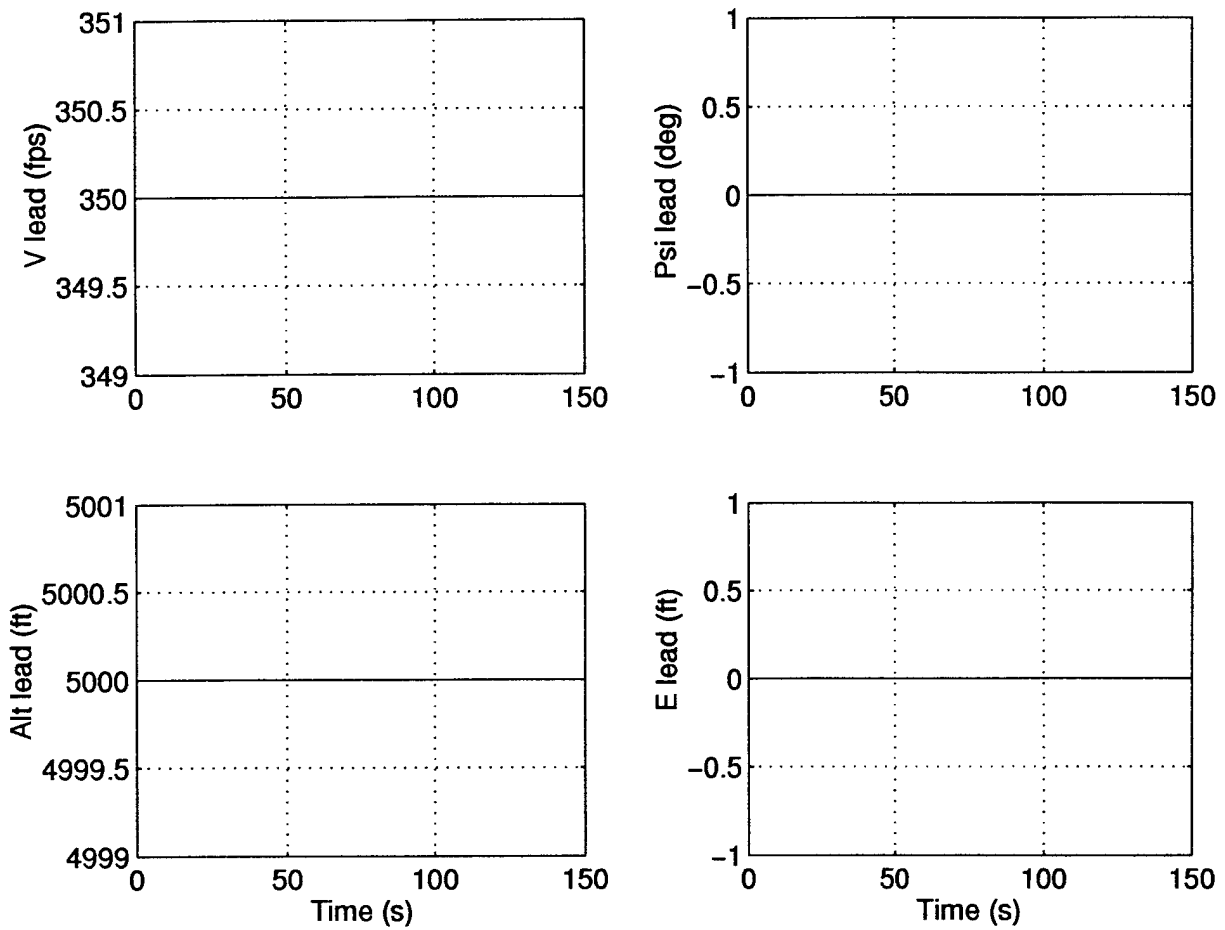
Figure 5.28   Lead Aircraft Responses for an Increase in X-Separation from $500ft$ to $1000ft$ (x inc) of the *Tight* Formation
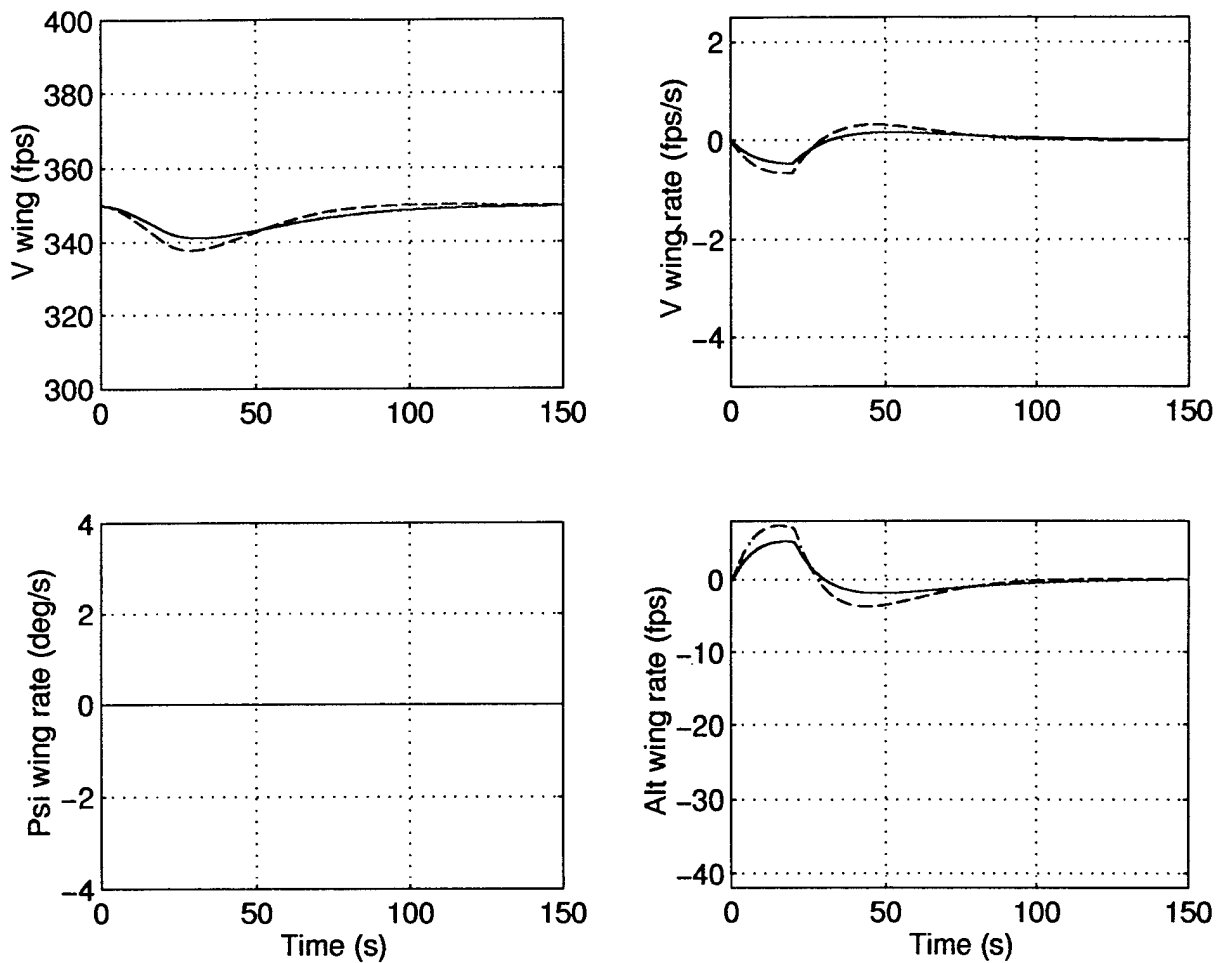
Figure 5.29   Rates of Wing Aircraft Responses for an Increase in X-Separation from 500 ft
to 1000 ft (x inc) of the *Tight* Formation

5.5.3 Composite Formation Heading Change Maneuver and Formation Geometry

Change. The responses due to a left diamond to right diamond geometry change with a 45° left turn (LD_RD_45L) maneuver are displayed in Figures (5.30) - (5.33). The nonlinear simulations for the optimal PIFF controller show that the wing aircraft/autopilot heading rate reaches positive saturation. However, the total costs difference between imposing or not imposing rate limits verifies that the encountered effects of rate saturation can be considered negligible.
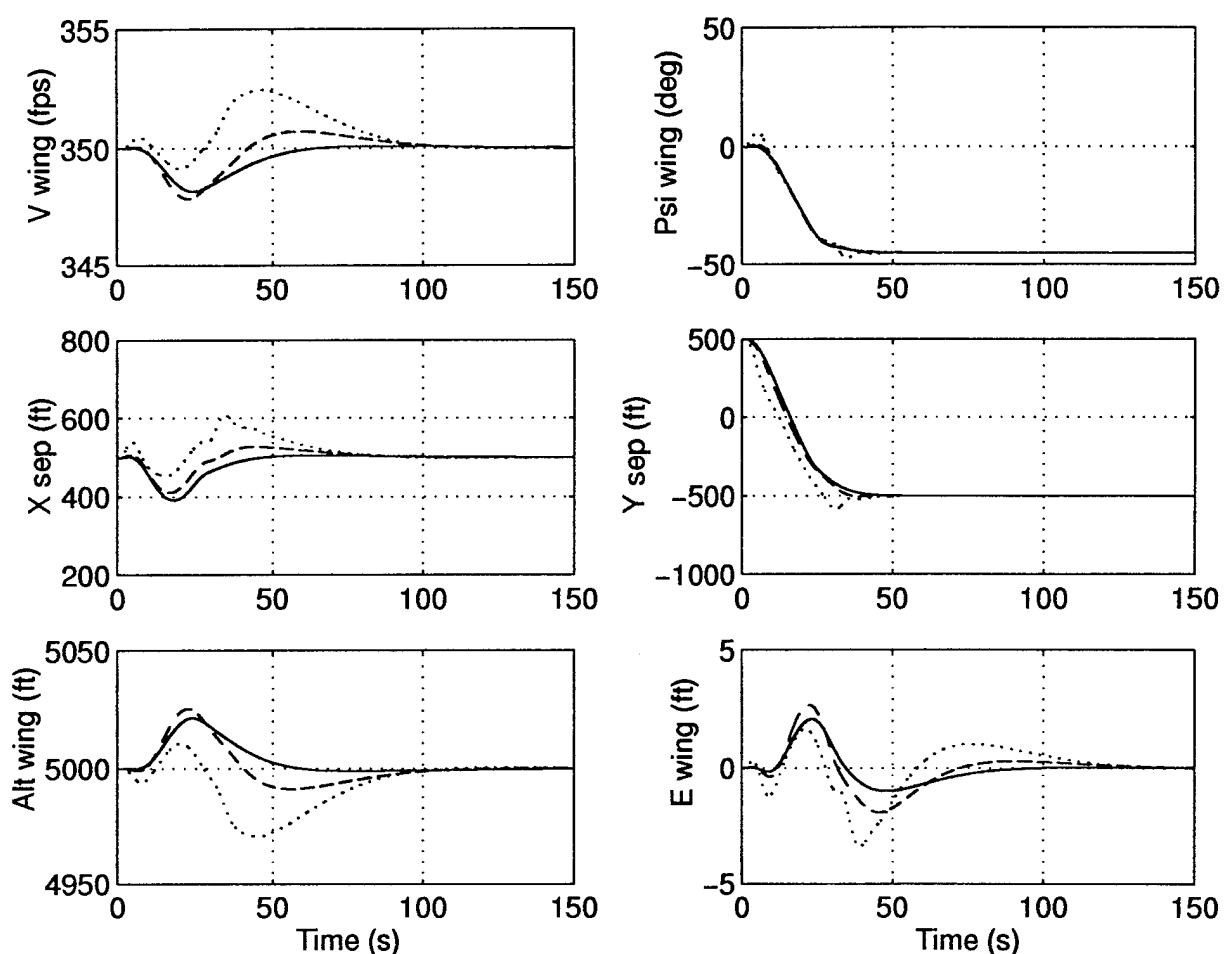
Figure 5.30   Wing Aircraft Responses for a Left Diamond to Right Diamond Geometry Change with a 45° Left Turn (LD_RD_45L) of the *Tight* Formation
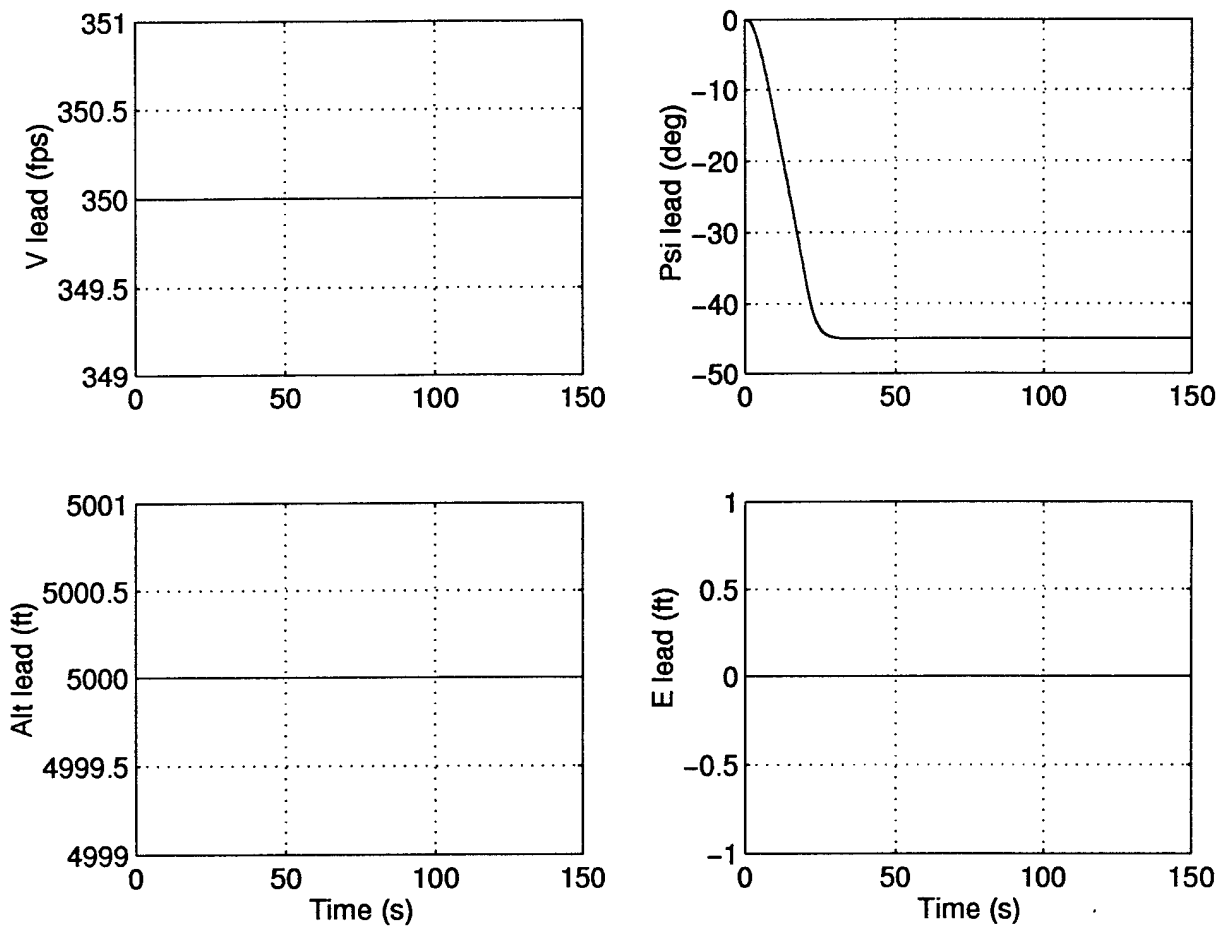
Figure 5.31   Lead Aircraft Responses for a Left Diamond to Right Diamond Geometry Change with a 45° Left Turn (LD_RD_45L) of the *Tight* Formation
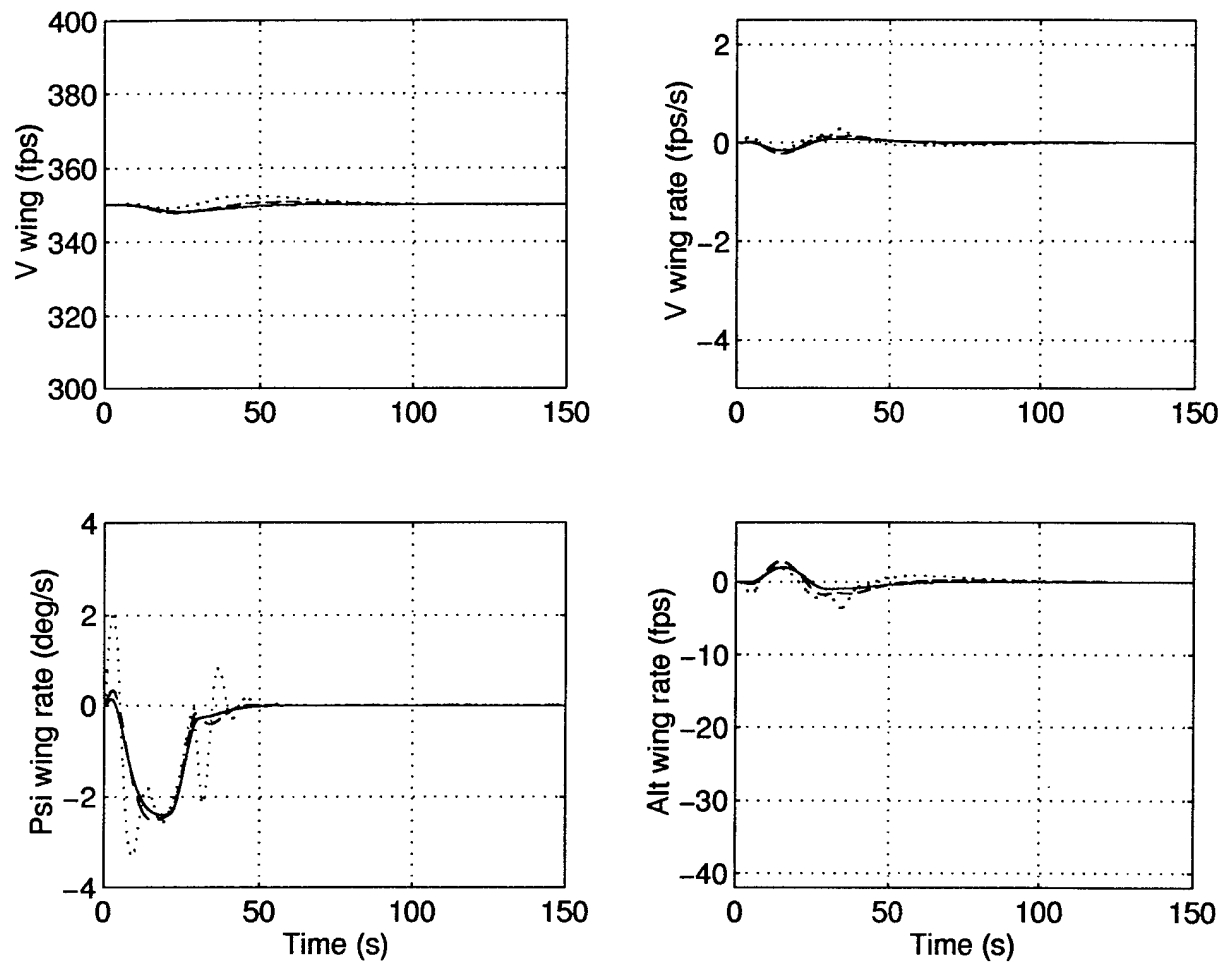
Figure 5.32　Rates of Wing Aircraft Responses for a Left Diamond to Right Diamond Geometry Change with a 45° Left Turn (LD_RD_45L) of the *Tight* Formation
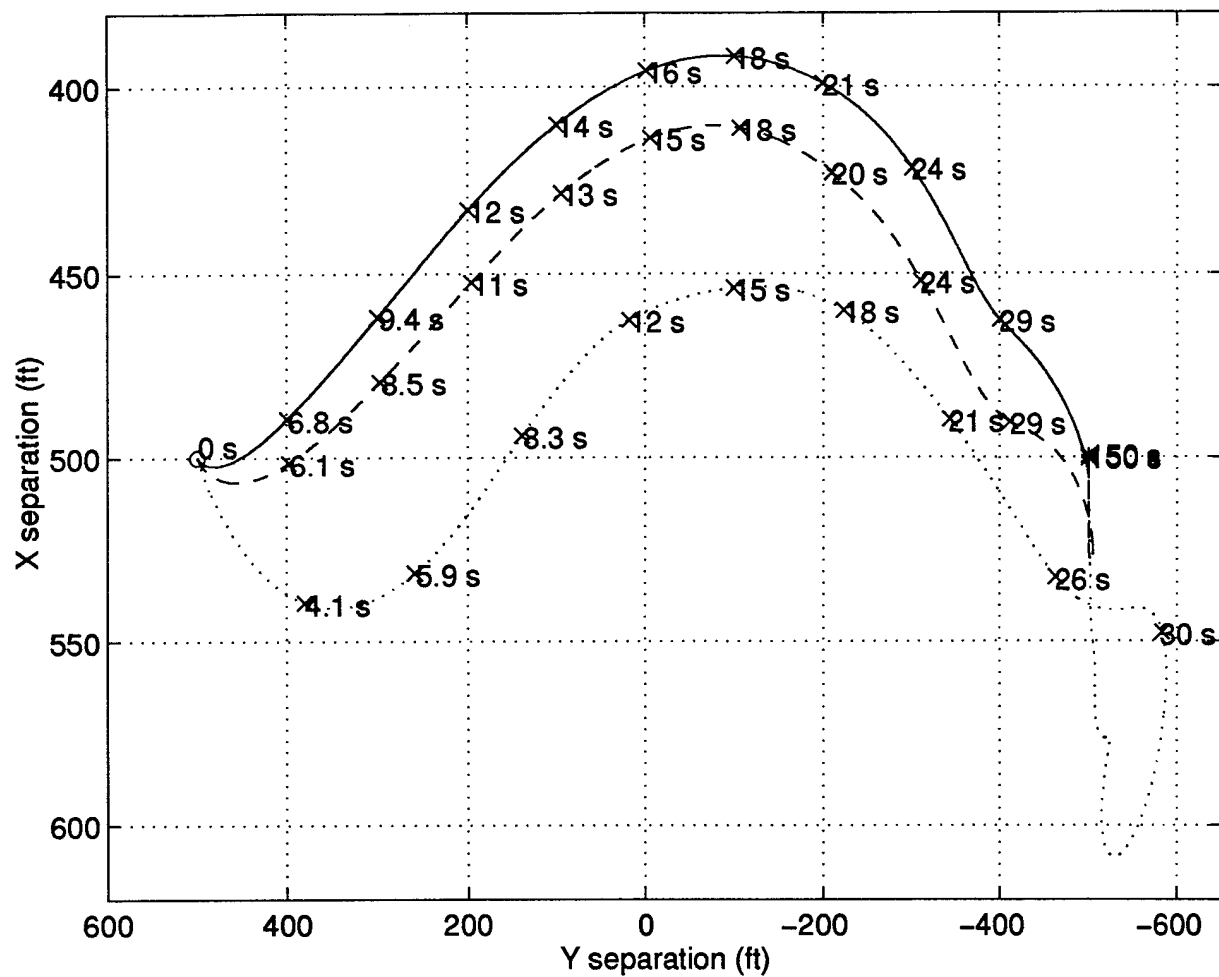
Figure 5.33   Lissajous Plots of Wing Aircraft Responses for a Left Diamond to Right Diamond Geometry Change with a 45° Left Turn (LD_RD_45L) of the *Tight* Formation

5.5.4 Dual Maneuver.
The responses during a dual maneuver, of a 45° left turn followed by a 45° right turn which returns the formation to its original heading, are displayed in Figures (5.34) - (5.37).
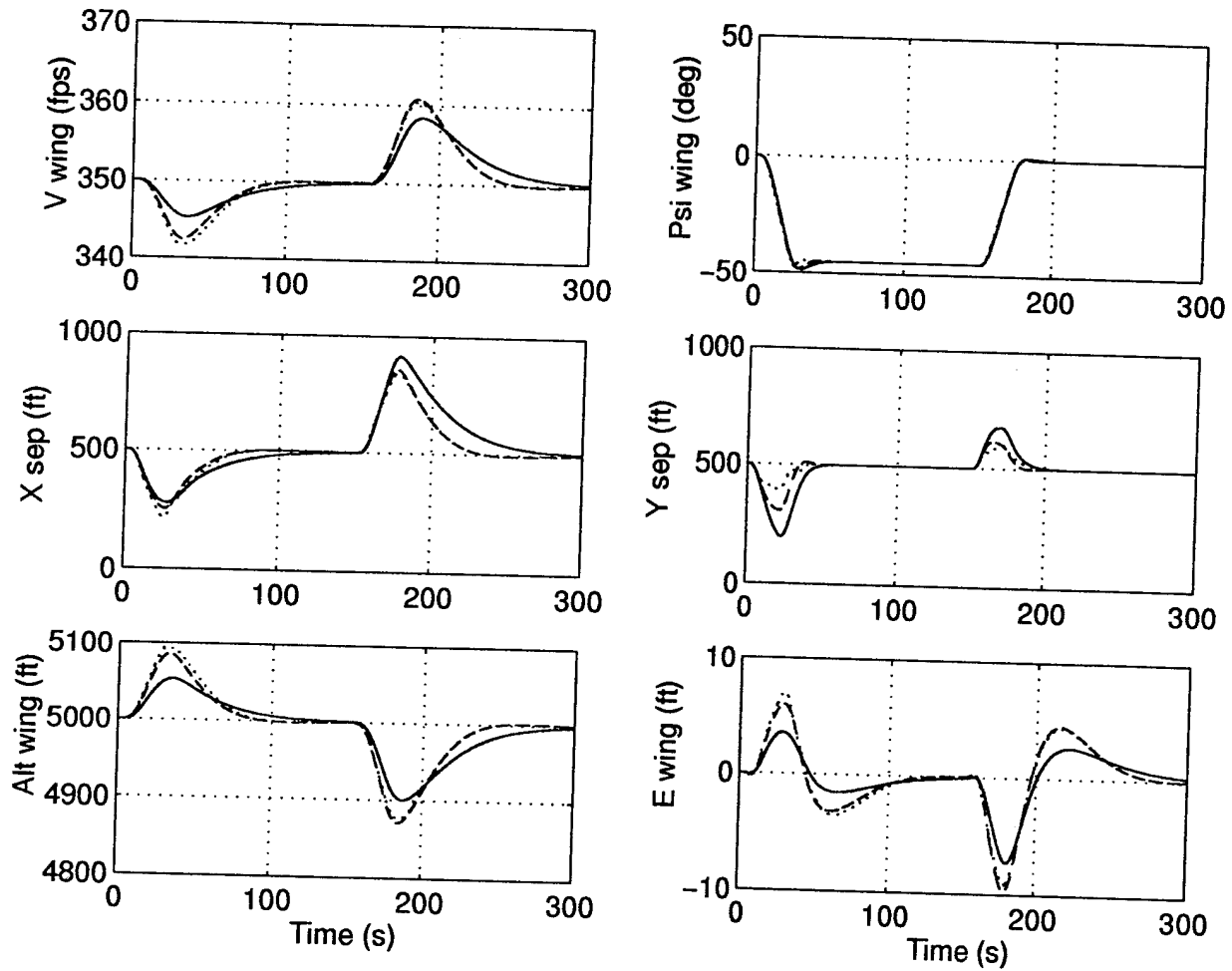
Figure 5.34   Wing Aircraft Responses for a 45° Left Turn and then a 45° Right Turn (45° left) of the *Tight* Formation
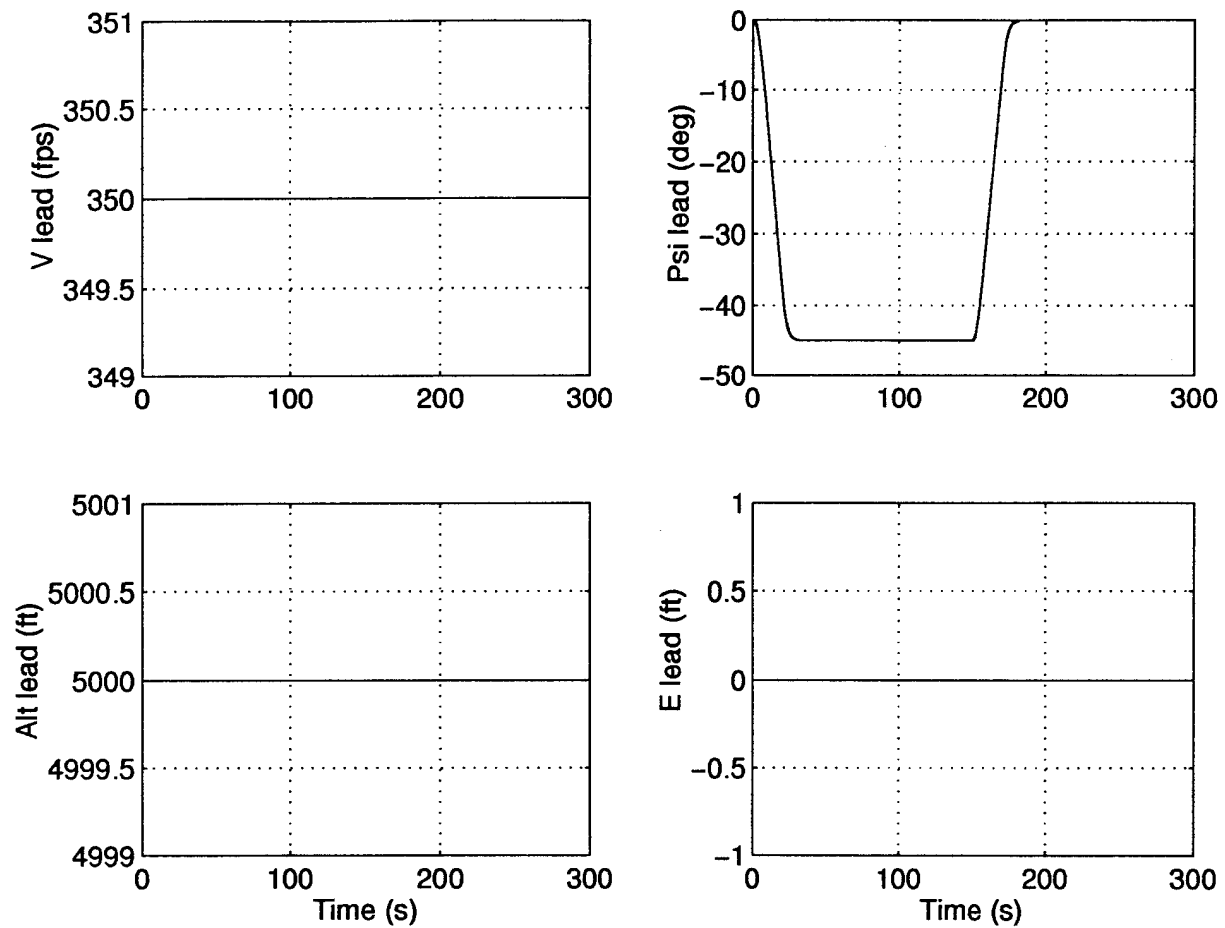
Figure 5.35 Lead Aircraft Responses for a 45° Left Turn and then a 45° Right Turn (45° left) of the *Tight* Formation
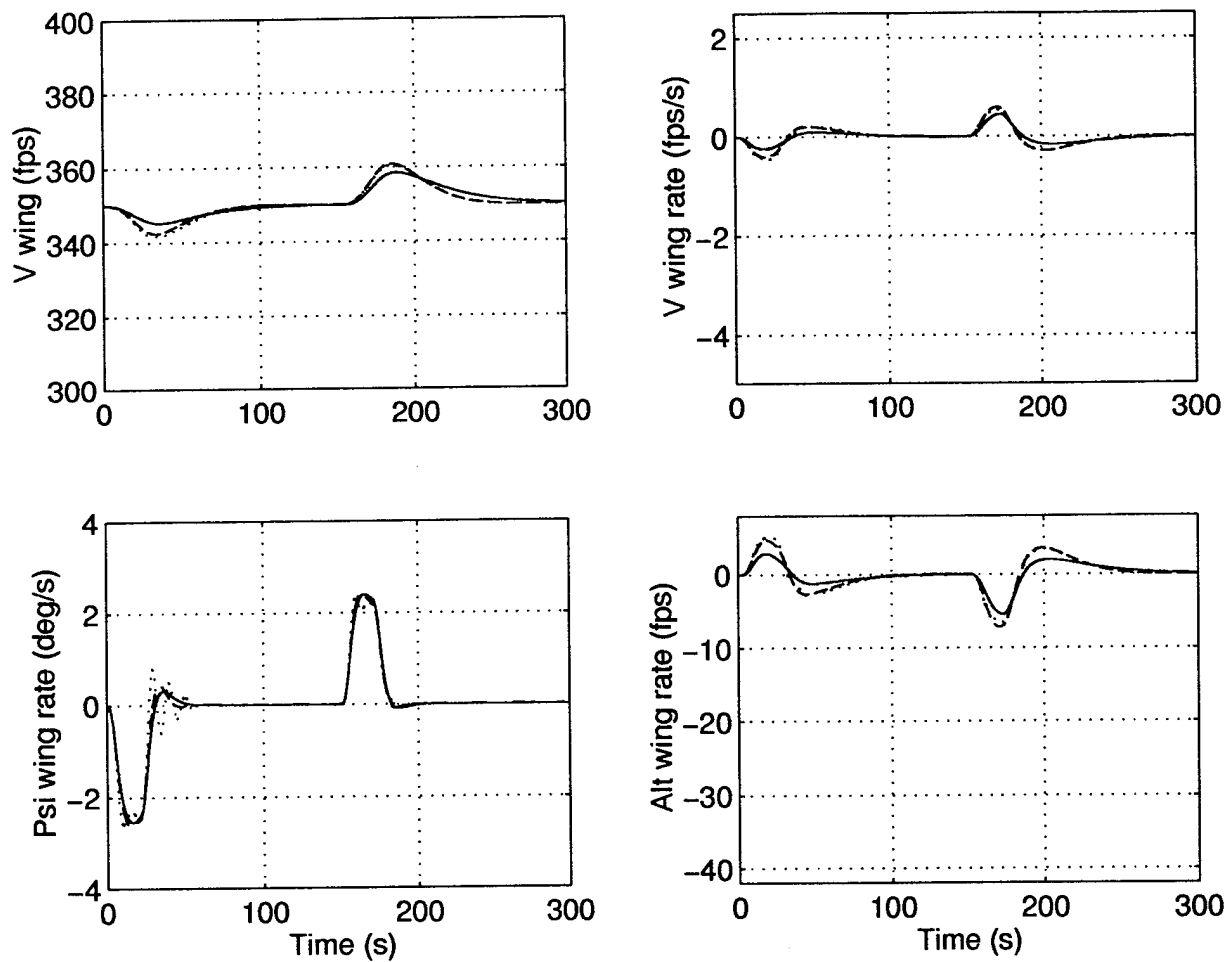
Figure 5.36   Rates of Wing Aircraft Responses for a 45° Left Turn and then a 45° Right
Turn (45° left) of the *Tight* Formation
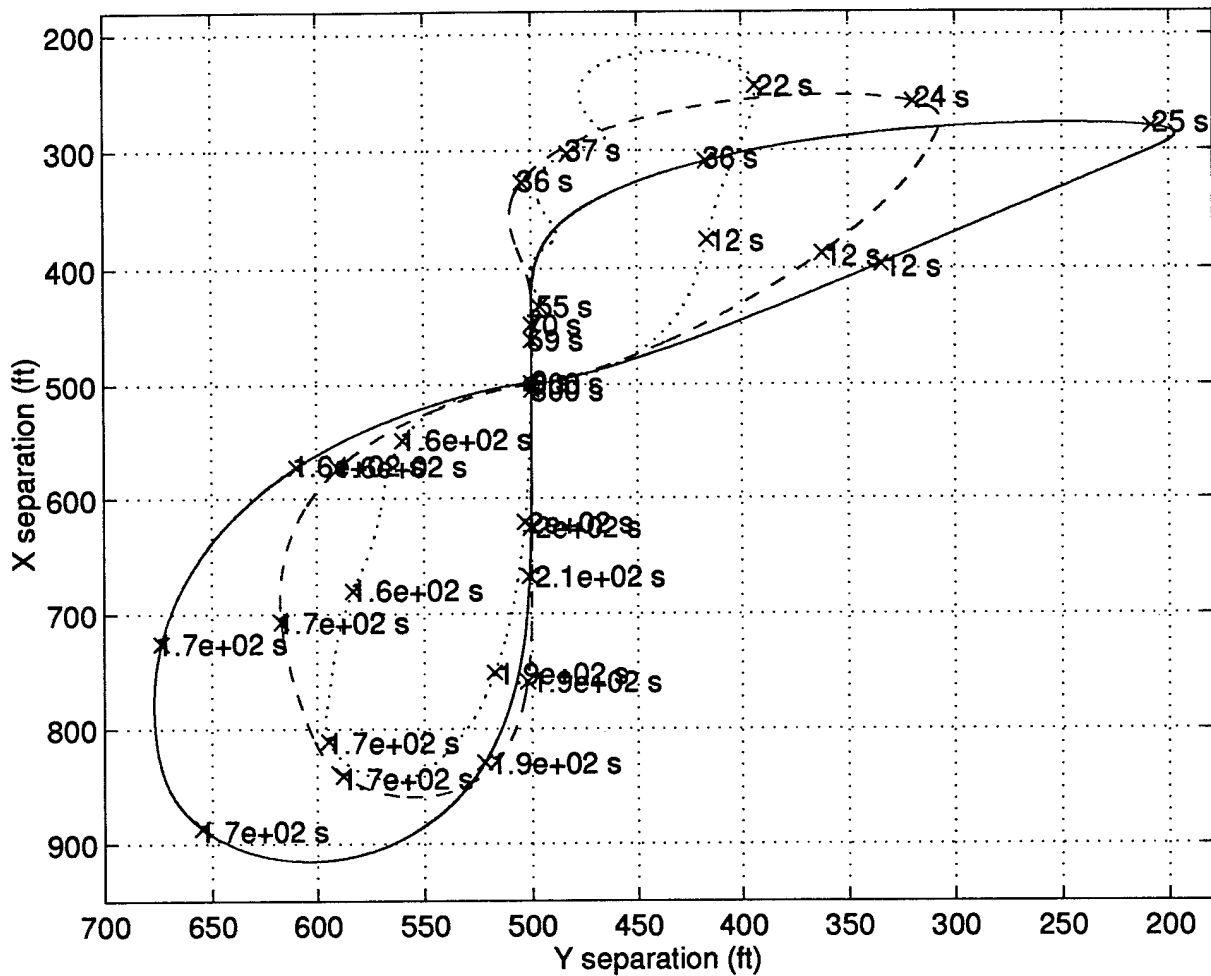
Figure 5.37   Lissajous Plots of Wing Aircraft Responses for a 45° Left Turn and then a
45° Right Turn (45° left) of the *Tight* Formation

5.6 Conclusion

Nonlinear simulations of *tight* formation geometry changes verify the improvement in performance and the robustness of optimal gains for both the PFF and PIFF controllers. The wide variety of formation maneuvers and geometry changes simulated yield a workable range for the optimal formation flight control system.

VI. Loose *Formation*

The optimization and testing of the Proportional plus FeedForward (PFF) and the Proportional plus Integral and FeedForward (PIFF) controller designs during *loose* formations are considered in this chapter. Optimal gains for each controller are determined via constrained optimization, which is available in MATLAB. The constrained optimization routine is applied to a wide variety of formation maneuvers and geometry changes initiated from the nominal *loose* formation. Comparison of optimization costs and formation responses are made for each controller design. The PFF design, with Veth's gains which were determined via root locus analysis [23], is used as the baseline.

6.1 Formation Changes

As in the previous chapter, a wide variety of formation maneuvers and geometry changes are simulated and used to optimize controller gains over the entire operational range of a formation flight autopilot. In this chapter a *loose* formation is considered. The nominal *loose* formation is a left diamond (echelon) formation with $\overline{X}$ = 3500 ft and $\overline{Y}$ = 1000 ft, at a velocity ($\overline{V}$) of $350\frac{ft}{sec}$, altitude ($\overline{H}$) of $5000ft$, and heading ($\overline{\Psi}$) of 0°. In addition, some *loose* trail formation maneuvers, with $\overline{X}$ = 3500 ft and $\overline{Y}$ = 0 ft, are also investigated for completeness.

The optimized *loose* formation maneuvers are the same as those optimized with the *tight* formation:

- 30° left turn

- 30° right turn

- 45° left turn

- 45° right turn

- 60° left turn

- 60° right turn

- altitude increase, or decrease, of $200ft$ (alt)

- velocity decrease of $25\frac{ft}{sec}$ (vel dn)

- velocity increase of $25\frac{ft}{sec}$ (vel up)

- 30° right turn, velocity decrease of $25\frac{ft}{sec}$, and altitude decrease of $100ft$ (rvuphdn)

- 60° left, or right, from trail formation (trail_60)

The formation geometry changes optimized are slightly different then those seen in the *tight* formation:

- left diamond to trail (LD_trail)

- trail to left diamond (trail_LD)

- left diamond to right diamond (LD_RD) or right diamond to left diamond (RD_LD)

- decrease in x-separation from $3500ft$ to $1000ft$ (x dec)

- increase in x-separation from $3500ft$ to $5000ft$ (x inc)

The geometry change maneuvers are different due to the increase in x- and y-separation distances. The wing aircraft changing to a lead position is not practical, from the *loose* formation, due to the large commanded x-separation change that is required and the attendant long simulation time. The composite formation geometry change and maneuvers optimized are:

- left diamond to right diamond with a 30° left turn (LD_RD_30L)

- left diamond to right diamond with a 30° right turn (LD_RD_30R)

- left diamond to right diamond with a 45° left turn (LD_RD_45L)

- left diamond to right diamond with a 45° right turn (LD_RD_45R)

- left diamond to right diamond with a 60° left turn (LD_RD_60L)

- left diamond to right diamond with a 60° right turn (LD_RD_60R)

The composite formation geometry changes and maneuvers, with the lead change, are not performed due to the large x-separation change that is required. Obviously, tracking such a large separation change takes longer than the 150 seconds established for a single

6-2

maneuver. An examples of the MATLAB code used to optimize the above maneuvers is listed in Appendix A.3.1.

The same dual formation changes are simulated for the *loose* formation, as are simulated for the *tight* formation. The dual formation changes include right and left heading changes, altitude increases and decreases, velocity increases and decreases, y-separation distance increases and decreases, and x-separation distance increases and decreases. See Appendix A.3.2 for an example of the MATLAB code used for dual formation maneuvers.

6.2   PFF Design Baseline

The baseline PFF gains, K_{xp} and K_{yp}, are listed in Table 6.1 [23]. Although these gains are designed for the *tight* formation, the basic characteristics of the *loose* formation are similar enough to the *tight* formation that the same gains should act as an adequate baseline.

Parameter	Value
K_{xp}	0.0250
K_{yp}	0.0187

Table 6.1   Veth's Gains For PFF

The baseline results for single formation changes are listed in Table 6.2, and the baselines results for dual formation changes are listed in Table 6.3. The total costs for *loose* formation changes is higher than that for comparable *tight* formation changes. Simulations involving left turns of greater than 30° cause the aircraft/autopilot model to encounter rate limits.

Once again, the cost for a dual maneuver in which the altitude first increases and then decreases is identical to the cost of an altitude decrease and then an increase maneuver. In like manner, for two dual formation geometry changes, the left diamond to right diamond and then a right diamond to left diamond formation maneuver yields identical costs to the right diamond to left diamond and then a left diamond to right diamond formation maneuver. To avoid redundancy these duplicate formation change costs are not included in Table 6.3. As before, the differences between the costs of complementary dual formation changes remain small.

6-3

Even for the *loose* formation, the PFF controller design is fairly robust over a wide variety of formation maneuvers and geometry changes.

Loose Formation Single Maneuver Results					
Maneuver	X Cost	Y Cost	Energy Cost	Total Cost	Saturation
30° left	192.98	58.69	81.29	332.97	L=NL
30° right	76.44	71.81	28.98	177.24	L=NL
45° left	311.93	79.92	129.20	521.05	L
	311.93	79.92	92.56	484.41	NL
45° right	79.52	108.65	27.02	215.19	L=NL
60° left	432.23	95.55	175.26	703.05	L
	432.23	95.55	201.59	729.37	NL
60° right	68.68	144.77	23.94	237.39	L=NL
alt	0	0	356.56	356.56	L=NL
vel dn	66.00	0	570.16	636.16	L=NL
vel up	65.90	0	626.78	692.68	L=NL
rvuphdn	115.92	69.80	228.67	414.40	L=NL
trail_60	181.89	120.82	78.81	381.52	L=NL
LD_trail	8.48	153.63	6.50	168.54	L=NL
trail_LD	13.80	153.76	7.20	174.76	L=NL
LD_RD	21.26	497.71	11.23	530.20	L=NL
x dec	547.87	0	193.83	741.70	L=NL
x inc	694.86	0	140.94	835.80	L=NL
LD_RD_30L	139.11	559.58	68.34	767.03	L=NL
LD_RD_30R	52.14	426.04	22.54	500.72	L=NL
LD_RD_45L	223.26	583.95	106.43	913.64	L
	223.26	583.95	103.16	910.37	NL
LD_RD_45R	31.64	391.21	25.16	448.01	L=NL
LD_RD_60L	301.17	604.40	139.15	1044.72	L
	301.17	604.40	106.29	1011.86	NL
LD_RD_60R	71.71	358.90	46.75	477.36	L=NL

Table 6.2   Costs Due to Single Maneuvers of the *Loose* Formation Using Veth's Gains (Baseline)

Loose Formation Dual Maneuver Results					
Maneuver	X Cost	Y Cost	Energy Cost	Total Cost	Saturation
30° left	134.23	65.19	56.12	255.54	L=NL
30° right	134.38	65.30	55.50	255.18	L=NL
45° left	195.01	94.13	79.98	369.12	L
	195.01	94.13	61.65	350.80	NL
45° right	195.29	94.37	78.67	368.34	L
	195.29	94.37	60.14	349.81	NL
60° left	249.57	119.89	102.07	471.54	L
	249.57	119.89	115.24	484.70	NL
60° right	249.57	120.28	100.27	470.53	L
	249.57	120.28	115.46	485.71	NL
alt	0	0	356.62	356.62	L=NL
vel dn	66.00	0	570.16	636.16	L=NL
vel up	65.90	0	626.78	692.68	L=NL
LD_trail	11.15	58.32	6.81	76.29	L=NL
trail_LD	11.35	58.32	6.80	76.46	L=NL
LD_RD	21.97	116.50	11.13	149.60	L=NL
x dec	395.18	0	169.02	564.20	L=NL
x inc	393.74	0	170.51	564.26	L=NL

Table 6.3   Costs Due to Dual Maneuvers of the *Loose* Formation Using Veth's Gains (Baseline)

6.3 PFF Design Optimization

The optimal gains, K_x^* and K_y^*, for the PFF controller design are listed in Table 6.4. These optimal gains for the *loose* formation controller are determined in the same manner as for the *tight* formation PFF controller, see Chapter V. These *loose* formation optimal gains are larger then the baseline gains, but different than the optimal gains for *tight* formations. Optimization of controller gains using the *loose* formation restricts the x-channel gain, but relaxes restrictions on the y-channel gain. As a result, the optimal x-channel gain, K_x^*, is smaller for *loose* formations than it is for *tight* formations and the y-channel gain, K_y^*, is larger for *loose* formations than it is for *tight* formations

Parameter	Value
K_{x^*}	0.03
K_y^*	1.00

Table 6.4   Optimal Gains For PFF

The results for single formation changes are listed in Table 6.5, and the results for dual formation changes are listed in Table 6.6. With one exception, the optimal PFF controller gains costs show a large improvement over the baseline gains. Once again, altitude maneuver costs remain the same since the altitude channel controller is not varied. The left diamond to right diamond geometry change with a 60° right turn is the only formation change which costs more with the optimal gains.

Simulations involving left turns of greater than 30° cause the aircraft/autopilot model to encounter rate limits. This suggests that the PFF controller is being driven harder with the optimal gains than it is with the baseline gains.

As with the *tight* formation, the optimal PFF controller design remains fairly robust over a wide variety of *loose* formation maneuvers and geometry changes.

Loose Formation Single Maneuver Results						
Maneuver	X Cost	Y Cost	Energy Cost	Total Cost	Sat	Compare
30° left	147.62	1.11	89.21	237.94	L=NL	better
30° right	80.52	1.36	46.69	128.57	L=NL	better
45° left	231.31	1.53	136.83	369.67	L	better
	231.31	1.53	104.09	336.92	NL	
45° right	103.20	2.08	56.91	162.18	L=NL	better
60° left	313.84	1.87	180.70	496.41	L	better
	313.84	1.87	236.06	551.77	NL	
60° right	120.05	2.81	62.19	185.05	L=NL	better
alt	0	0	356.56	356.56	L=NL	same
vel dn	55.56	0	570.99	626.55	L=NL	better
vel up	55.55	0	628.32	683.86	L=NL	better
rvuphdn	113.54	1.33	247.32	362.19	L=NL	better
trail_60	96.87	2.35	60.32	159.54	L=NL	better
LD_trail	8.27	96.48	8.18	112.93	L=NL	better
trail_LD	16.90	96.48	12.80	126.18	L=NL	better
LD_RD	24.46	383.35	18.51	426.33	L=NL	better
x dec	483.83	0	224.76	708.60	L=NL	better
x inc	633.50	0	159.57	793.06	L=NL	better
LD_RD_30L	95.63	384.53	66.71	546.87	L=NL	better
LD_RD_30R	48.66	382.02	28.33	459.00	L=NL	better
LD_RD_45L	135.20	385.04	94.78	615.02	L	better
	135.20	385.04	93.87	614.11	NL	
LD_RD_45R	35.60	381.36	28.64	445.60	L=NL	better
LD_RD_60L	165.32	385.51	115.69	666.52	L	better
	165.32	385.51	107.65	658.48	NL	
LD_RD_60R	56.13	369.17	65.42	490.72	L=NL	worse

Table 6.5   Costs Due to Single Maneuvers of the *Loose* Formation Using Optimal Gains (PFF)

Loose Formation Dual Maneuver Results						
Maneuver	X Cost	Y Cost	Energy Cost	Total Cost	Sat	Compare
30° left	114.16	1.23	68.24	183.63	L=NL	better
30° right	114.12	1.23	68.12	183.47	L=NL	better
45° left	167.39	1.80	97.49	266.68	L	better
	167.39	1.80	81.11	250.30	NL	
45° right	167.31	1.80	97.26	266.37	L	better
	167.31	1.80	80.86	249.97	NL	
60° left	217.12	2.34	122.52	341.98	L	better
	217.12	2.34	150.21	369.66	NL	
60° right	216.99	2.34	122.13	341.46	L	better
	216.99	2.34	150.34	369.67	NL	
alt	0	0	356.62	356.62	L=NL	same
vel dn	55.58	0	578.56	634.14	L=NL	better
vel up	55.57	0	621.49	677.07	L=NL	better
LD_trail	12.59	1.12	10.49	24.19	L=NL	better
trail_LD	12.60	1.12	10.45	24.17	L=NL	better
LD_RD	24.61	2.20	18.38	45.20	L=NL	better
x dec	333.71	0	192.45	526.16	L=NL	better
x inc	333.61	0	193.89	527.50	L=NL	better

Table 6.6 Costs Due to Dual Maneuvers of the *Loose* Formation Using Optimal Gains (PFF)

6.4 PIFF Design Optimization

The optimal gains for the PIFF controller design, K_x^*, K_y^*, and K_{yi}^*, are listed in Table 6.7. These optimal gains for the *loose* formation controller are determined in the same manner as for the *tight* formation PIFF controller, see Chapter V. The optimal x-channel PIFF gain is the same as in the PFF optimization since the x-channel is not modified.

Parameter	Value
K_x^*	0.03
K_y^*	1.00
K_{yi}^*	0.75

Table 6.7 Optimal Gains For PIFF

The results for single formation change maneuvers are listed in Table 6.8, and the results for dual formation changes are listed in Table 6.9. The first column under the "Compare" heading is the optimal PIFF comparison with the PFF baseline, and the second column is the optimal PIFF comparison with the PFF with optimal gains.

The optimal PIFF controller gains costs are better than the baseline for all the formation changes, except altitude. The altitude maneuver costs remain the same since the altitude channel is not varied. Furthermore, there is only one instance for which the optimized PIFF controller costs are worse than the optimized PFF controller costs. The 60° right turn maneuver is the only formation change which costs more with the optimal PIFF gains. Simulations involving left turns of greater than 30° cause the aircraft/autopilot model to encounter rate limits. This suggests that the PIFF controller, like the PFF controller, is being driven hard. This should come as no surprise, since one explicitly accounts for the saturation in the optimization. This affords more aggressive control in the presence of saturation, as opposed to more ad hoc approaches, where saturation is only implicitly acknowledged or is being avoided. The payoff is improved performance.

As with the *tight* formation, the optimal PIFF controller design applied to the *loose* formation is able to perform well despite receiving less feedforward information than the PFF controller design.

Loose Formation Single Maneuver Results						
Maneuver	X Cost	Y Cost	Energy Cost	Total Cost	Sat	Compare
30° left	147.06	0.27	89.01	236.33	L=NL	better/better
30° right	81.11	0.27	47.23	128.60	L=NL	better/close
45° left	230.18	0.40	136.35	366.92	L	better/better
	230.18	0.40	103.37	333.96	NL	
45° right	104.41	0.40	57.91	162.72	L=NL	better/close
60° left	312.09	0.53	179.92	492.54	L	better/better
	312.09	0.53	232.54	545.16	NL	
60° right	122.02	0.53	63.68	186.23	L=NL	better/worse
alt	0	0	356.56	356.56	L=NL	same/same
vel dn	55.56	0	570.99	626.55	L=NL	better/same
vel up	55.55	0	628.32	683.86	L=NL	better/same
rvuphdn	114.12	0.27	247.82	362.21	L=NL	better/close
trail_60	95.00	0.53	59.21	154.74	L=NL	better/better
LD_trail	8.28	95.72	8.19	112.19	L=NL	better/close
trail_LD	16.99	95.72	12.89	125.60	L=NL	better/close
LD_RD	24.55	381.51	18.61	424.66	L=NL	better/better
x dec	483.83	0	224.76	708.60	L=NL	better/same
x inc	633.50	0	159.57	793.06	L=NL	better/same
LD_RD_30L	94.80	381.25	66.30	542.35	L=NL	better/better
LD_RD_30R	48.95	381.77	28.44	459.15	L=NL	better/close
LD_RD_45L	133.54	381.13	93.88	608.54	L	better/better
	133.54	381.13	93.28	607.95	NL	
LD_RD_45R	35.93	381.90	28.59	446.42	L=NL	better/close
LD_RD_60L	162.75	381.00	114.29	658.04	L	better/better
	162.75	381.00	107.76	651.51	NL	
LD_RD_60R	44.26	382.04	43.15	469.45	L=NL	better/better

Table 6.8 Costs Due to Single Maneuvers of the *Loose* Formation Using Optimal Gains (PIFF)

Loose Formation Dual Maneuver Results						
Maneuver	X Cost	Y Cost	Energy Cost	Total Cost	Sat	Compare
30° left	114.17	0.27	68.40	182.84	L=NL	better/close
30° right	114.14	0.27	68.29	182.67	L=NL	better/close
45° left	167.43	0.40	97.74	265.57	L	better/better
	167.43	0.40	81.25	249.07	NL	
45° right	167.35	0.40	97.52	265.28	L	better/better
	167.35	0.40	81.00	248.75	NL	
60° left	217.23	0.53	122.87	340.63	L	better/better
	217.23	0.53	149.18	366.94	NL	
60° right	217.11	0.53	122.48	340.12	L	better/better
	217.11	0.53	149.31	366.95	NL	
alt	0	0	356.62	356.62	L=NL	better/same
vel dn	55.58	0	578.56	634.14	L=NL	better/same
vel up	55.57	0	621.49	677.07	L=NL	better/same
LD_trail	12.64	0.58	10.54	23.76	L=NL	better/close
trail_LD	12.65	0.58	10.50	23.73	L=NL	better/close
LD_RD	24.70	0.59	18.48	43.77	L=NL	better/better
x dec	333.71	0	192.45	526.16	L=NL	better/same
x inc	333.61	0	193.89	527.50	L=NL	better/same

Table 6.9   Costs Due to Dual Maneuvers of the *Loose* Formation Using Optimal Gains (PIFF)

6.5 Formation Changes/Maneuvers Optimization

Further insight is gained by comparing nonlinear formation responses during *loose* formations for the PFF baseline, optimized PFF, and optimized PIFF controllers. For selected formation changes, the wing aircraft/autopilot responses, wing aircraft/autopilot rates, and lead aircraft/autopilot responses are plotted. Lissajous figures, that show the variation in both x and y-separation distances during formation maneuvers, are also included. For all nonlinear simulation responses, the following legend is used:

PFF (Baseline):   "___"

PFF (Optimal):   "_ _ _"

PIFF (Optimal):   ". . ."

The units for each formation change response plot remains consistent; where heading change angles are in units of *degrees* (*deg*), altitude and separation distances are in units of *feet* (*ft*), and velocities and rates are in units of *feet per second* (*fps*). The lead aircraft/autopilot is not effected by changes in the formation autopilot residing on the wing aircraft, so only one lead aircraft/autopilot response appears in each nonlinear simulations. For the wing aircraft/autopilot rate, the plotted data is sampled before the limits are imposed to show how heavy into saturation the rates would go if clipping does not occur.

6.5.1 Formation Maneuvers. Six different *loose* formation maneuvers are presented, including left and right heading changes, a velocity increase, an altitude increase, a heading change from trail, and a 3-D maneuver. The responses due to a 45° left turn maneuver are displayed in Figures (6.1) - (6.4). The wing aircraft/autopilot reaches positive altitude rate saturation during the 45° left turn maneuver.
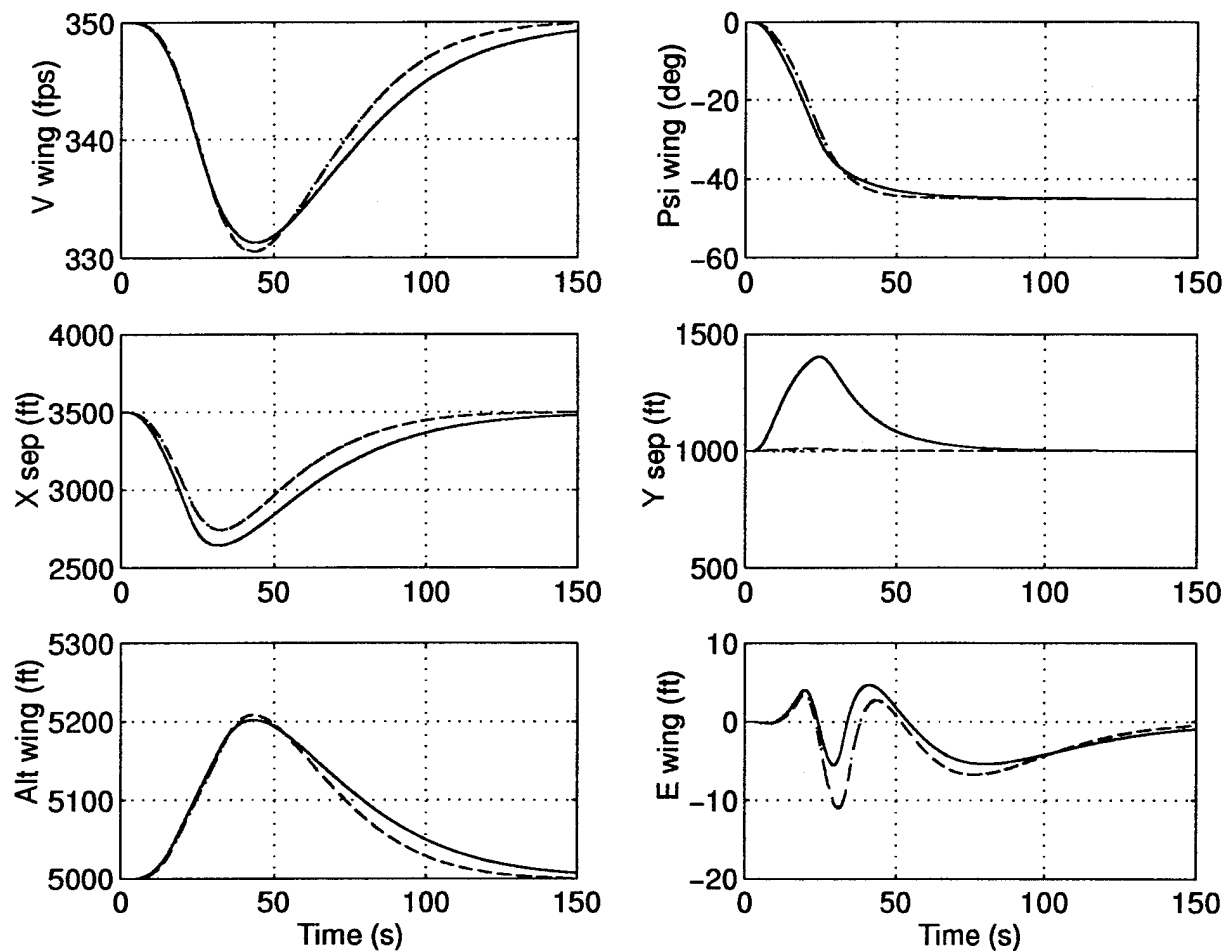

Figure 6.1   Wing Aircraft Responses for a 45° Left Turn (45° left) of the *Loose* Formation
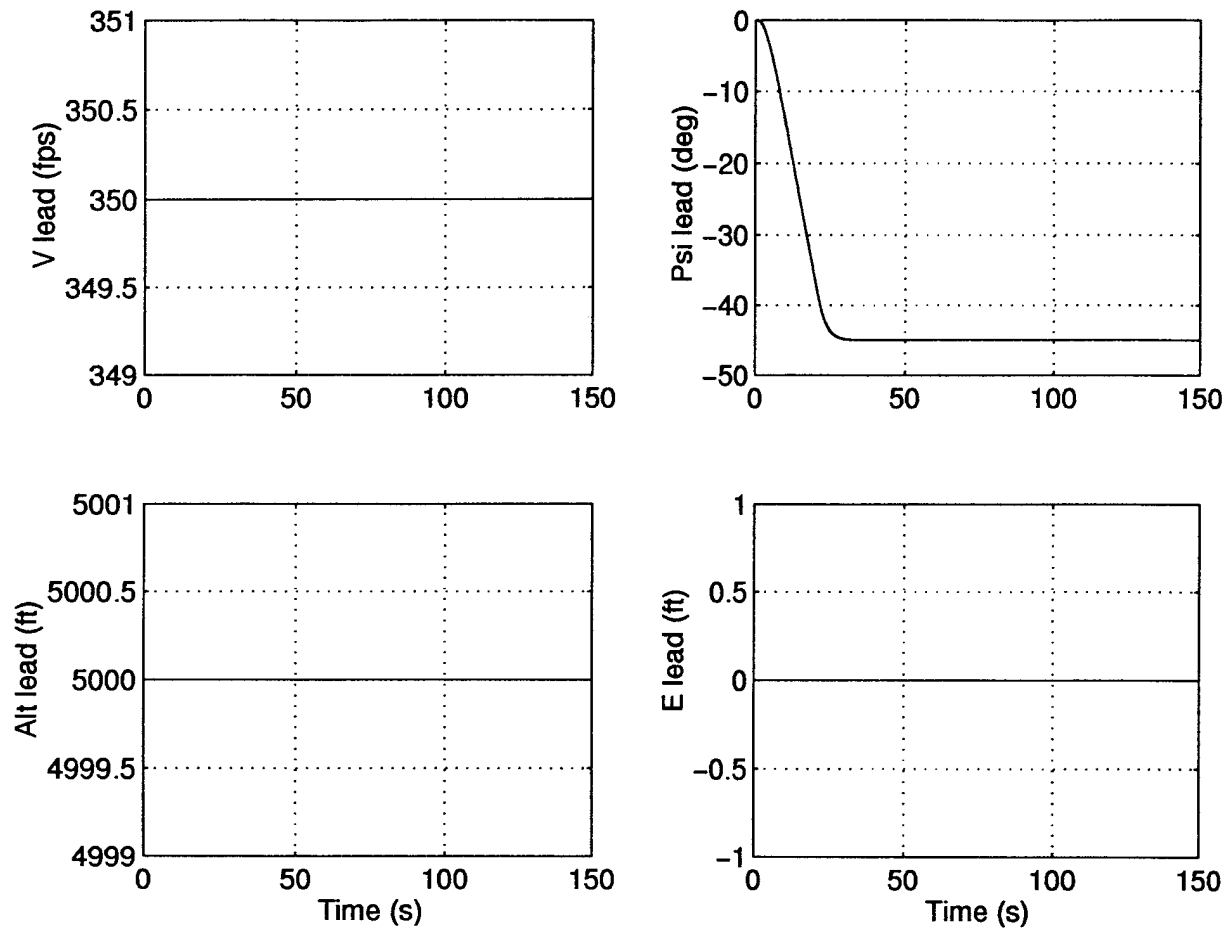
Figure 6.2   Lead Aircraft Responses for a 45° Left Turn (45° left) of the *Loose* Formation
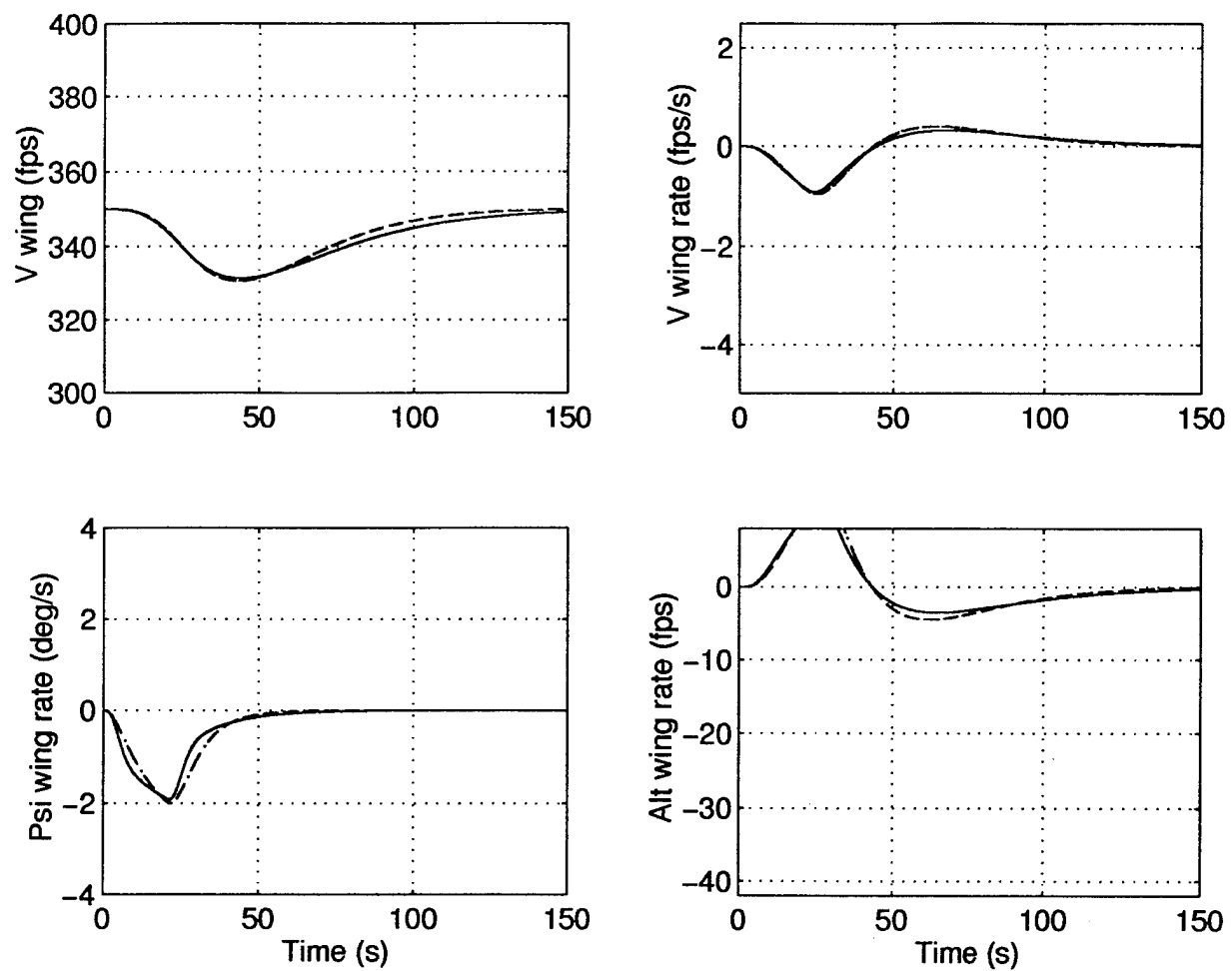
Figure 6.3   Rates of Wing Aircraft Responses for a 45° Left Turn (45° left) of the *Loose* Formation
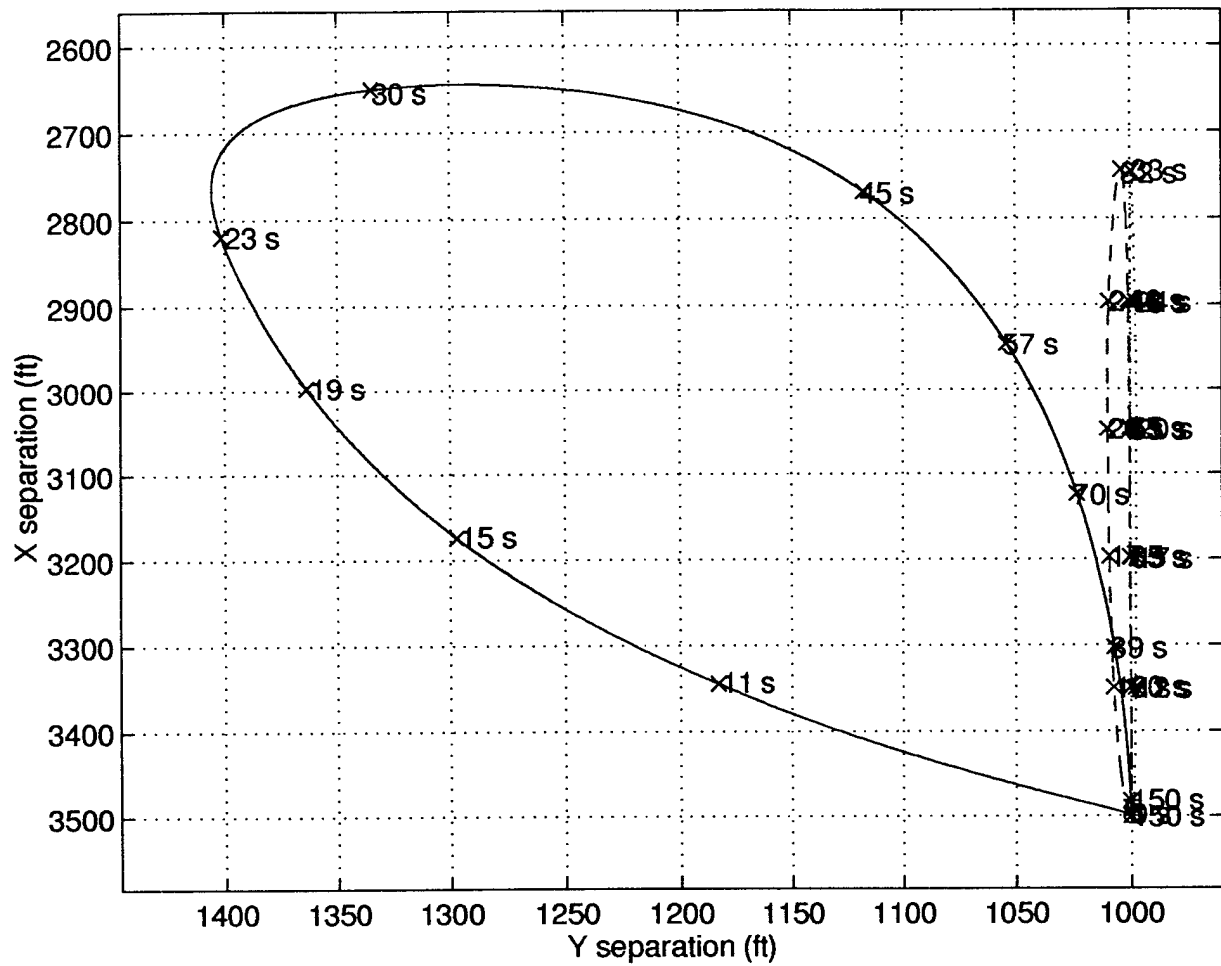
Figure 6.4   Lissajous Plots of Wing Aircraft Responses for a 45° Left Turn (45° left) of the *Loose* Formation

The responses due to a 45° right turn maneuver are displayed in Figures (6.5) - (6.8).
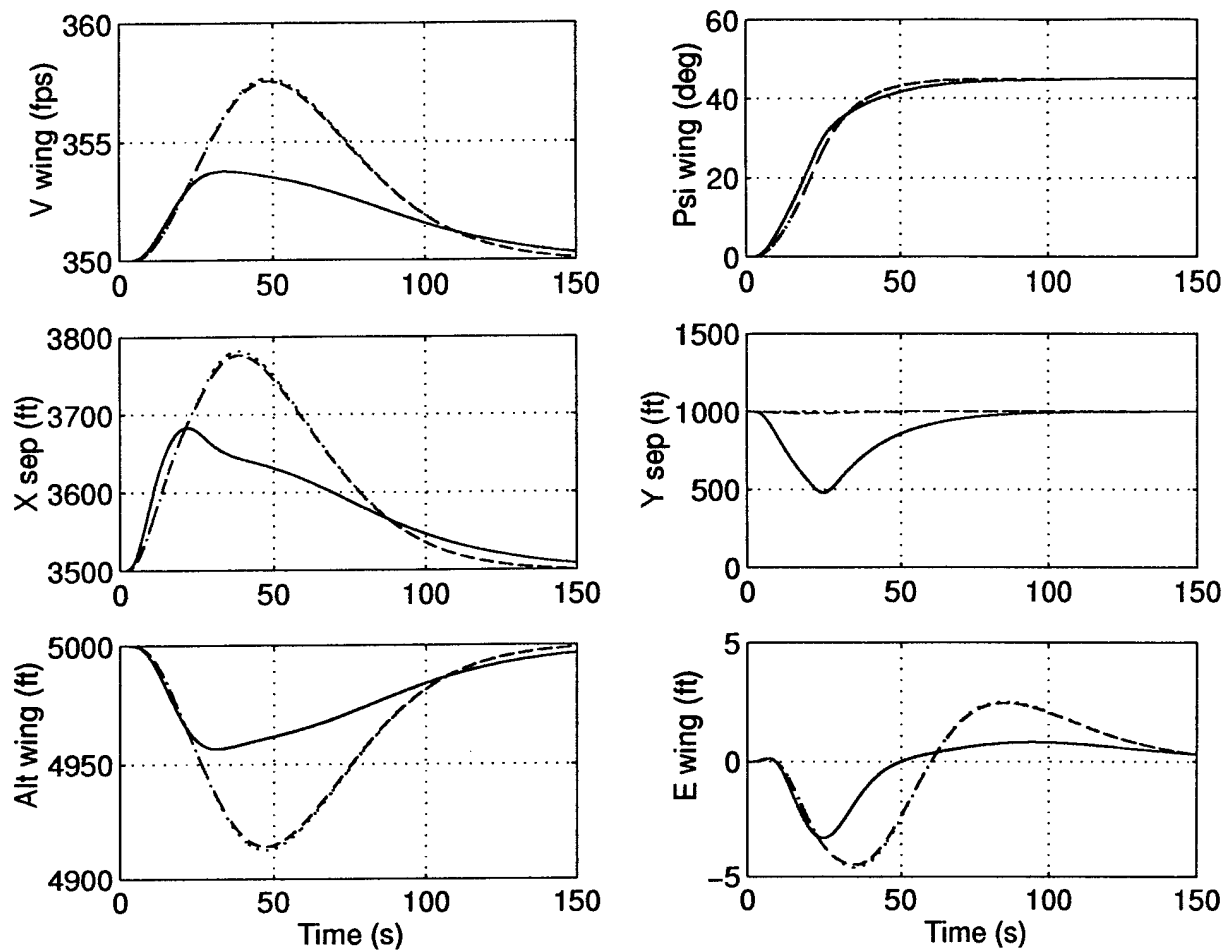

Figure 6.5 Wing Aircraft Responses for a 45° Right Turn (45° right) of the *Loose* Formation
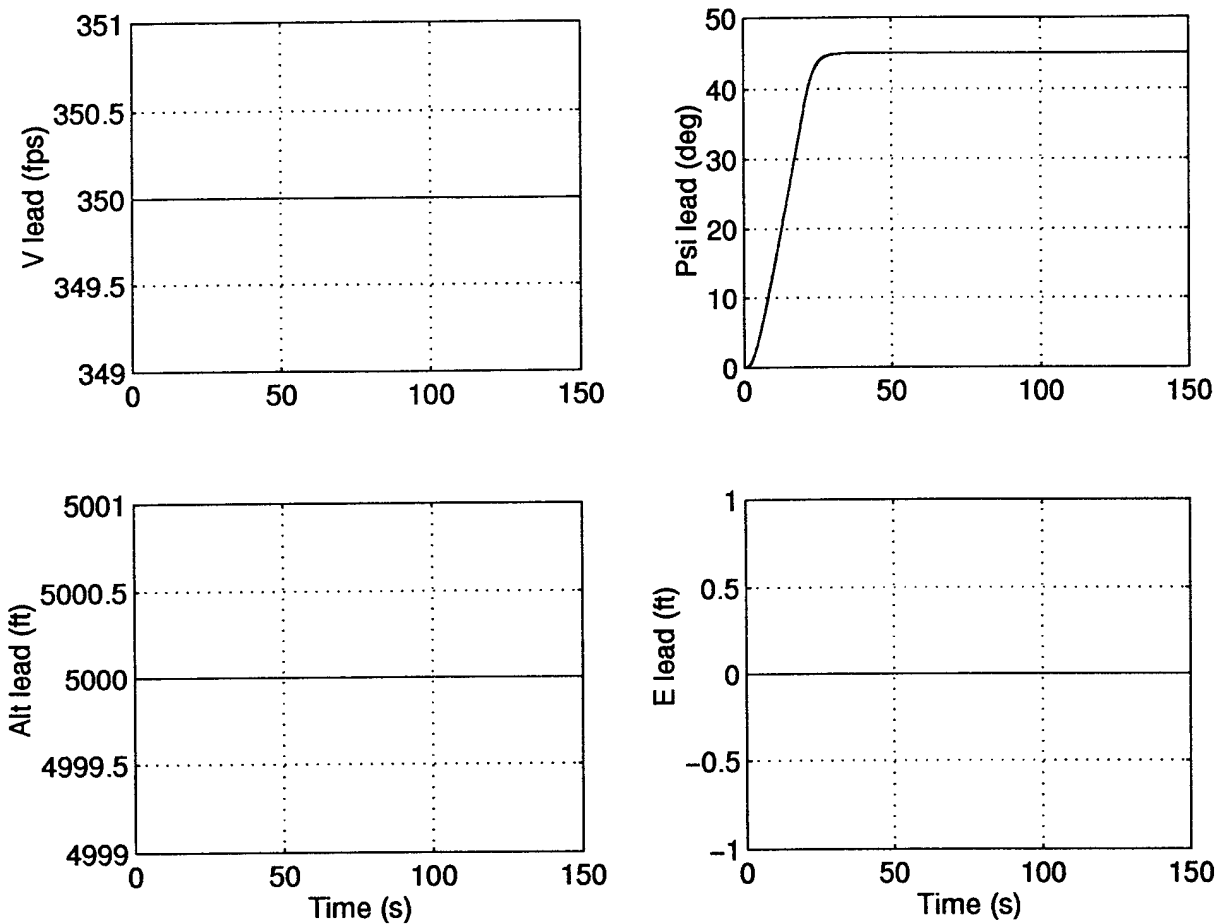
Figure 6.6   Lead Aircraft Responses for a 45° Right Turn (45° right) of the *Loose* Formation
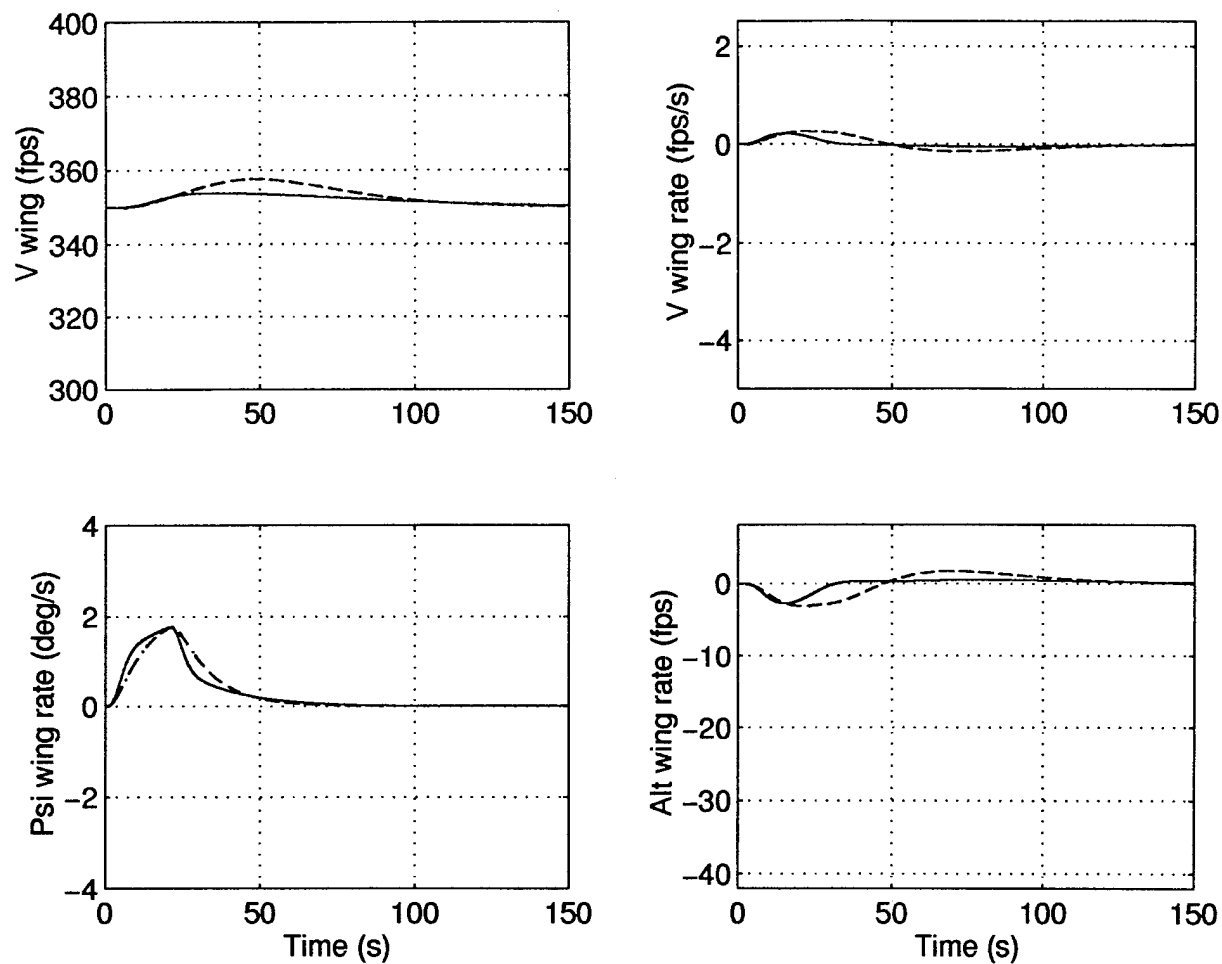
Figure 6.7   Rates of Wing Aircraft Responses for a 45° Right Turn (45° right) of the *Loose* Formation
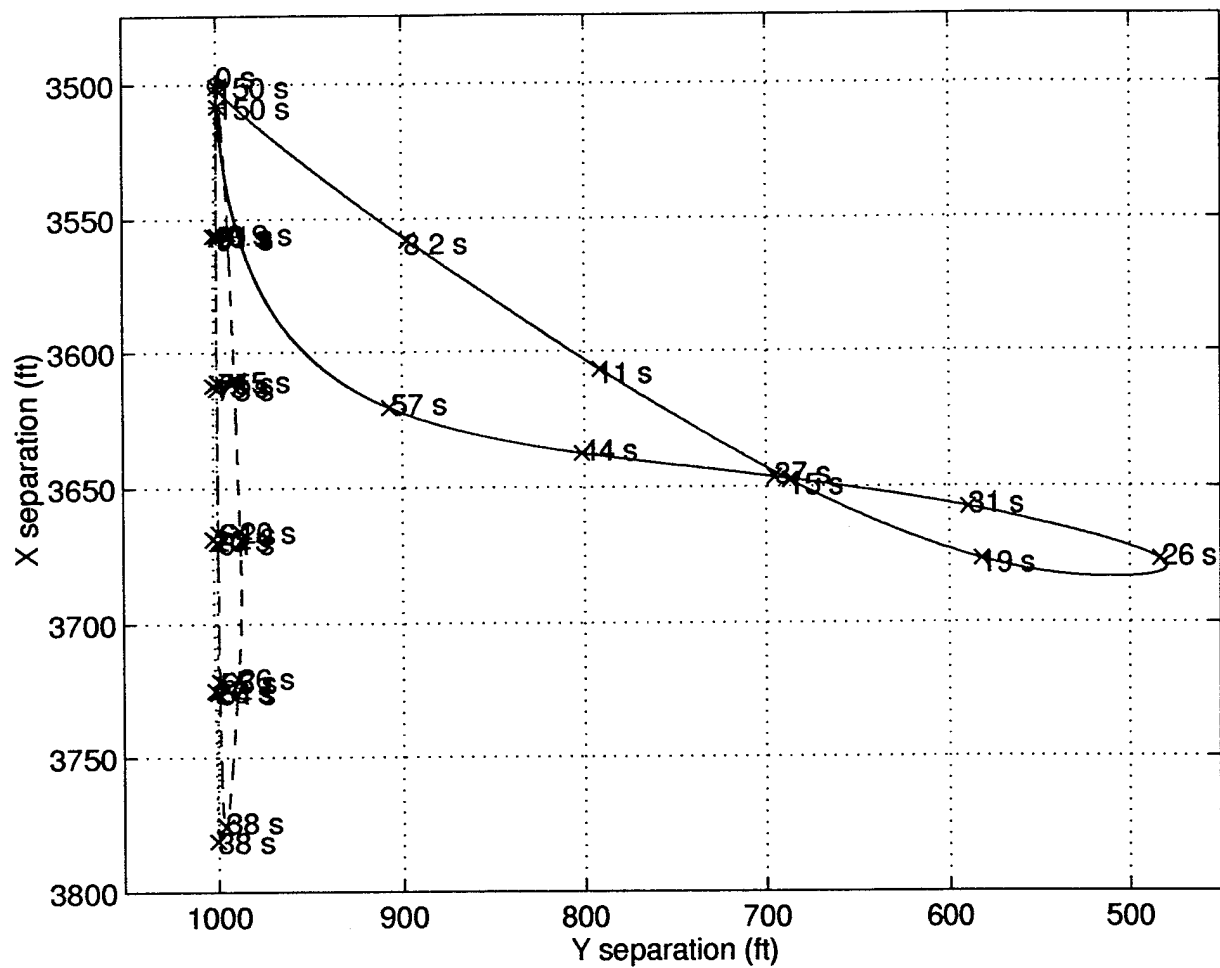
Figure 6.8   Lissajous Plots of Wing Aircraft Responses for a 45° Right Turn (45° right) of the *Loose* Formation

The responses due to a formation velocity increase of $25\frac{ft}{sec}$ (vel up) maneuver are displayed in Figures (6.9) - (6.11). The optimized PFF and PIFF formation flight controller responses coincide, since the x-channel characteristics of the two controllers are identical.

Figure 6.9 Wing Aircraft Responses for a $25\frac{ft}{sec}$ Velocity Increase (vel up) of the *Loose* Formation

Figure 6.10   Lead Aircraft Responses for a $25\frac{ft}{sec}$ Velocity Increase (vel up) of the *Loose* Formation
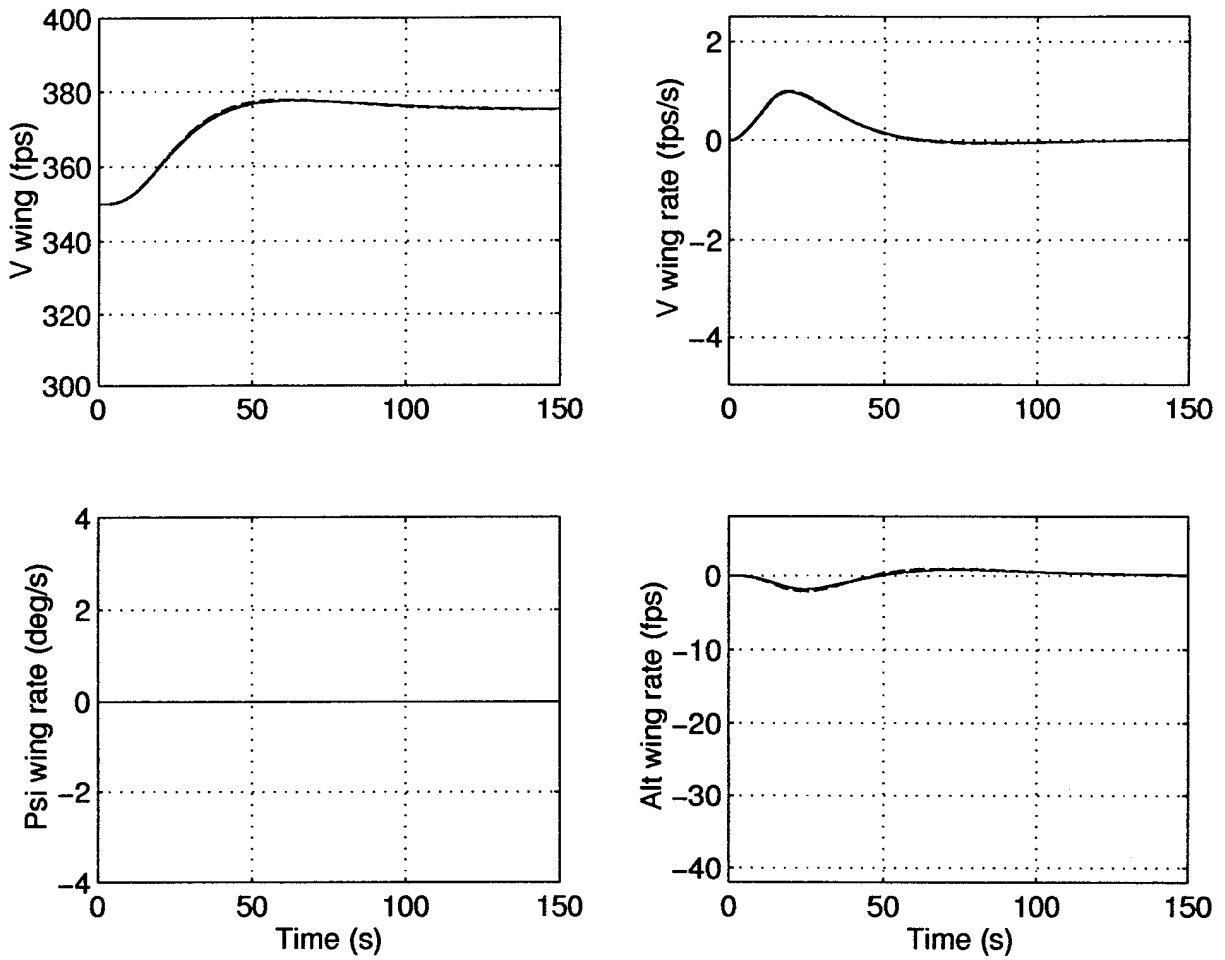
Figure 6.11   Rates of Wing Aircraft Responses for a $25\frac{ft}{sec}$ Velocity Increase (vel up) of the *Loose* Formation

The responses due to a altitude increase maneuver of $200\,ft$ (alt) are displayed in Figures (6.12) - (6.14). The optimized PFF and PIFF formation flight controller responses coincide, since the x-channel characteristics of the two controllers are identical.
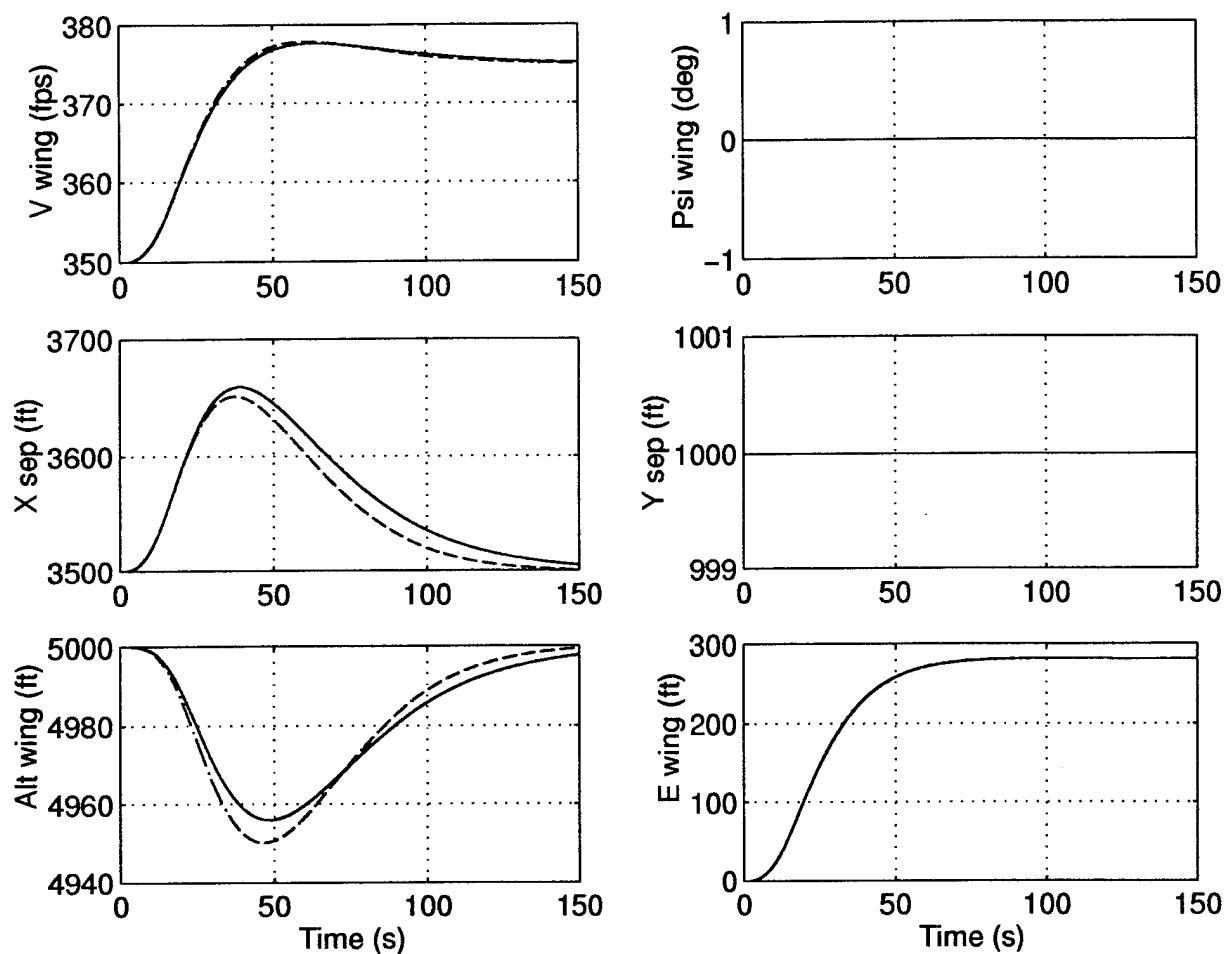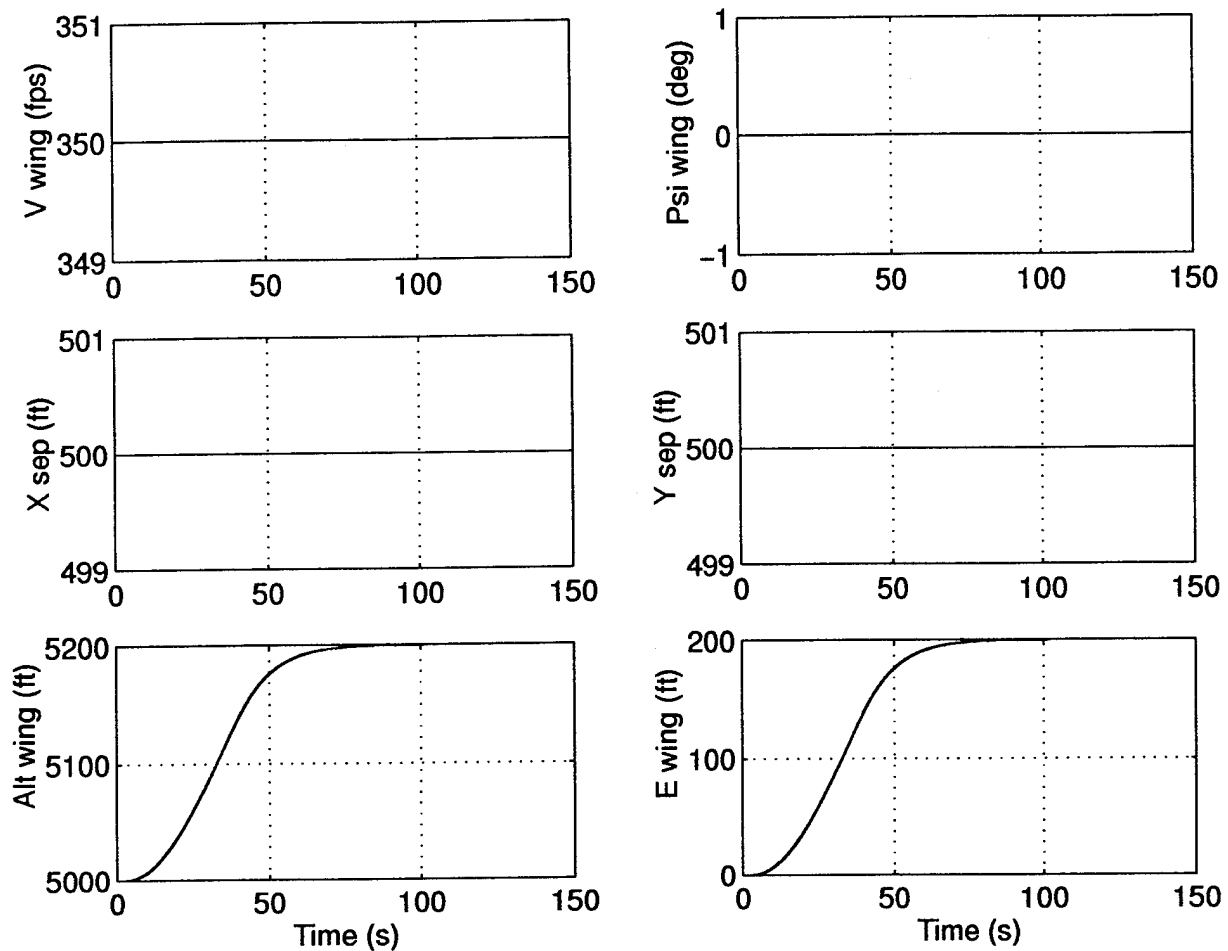

Figure 6.12   Wing Aircraft Responses for an $200\,ft$ Altitude Increase (alt) of the *Loose* Formation

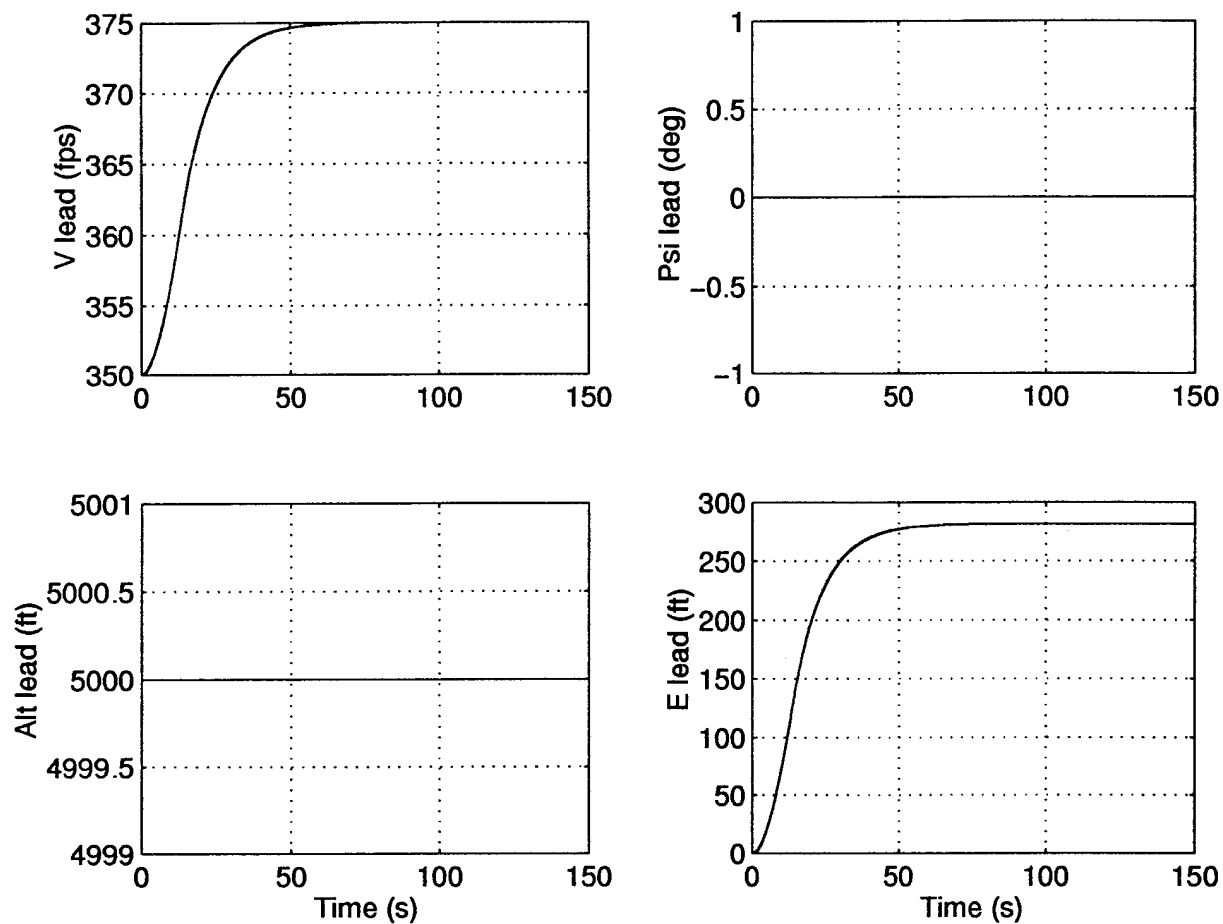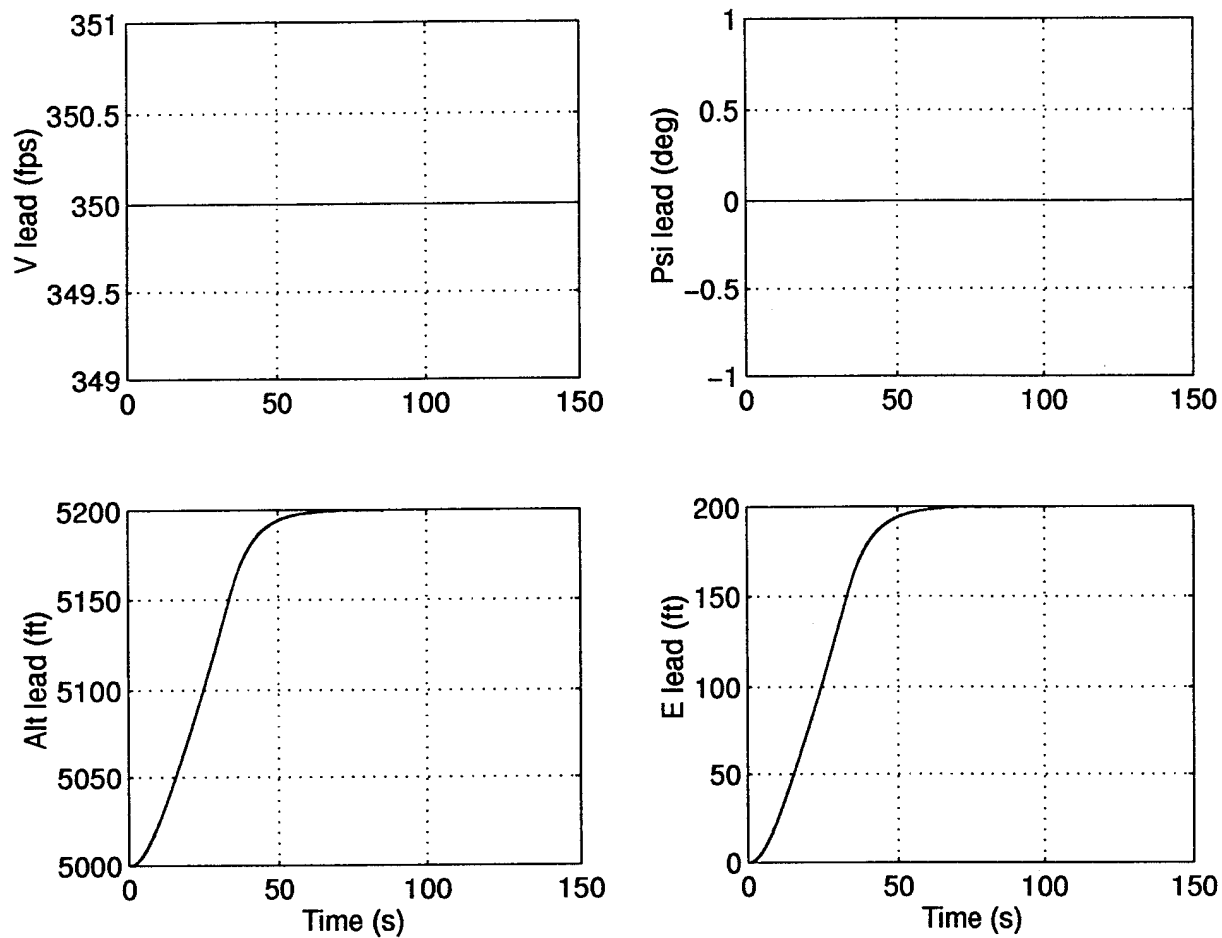Figure 6.13   Lead Aircraft Responses for an 200ft Altitude Increase (alt) of the *Loose* Formation
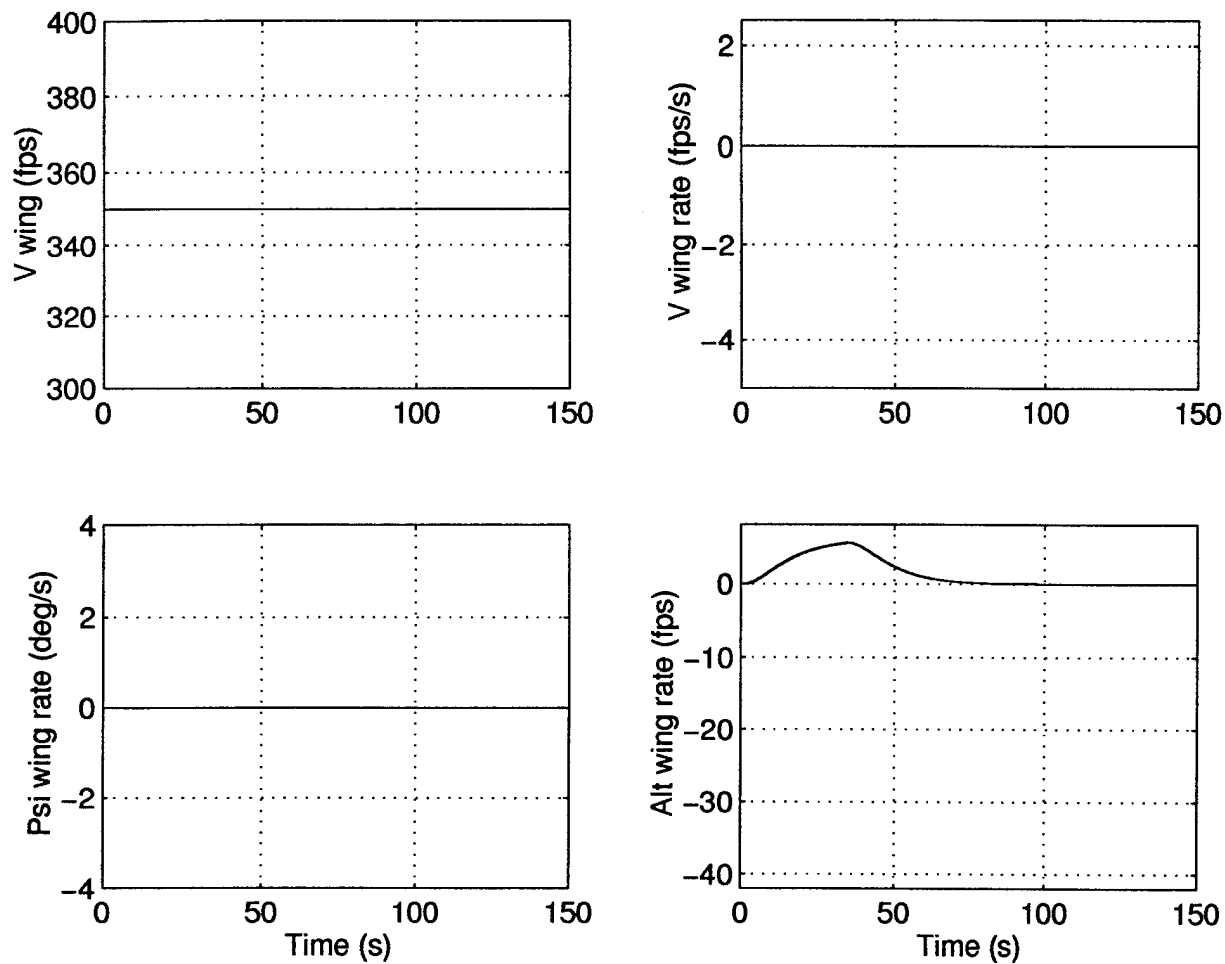
Figure 6.14   Rates of Wing Aircraft Responses for an 200 *ft* Altitude Increase (alt) of the *Loose* Formation

The responses during to a 60° left turn maneuver of a trail formation(trail_60) are displayed in Figures (6.15) - (6.18). By symmetry, a right turn maneuver of a trail formation is simply a mirror image of these responses and is not shown. The Lissajous Figure 6.18 shows that the PIFF controller design's largest improvement over the PFF design is in heading changes of the trail formation, regardless of the x-separation distance.
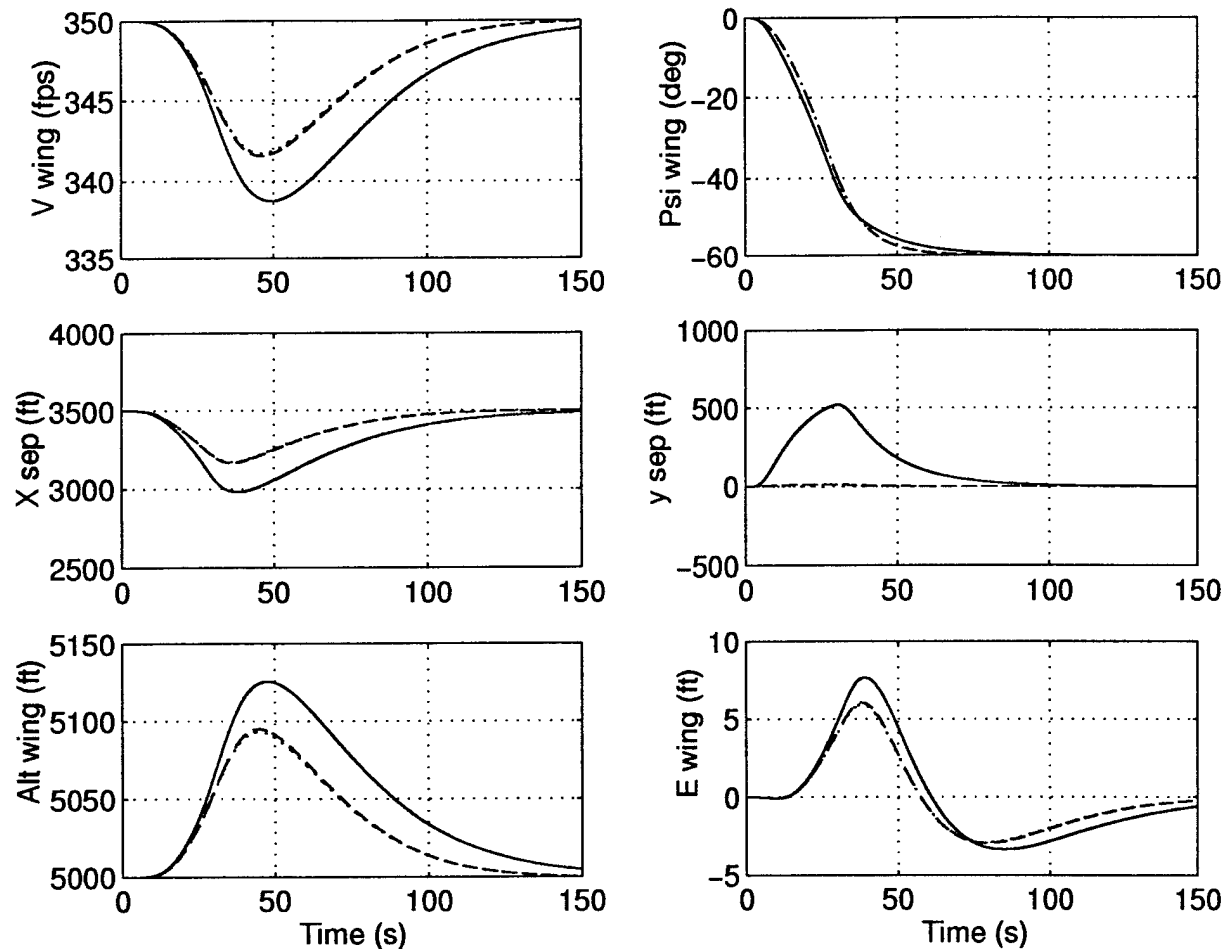
Figure 6.15   Wing Aircraft Responses for a 60° Left Turn of the *Loose* Trail Formation (trail_60)
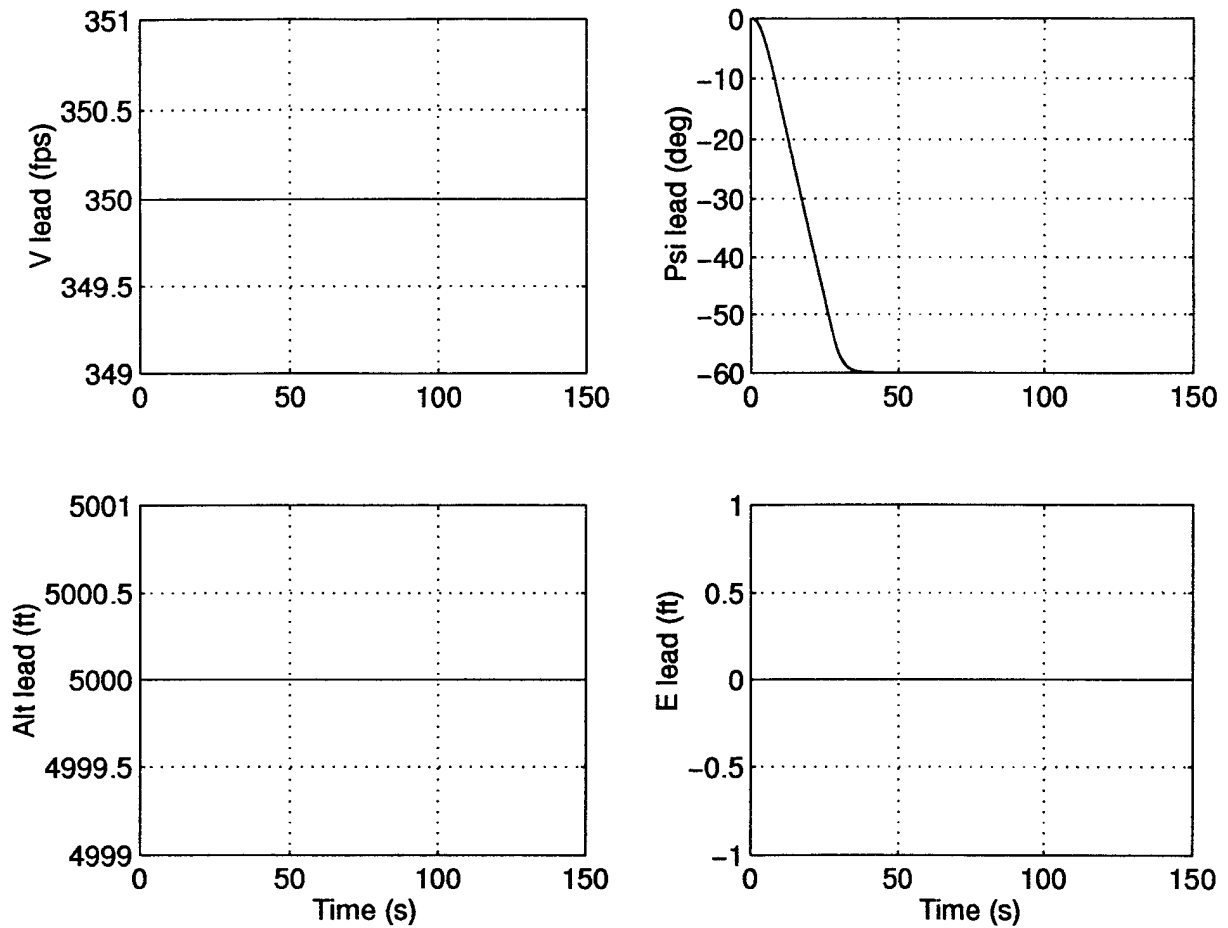
Figure 6.16   Lead Aircraft Responses for a 60° Left Turn of the *Loose* Trail Formation (trail_60)
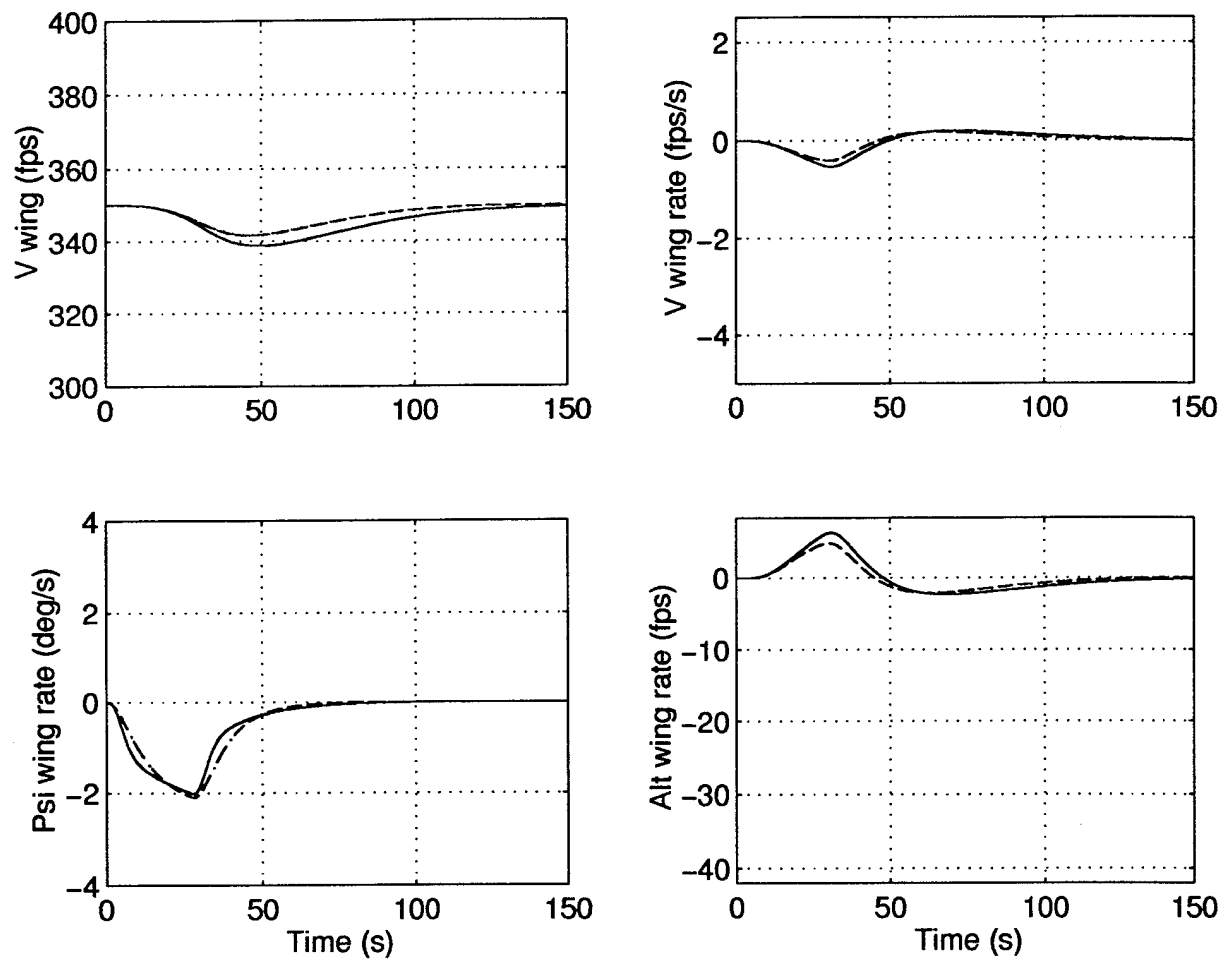
Figure 6.17   Rates of Wing Aircraft Responses for a 60° Left Turn of the *Loose* Trail
Formation (trail_60)
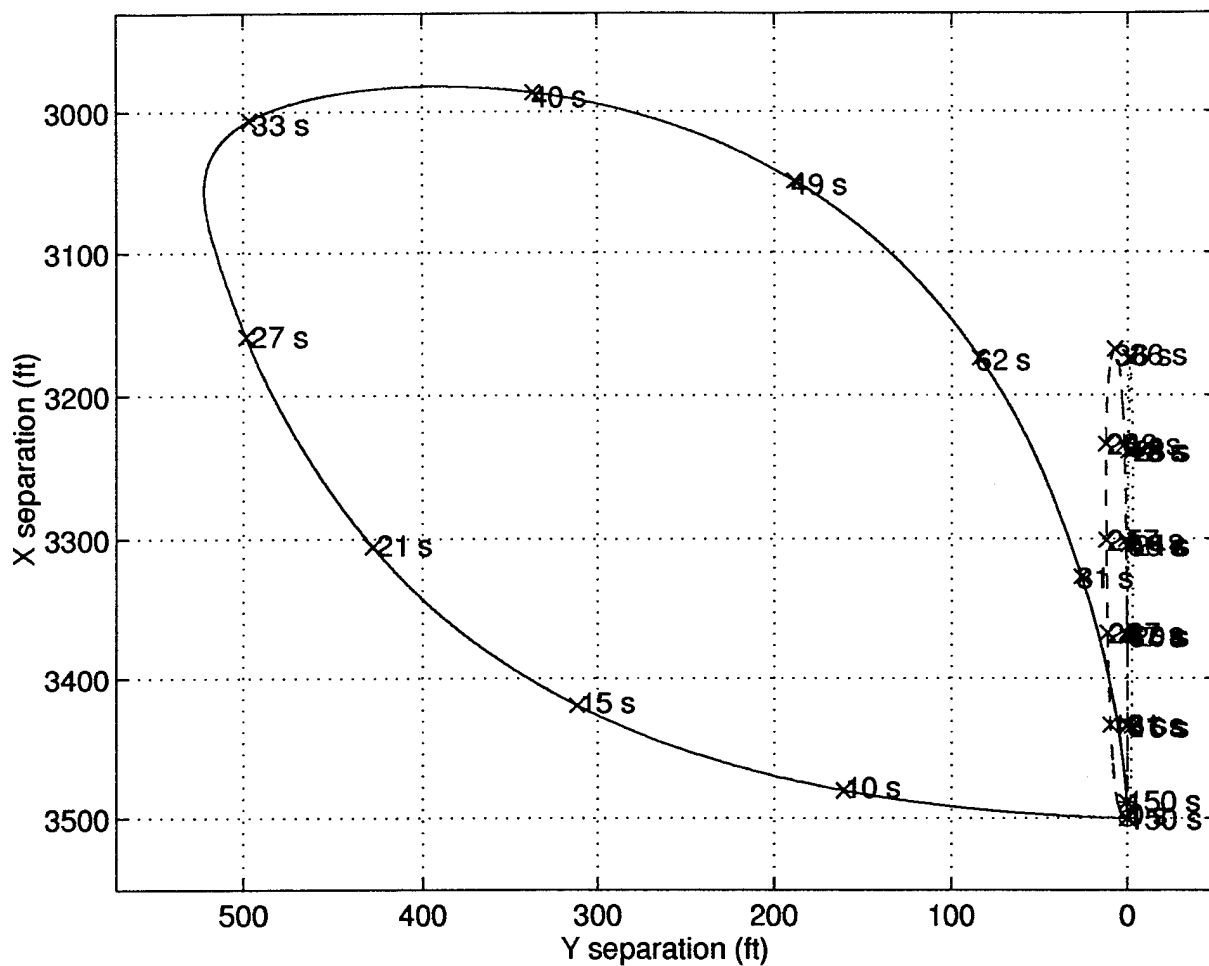
Figure 6.18   Lissajous Plots of Wing Aircraft Responses for a 60° Left Turn of the *Loose* Trail Formation (trail_60)

The responses due to a combined 30° right turn, velocity increase of $25\frac{ft}{sec}$, and altitude decrease of $100ft$ (rvuphdn) formation maneuver are displayed in Figures (6.19) - (6.22).
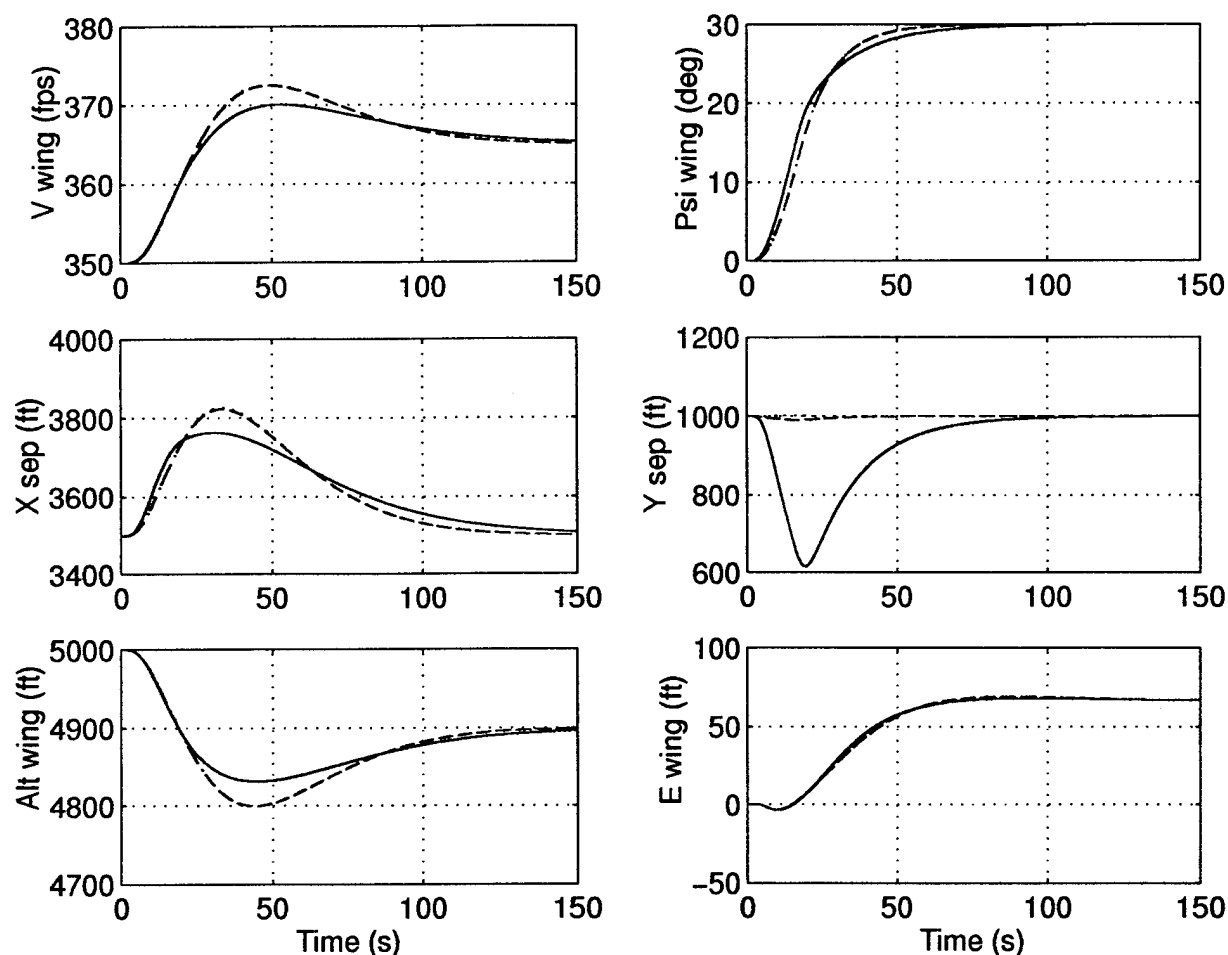
Figure 6.19   Wing Aircraft Responses for a 30° Right Turn, $25\frac{ft}{sec}$ Velocity Increase, and $100ft$ Altitude Decrease (rvuphdn) of the *Loose* Formation
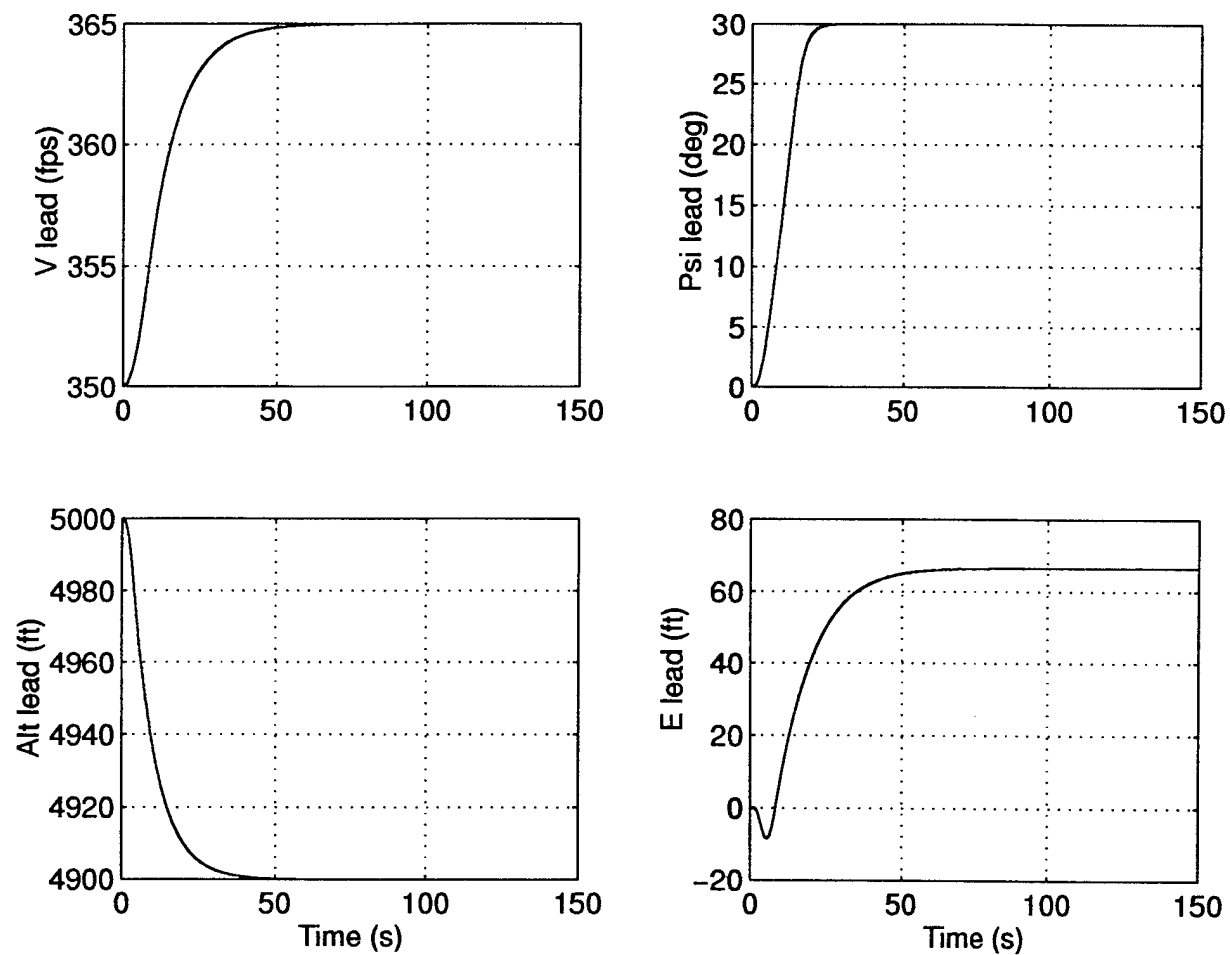
Figure 6.20   Lead Aircraft Responses for a 30° Right Turn, $25\frac{ft}{sec}$ Velocity Increase, and 100 ft Altitude Decrease (rvuphdn) of the *Loose* Formation
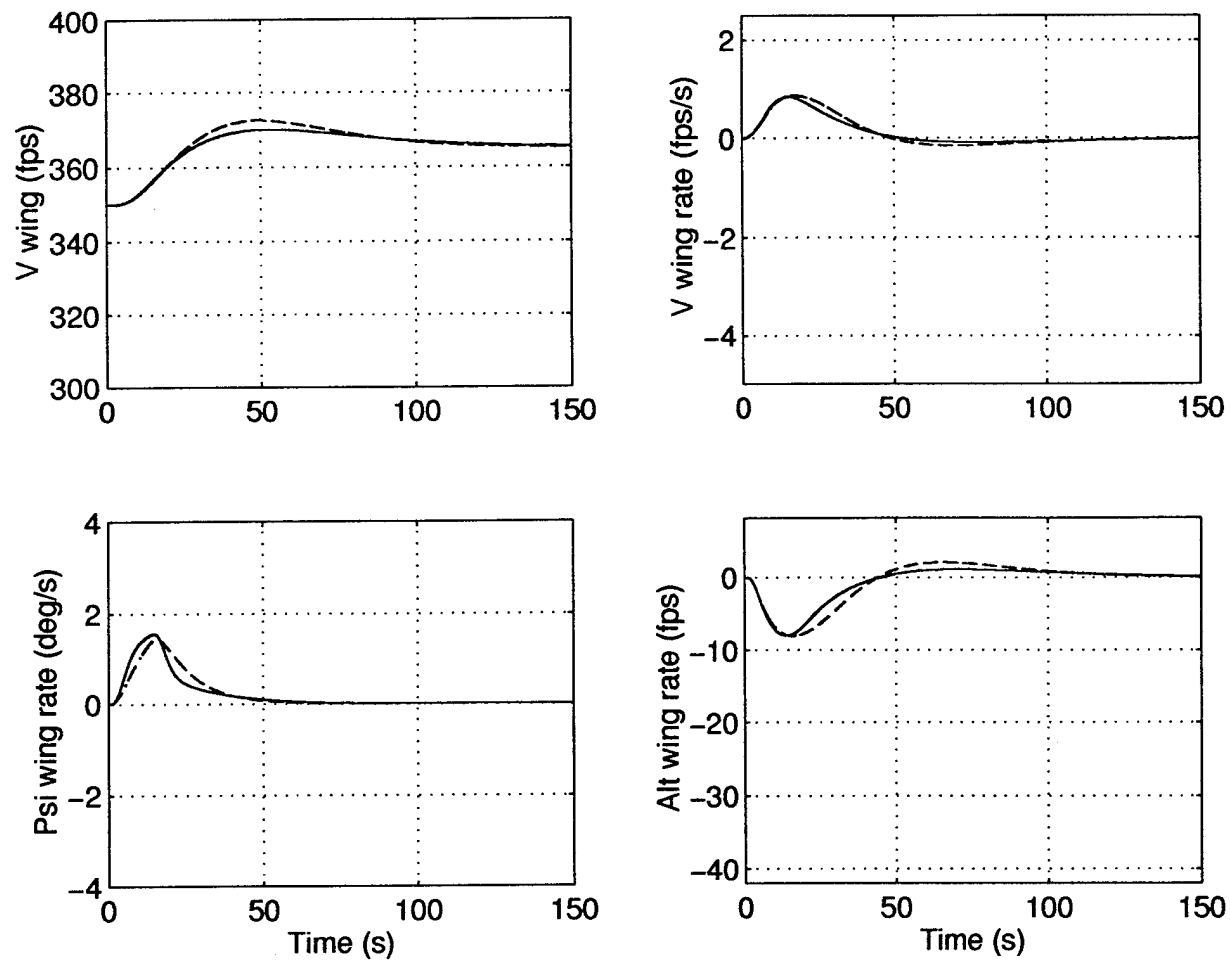
Figure 6.21   Rates of Wing Aircraft Responses for a 30° Right Turn, $25\frac{ft}{sec}$ Velocity Increase, and $100ft$ Altitude Decrease (rvuphdn) of the *Loose* Formation
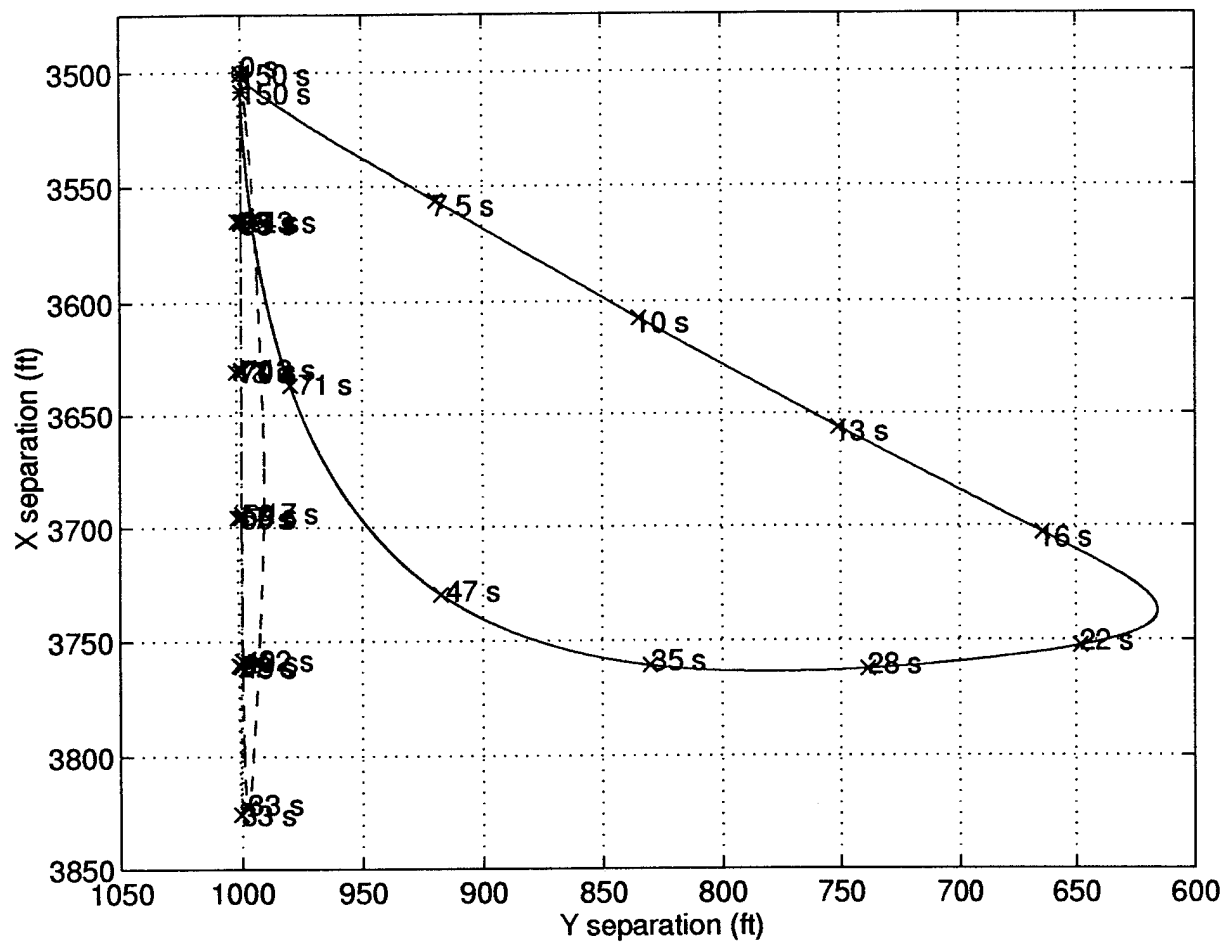
Figure 6.22   Lissajous Plots of Wing Aircraft Responses for a 30° Right Turn, $25\frac{ft}{sec}$ Velocity Increase, and $100\,ft$ Altitude Decrease (rvuphdn) of the *Loose* Formation

6.5.2 Formation Geometry Changes. The two different *loose* formation changes presented are a left diamond to trail and an increase in x-separation formation geometry change. The responses due to a left diamond to trail (LD_trail) geometry change are displayed in Figures (6.23) - (6.26). There is no change in the lead aircraft's heading, altitude, velocity, or energy, since the change in geometry is performed by the wing aircraft.
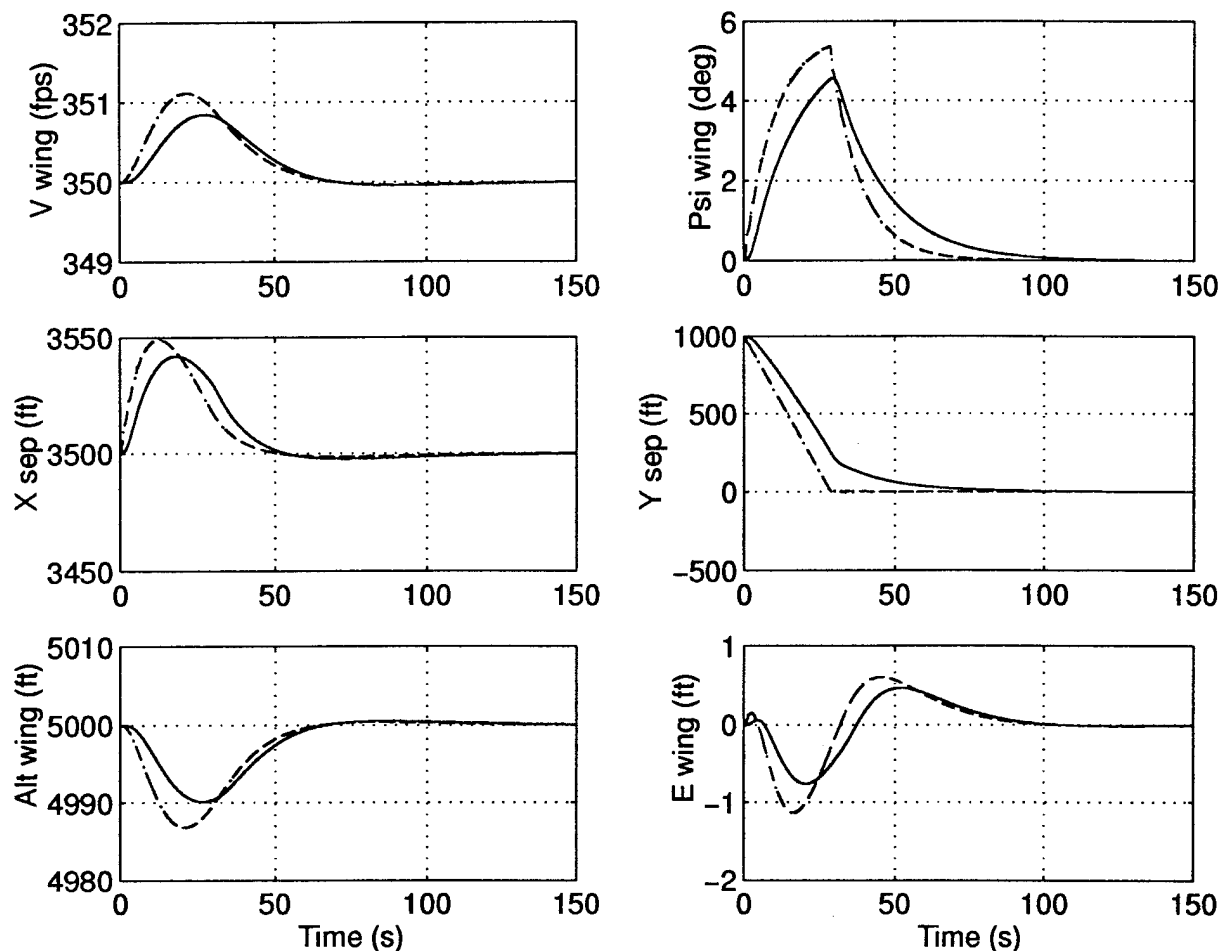
Figure 6.23   Wing Aircraft Responses for a Left Diamond to Trail Formation Geometry Change (LD_trail) of the *Loose* Formation
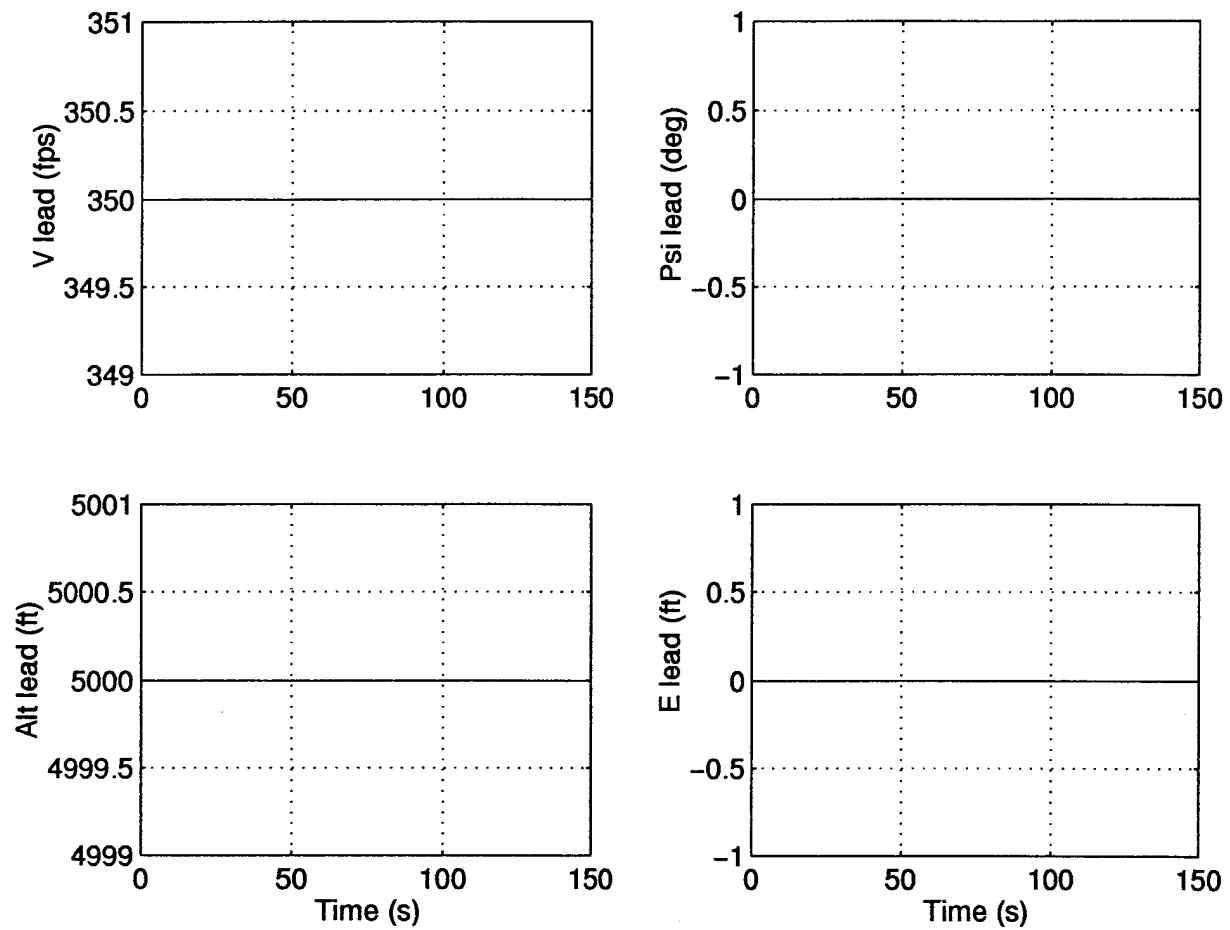
Figure 6.24   Lead Aircraft Responses for a Left Diamond to Trail Formation Geometry
Change (LD_trail) of the *Loose* Formation
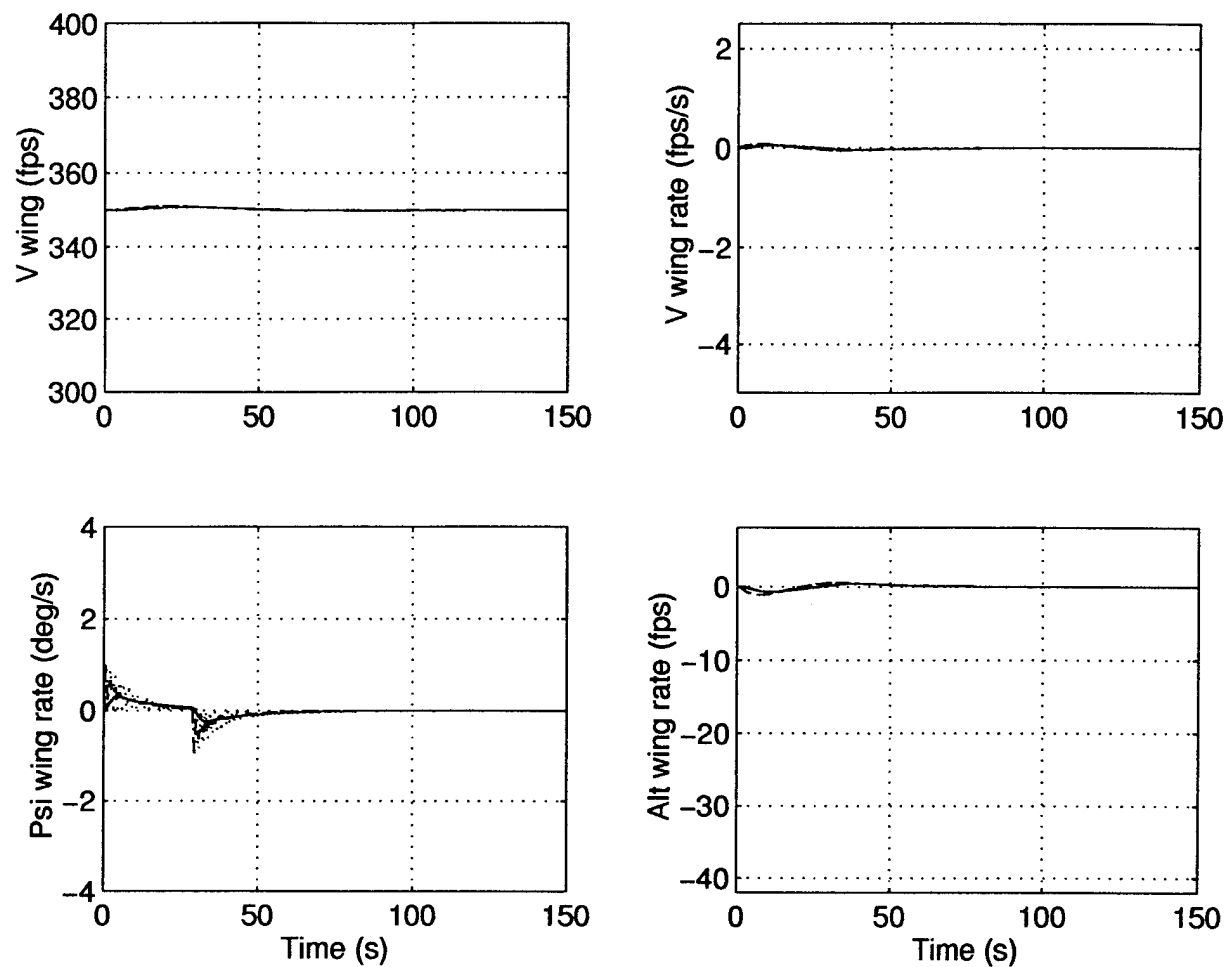
Figure 6.25   Rates of Wing Aircraft Responses for a Left Diamond to Trail Formation
Geometry Change (LD_trail) of the *Loose* Formation
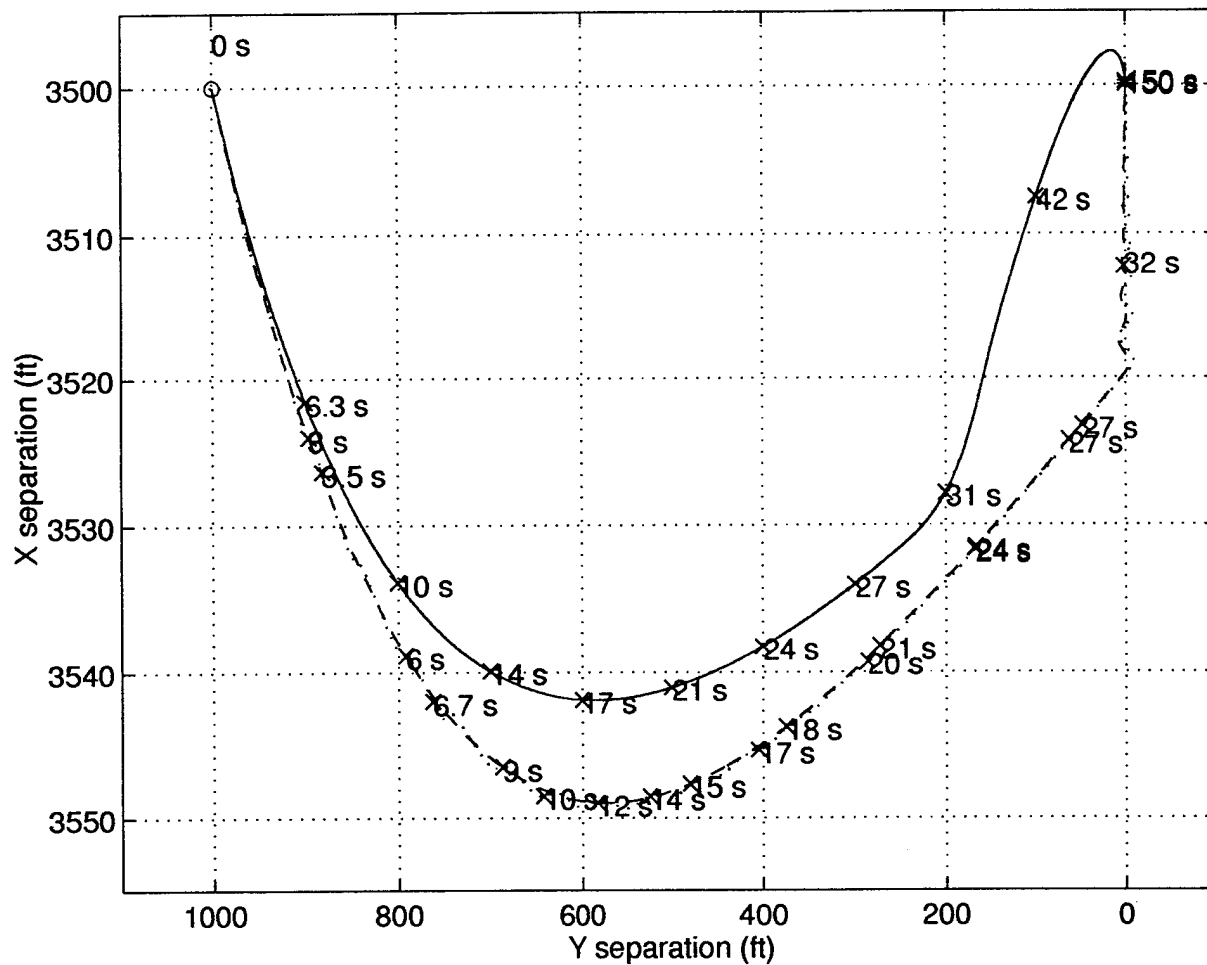
Figure 6.26   Lissajous Plots of Wing Aircraft Responses for a Left Diamond to Trail
Formation Geometry Change (LD_trail) of the *Loose* Formation

The responses due to an increase in x-separation from $3500ft$ to $5000ft$ (x inc) formation geometry change are displayed in Figures (6.27) - (6.29). There is no change in the lead aircraft's heading, altitude, velocity, or energy, since the change in geometry is performed by the wing aircraft. The optimized PFF and PIFF formation flight controller responses coincide, since the x-channel characteristics of the two controllers are identical.
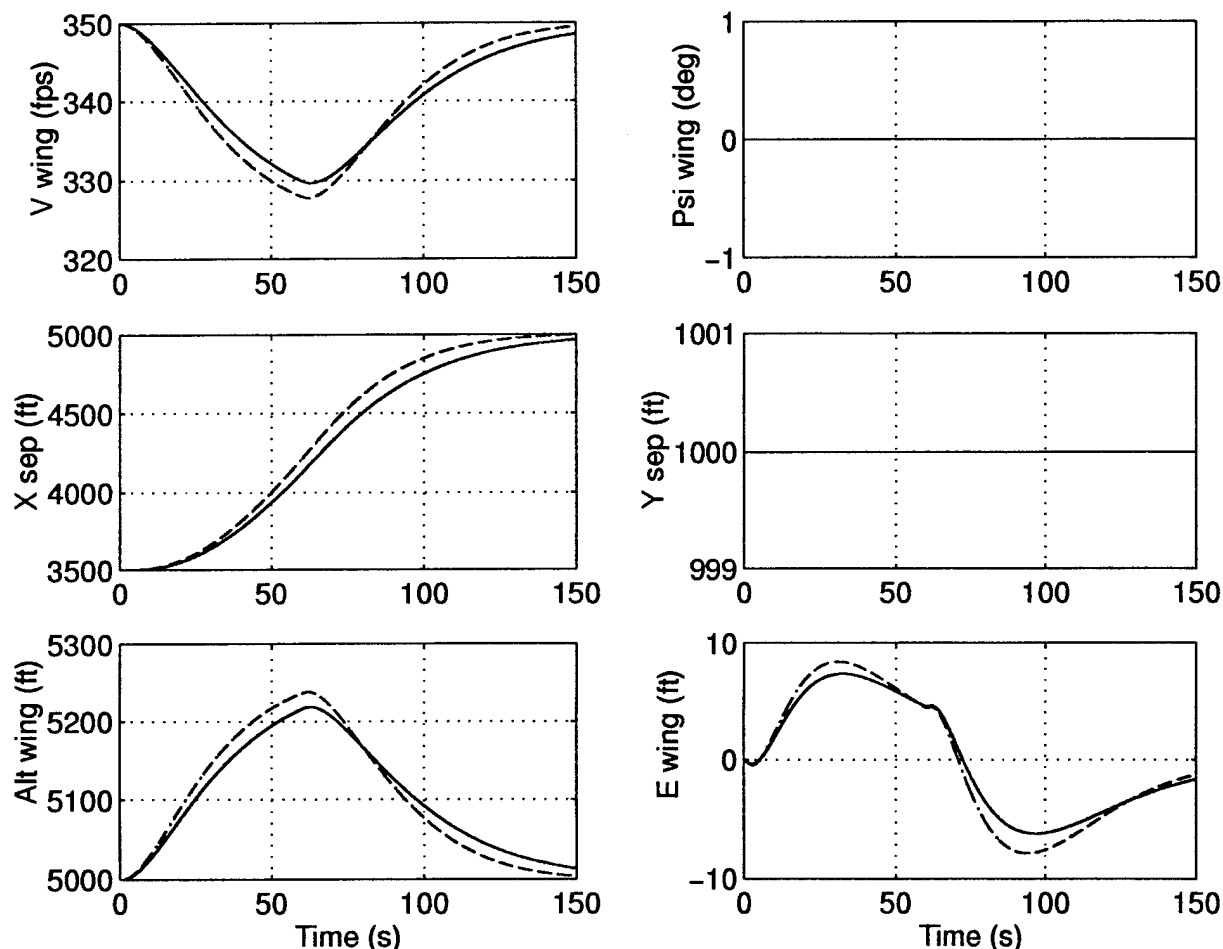
Figure 6.27   Wing Aircraft Responses for an Increase in X-Separation from $3500ft$ to $5000ft$ (x inc) of the *Loose* Formation
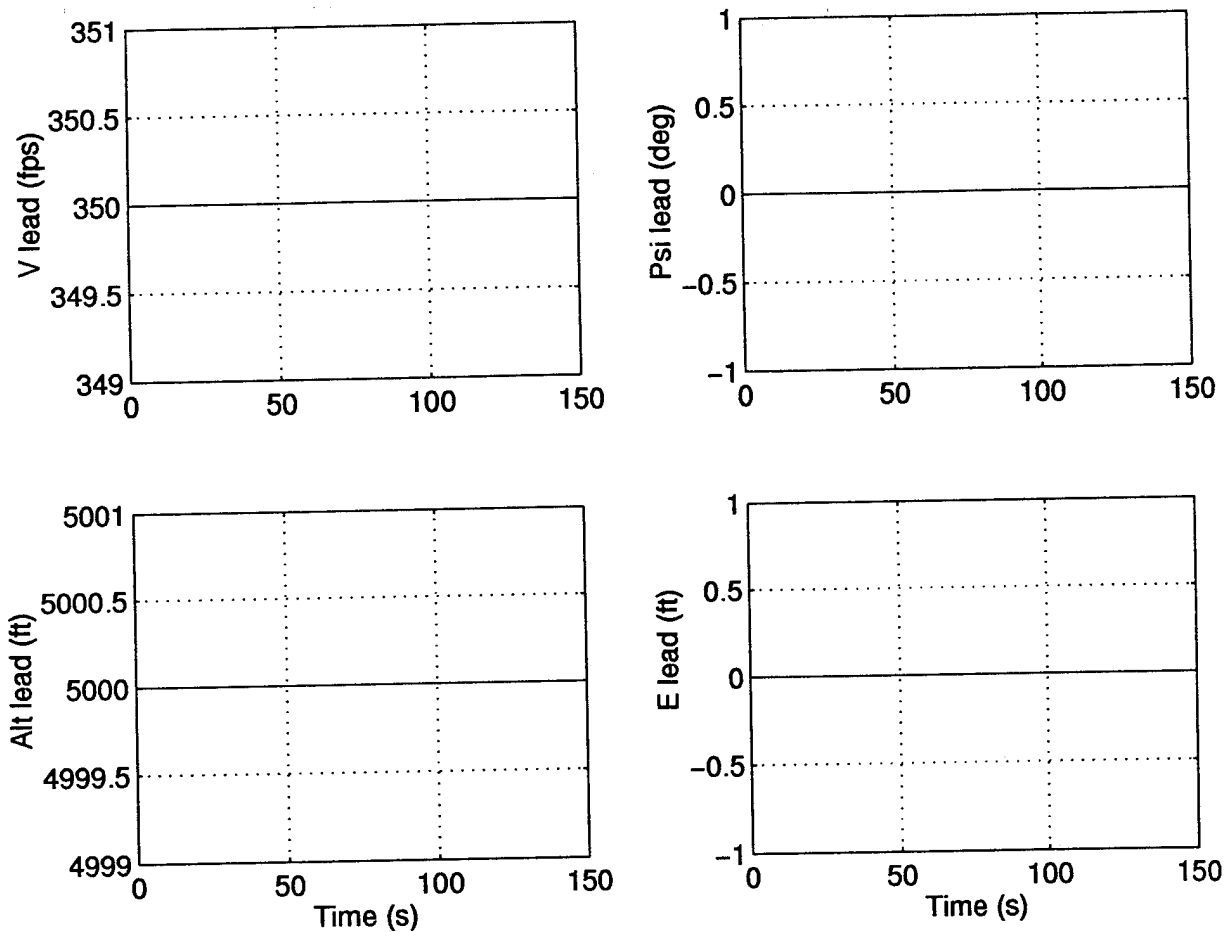
Figure 6.28   Lead Aircraft Responses for an Increase in X-Separation from $3500ft$ to $5000ft$ (x inc) of the *Loose* Formation
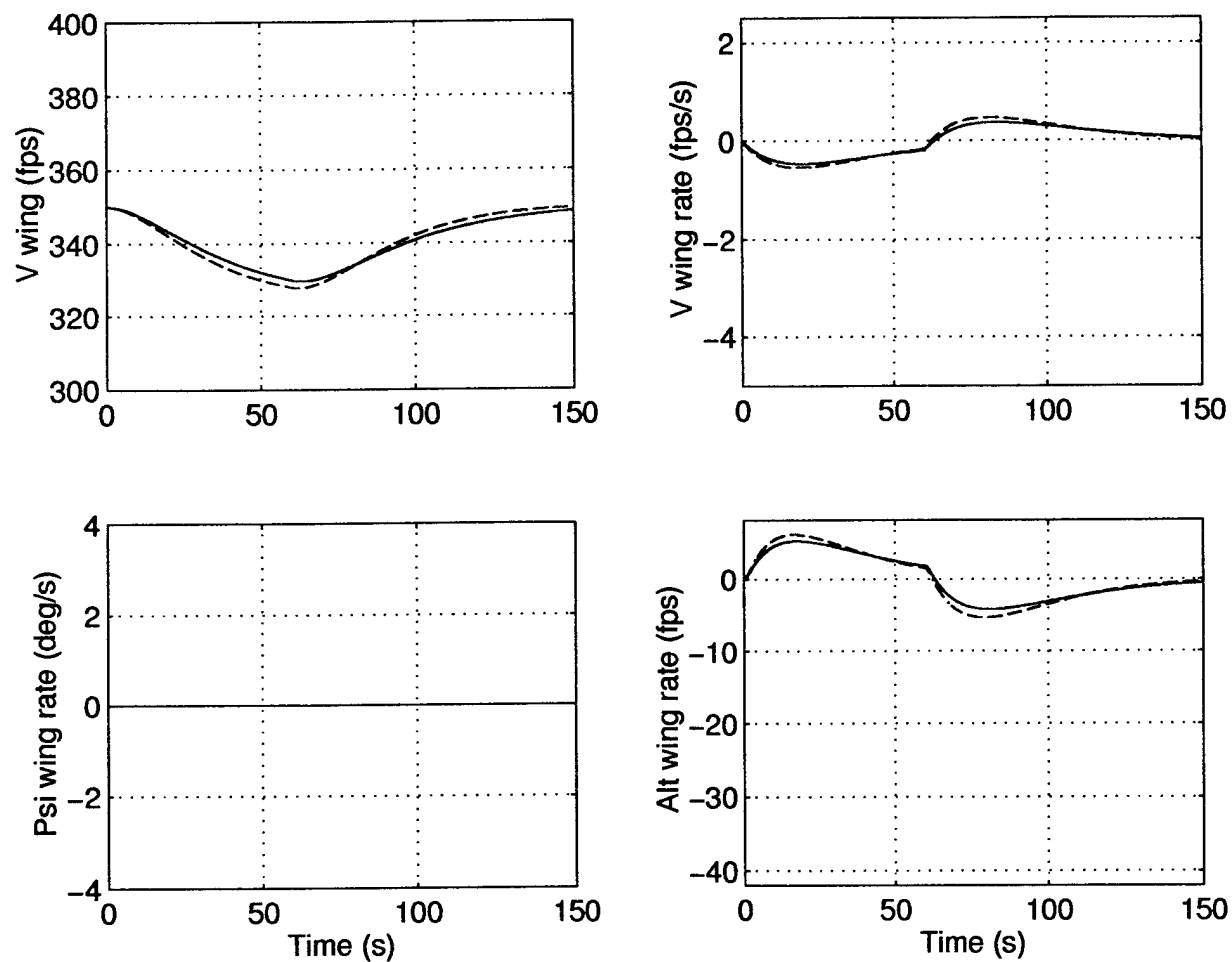
Figure 6.29 Rates of Wing Aircraft Responses for an Increase in X-Separation from 3500ft to 5000ft (x inc) of the *Loose* Formation

6.5.3 *Composite Formation Heading Change Maneuver and Formation Geometry*

hange. The responses due to a left diamond to right diamond formation geome-
y change with a 45° left turn (LD_RD_45L) maneuver are displayed in Figures (6.30)
6.33). The nonlinear simulations for the optimal PIFF controller show that the wing
rcraft/autopilot altitude rate reaches positive saturation. However, the total costs dif-
ence between imposing or not imposing rate limits verifies that the encountered effects
rate saturation can be considered negligible.
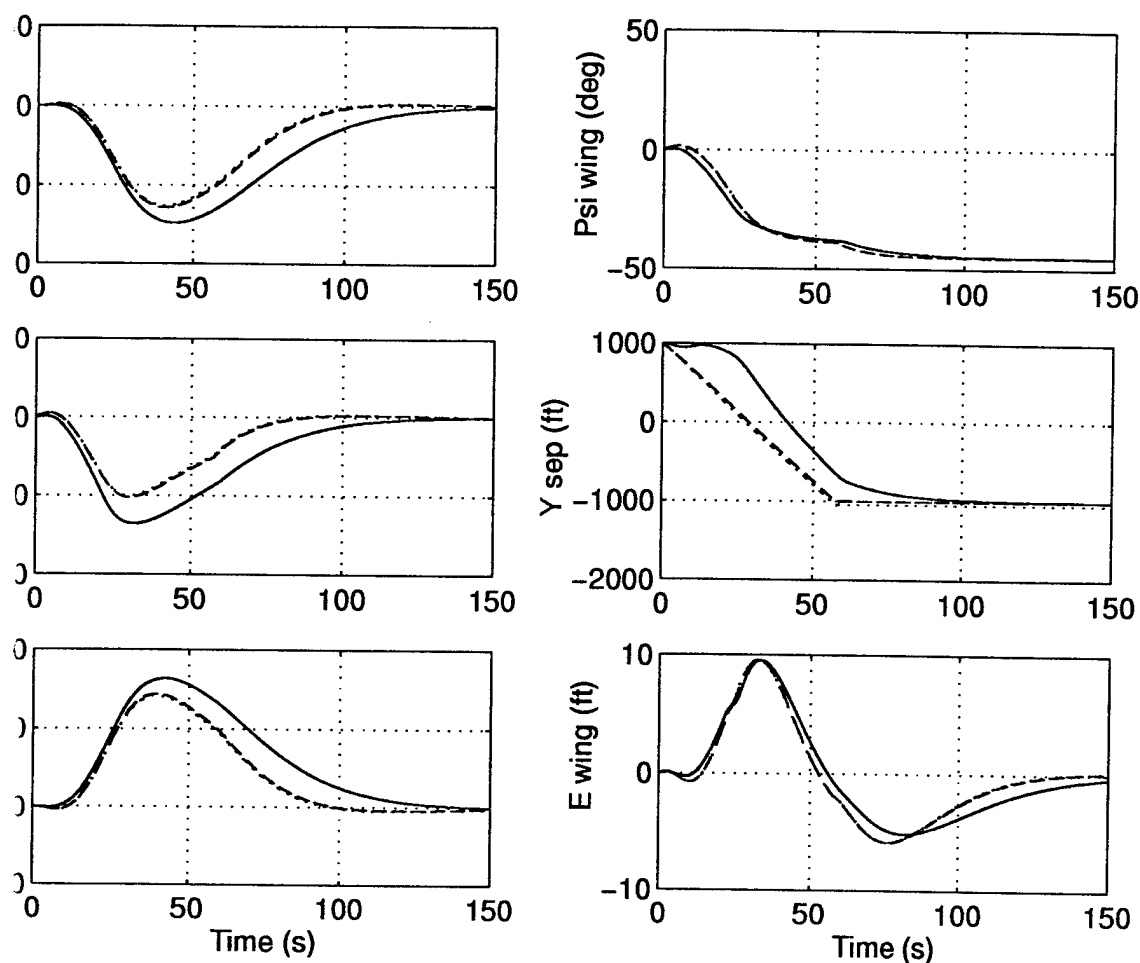
ıre 6.30   Wing Aircraft Responses for a Left Diamond to Right Diamond Geometry
Change with a 45° Left Turn (LD_RD_45L) of the *Loose* Formation

6-42
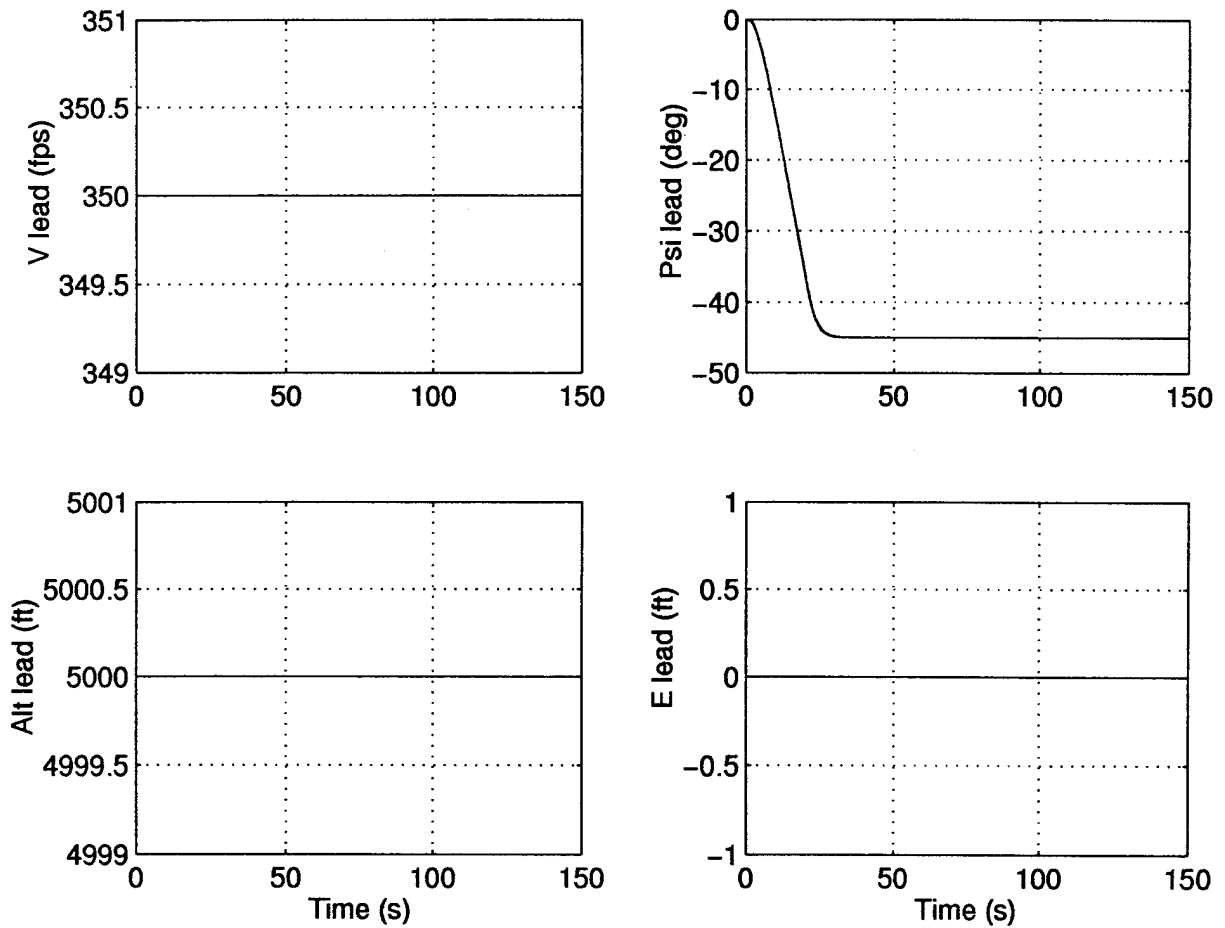
Figure 6.31   Lead Aircraft Responses for a Left Diamond to Right Diamond Geometry
Change with a 45° Left Turn (LD_RD_45L) of the *Loose* Formation
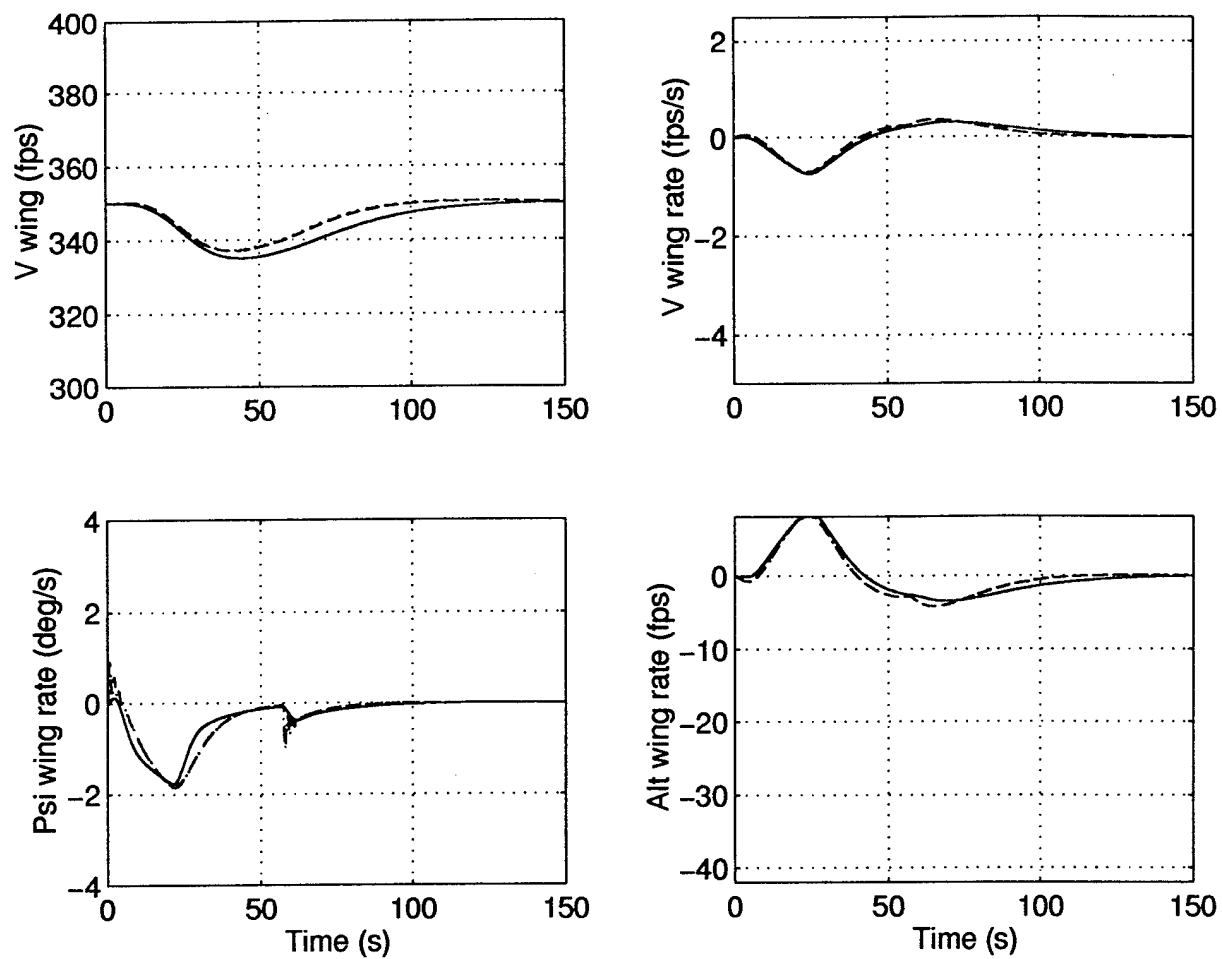
Figure 6.32   Rates of Wing Aircraft Responses for a Left Diamond to Right Diamond
Geometry Change with a 45° Left Turn (LD_RD_45L) of the *Loose* Formation
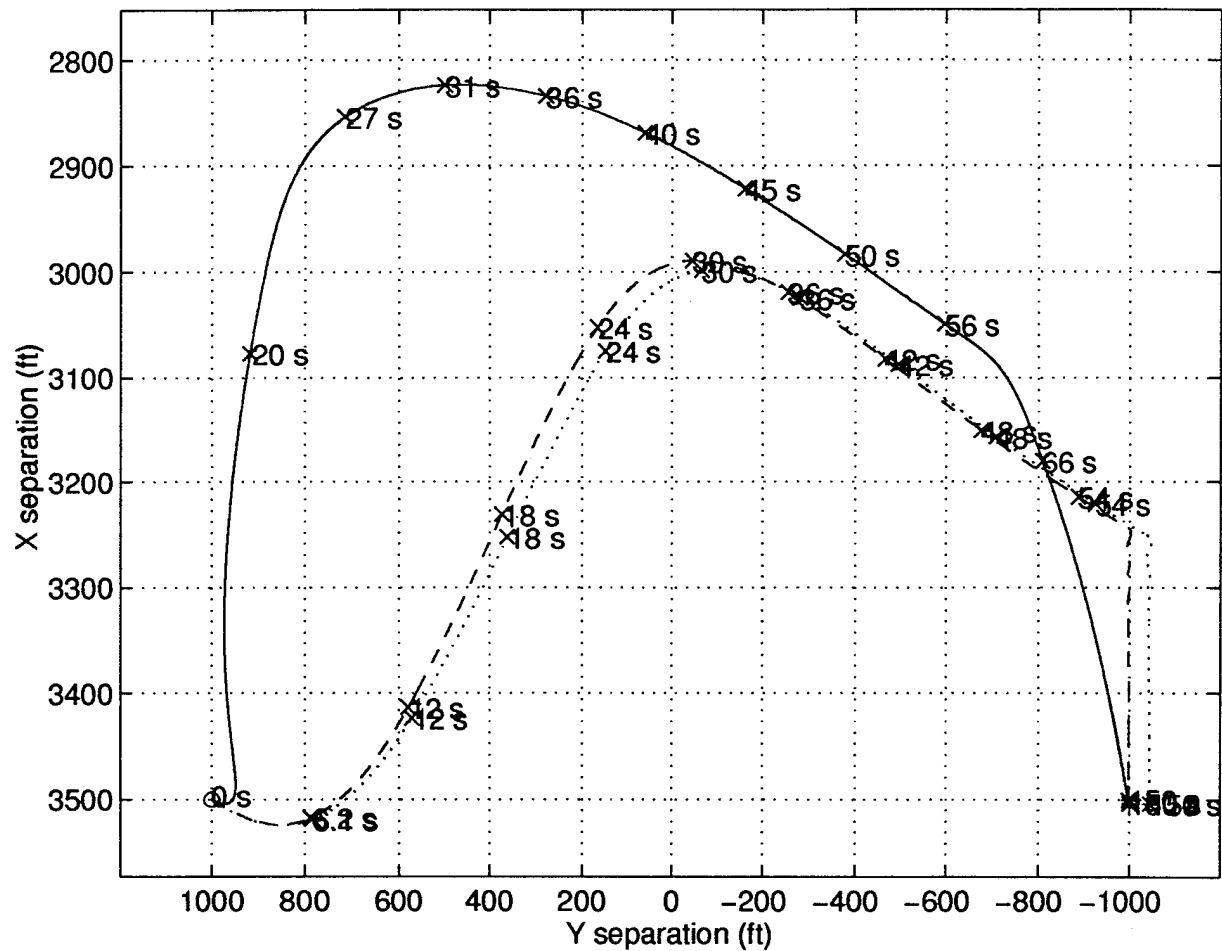
Figure 6.33 Lissajous Plots of Wing Aircraft Responses for a Left Diamond to Right Diamond Geometry Change with a 45° Left Turn (LD_RD_45L) of the *Loose* Formation

6.5.4 Dual Maneuver. The responses during a dual maneuver of a 45° left turn followed by a 45° right turn which returns the formation to its original heading are displayed in Figures (6.34) - (6.37). The wing aircraft/autopilot reaches positive altitude rate saturation during the dual maneuver of a 45° left turn followed by a 45° right turn.
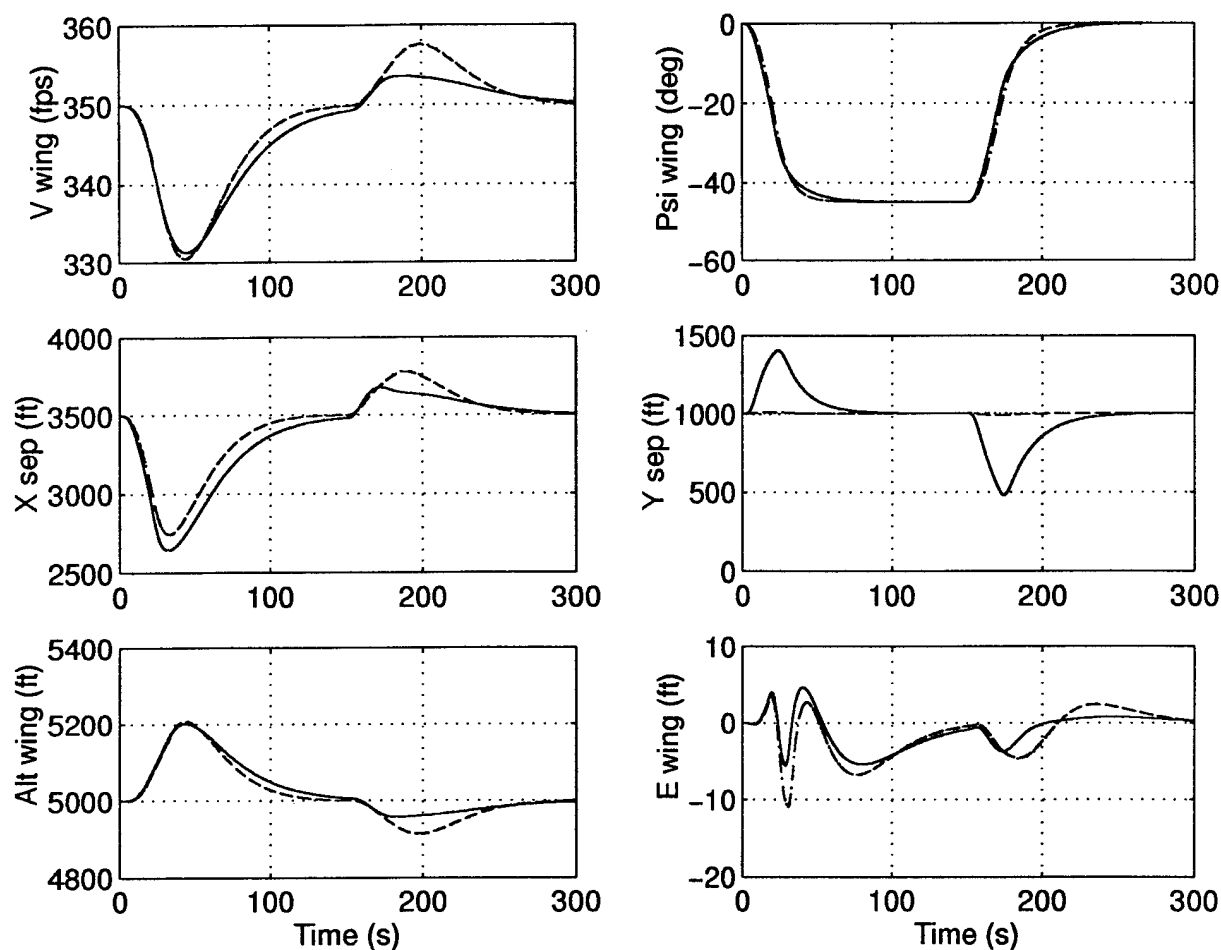
Figure 6.34   Wing Aircraft Responses for a 45° Left Turn and then a 45° Right Turn (45° left) of the *Loose* Formation
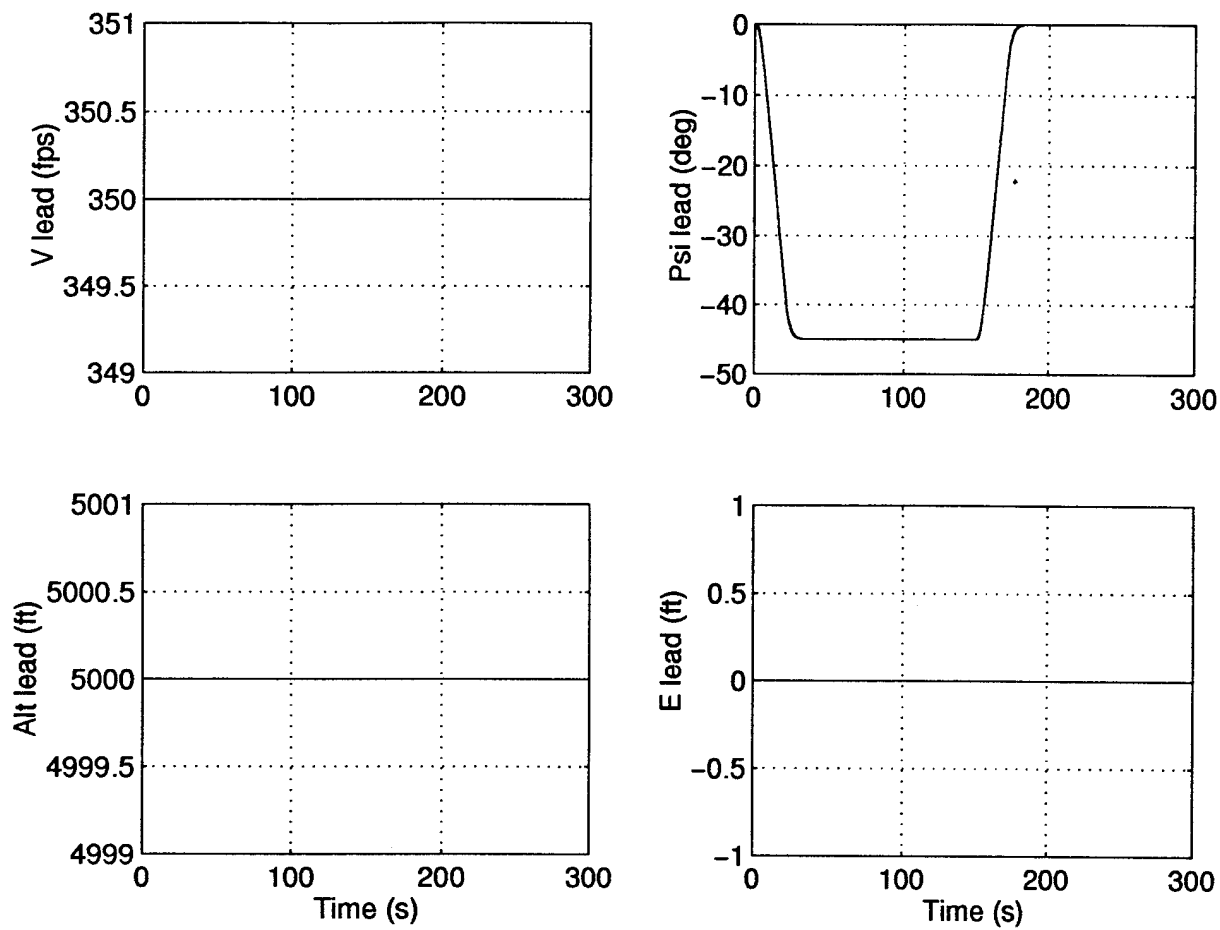
Figure 6.35 Lead Aircraft Responses for a 45° Left Turn and then a 45° Right Turn (45° left) of the *Loose* Formation
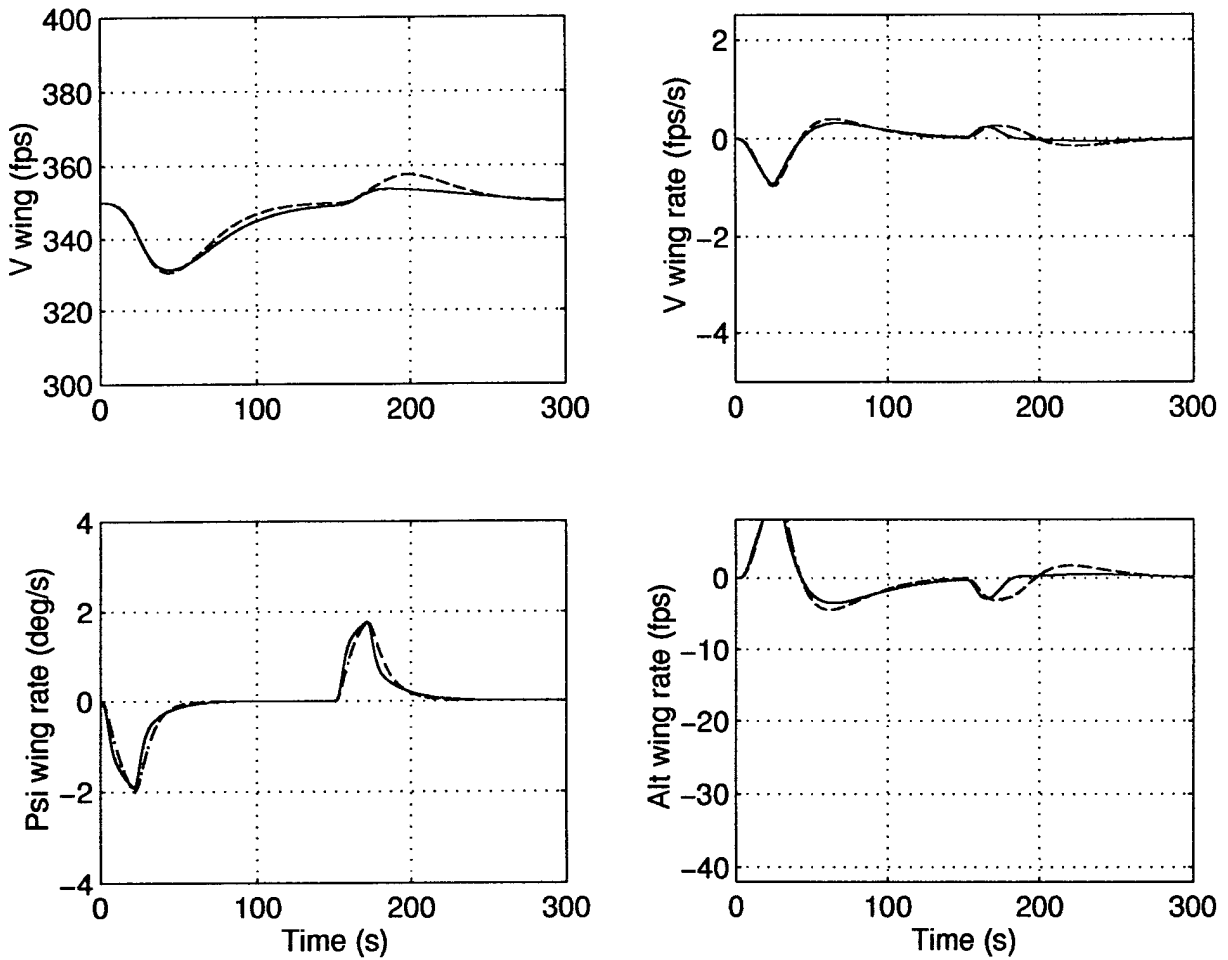
Figure 6.36   Rates of Wing Aircraft Responses for a 45° Left Turn and then a 45° Right Turn (45° left) of the *Loose* Formation
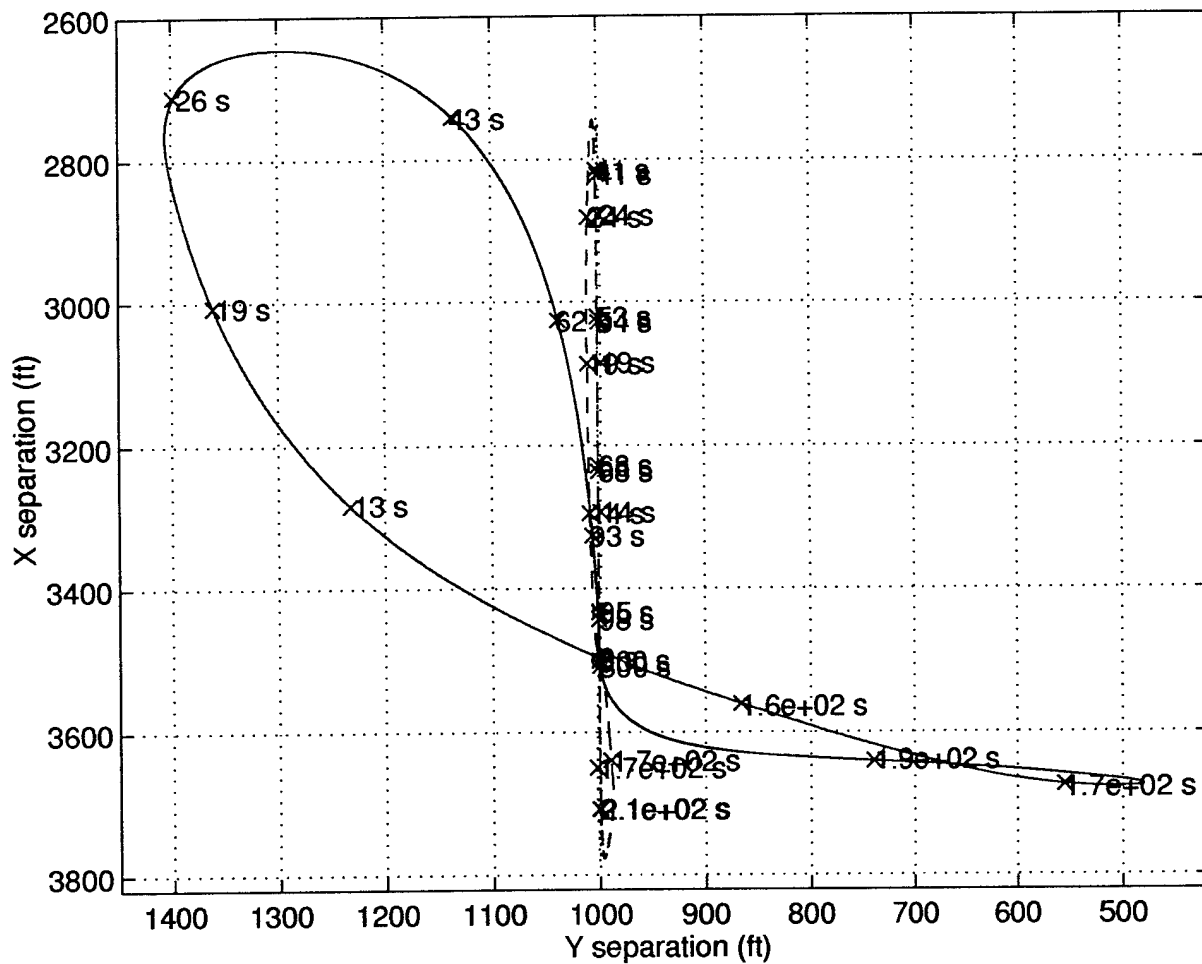
Figure 6.37 Lissajous Plots of Wing Aircraft Responses for a 45° Left Turn and then a 45° Right Turn (45° left) of the *Loose* Formation

6.6 Conclusion

Optimization of both the PFF and PIFF formation flight controllers for the *loose* formation geometries, including the nonlinearities, verifies the achievable performance improvement and robustness with optimized gains. The wide variety of formation maneuvers and geometry changes investigated represent an operational range for the optimal formation flight control system, and thus validate the robustness of the optimized formation flight controllers.

VII. Analysis and Conclusions

7.1 Objectives of Research Met

The objective of this research is to extend the work of Rohs, Dargan, Buzogany, Reyna, and Veth by continuing the development of formation flight control. Specifically, optimization techniques are applied for determining optimal gains in fixed structure controllers. First, a new Proportional plus Integral and FeedForward (PIFF) controller is considered for second-order aircraft/autopilot models. Second, a MATLAB constrained optimization routine is employed for the formation flight controller optimization. Next, the optimization and testing of the Proportional plus FeedForward (PFF) controller and the new PIFF controller are conducted for *tight* formations. Finally, the optimization and testing of the PFF and PIFF controller designs are performed for *loose* formations. All of the above objectives have been met.

7.1.1 Controller design.

The new three-dimensional PIFF formation flight control law combines proportional control and direct V_L signal feedforward in the x-channel, proportional plus integral control in the y-channel, and wing aircraft energy swing reduction. The integral action replaces the Ψ_L information used in the PFF control law. The energy tracking controller's role is to reduce wing aircraft energy swings by using the lead aircraft/autopilot altitude (H_L) signal feedforward in the altitude channel. The decoupling between the heading, altitude, and airspeed states provided by the conventional autopilots allow the outer-loop formation flight controller to command moderate altitude excursions which reduce energy swings by the wing aircraft. The new PIFF controller's superior performance with second-order aircraft/autopilot models is validated through extensive nonlinear simulations.

7.1.2 Optimization.

A MATLAB constrained optimization routine for determining the nonlinear formation flight control system gains is used. The MATLAB constrained optimization routine used in this thesis is based on a Sequential Quadratic Programming (SQP) algorithm. The saturation/rate limits on the C-130 second-order aircraft/autopilot models are incorporated into the optimization as constraints. The cost function is based

on the weighted average of x-separation, y-separation, and energy fluctuations throughout each maneuver. The weights for the x- and y-channels are set equal to one, but energy fluctuation weighting is determined by the altitude component of the wing aircraft's total specific energy. Optimization of formation changes throughout the operational range of the formation flight autopilot leads to the specification of the best gains for the selected optimization conditions.

7.1.3 Loose *and* Tight *Formations.* The operational range of formation changes involves a wide variety of maneuvers and geometry changes. The maneuvers involve heading, altitude, and velocity changes and commanded geometry changes involve variations in x- and y-separation distances. Obviously, the formation responses are in part determined by the initial nominal formation geometry before a formation maneuver or a formation change is commanded. Two initial nominal formations are considered in this thesis. First, the nominal *tight* formation is used to compare results with previous research. The nominal *tight* formation is a left diamond formation with separations of $\overline{X} = 500$ ft and $\overline{Y} = 500$ ft, at a velocity $(\overline{V})$ of $350\frac{ft}{sec}$, altitude $(\overline{H})$ of $5000 ft$, and heading $(\overline{\Psi})$ of $0°$. The additional formation considered is a nominal *loose* formation. The nominal *loose* formation is a left diamond formation with separations of $\overline{X} = 3500$ ft and $\overline{Y} = 1000$ ft, at a velocity $(\overline{V})$ of $350\frac{ft}{sec}$, altitude $(\overline{H})$ of $5000 ft$, and heading $(\overline{\Psi})$ of $0°$. The increased nominal x- and y-separation distances of the *loose* formation are closer to conventional formation flight conditions used by C-130 pilots. The *tight* and *loose* formations are both useful in the analysis of the optimal formation flight control system.

7.2 Conclusions and Specific Lessons Learned

The following conclusions are drawn from this thesis research:

- The formation flight controller's Ψ_L information can be replaced with integral action without deleterious effects.

- The PIFF controller design tends to be slightly less robust than the PFF controller design due to rate saturation.

- Ramping of input commands is necessary in order to avoid rate saturations in the lead aircraft/autopilot models and to further delay saturation in the wing aircraft/autopilot.

- Optimization techniques can be successfully applied to the formation flight control problem.

- Optimal controller gains can be selected which are robust with respect to wide variations in formation maneuvers, formation geometry changes, and initial nominal formation geometry.

- It was found that the optimized PFF and PIFF controller designs are even more robust if the optimal y-channel gain(s) for the *tight* formation and the optimal x-channel gain for the *loose* formation are used. However, simulations are not presented for this optimal gain combination.

7.3 Recommendations for Further Study

This thesis addresses one part of the formation flight control problem. The problem has proven to be quite rich and suggestions for future study are made:

- Investigate the incorporation of anti-collision algorithms into the formation flight controller.

- Extend the formation hold autopilot design to other aircraft, such as helicopters and high-performance aircraft.

- Develop models of sensors and include them into the simulation. Sensor noise should also be added to determine its effect on formation flight control system performance.

- Develop a more accurate aircraft/autopilot model which includes the effects of inter channel cross-coupling. This will help to improve the realism of the simulation.

- Investigate the incorporation of air refueling modes, for both manned and unmanned wing aircraft, into the formation flight autopilot.

7.4 Summary

In this thesis, formation flight control systems are designed and optimized. The Proportional plus FeedForward (PFF) control law is modified and a new Proportional plus Integral and FeedForward (PIFF) control law is considered. The PIFF controller combines proportional control and feedforward of v_L in the x-channel, proportional plus integral control in the y-channel, and energy tracking. The three-dimensional energy tracking formation flight controller reduces energy excursions of the wing aircraft by commanding appropriate wing aircraft altitude changes. The formation flight control system is designed by utilizing the more accurate second-order models for an aircraft/autopilot developed by Buzogany [2]. A MATLAB constrained optimization routine is applied to both the PFF and PIFF controllers to determine the best gains for the workable range of the formation flight autopilot. In addition, two initial nominal formation geometries, *tight* and *loose*, are considered. The *tight* and *loose* formations are both useful in the study of the optimal formation flight control system. Extensive nonlinear responses of the optimal formation flight control system are analyzed in order to validate the formation flight control design and optimization process.

Appendix A. Sample MATLAB and SIMULINK Code

Samples of various MATLAB and SIMULINK code are listed in this Appendix.

A.1 SIMULINK Block Diagram

SIMULINK is an extension of MATLAB which allows for a more graphical representation and analysis of dynamic systems. Figure A.1 is a sample of the type of SIMULINK block diagram used in simulating the formation flight system.

A.2 SIMULINK Variables

The variables of the SIMULINK block diagrams are initialized from MATLAB files. For instance, the variables for the Aircraft/Autopilot models are:

```
%  C-130 A:  Second order model
%
%  This file contains model data, including rate limits and time constants
%  for lead and wing A/C
%
%  Time constants:

t_v2_1 = 10;
t_v2_w = 10;


ahl = 1.625;
ahw = 1.625;
bhl = 0.13;
bhw = 0.13;


apsil = .544;
apsiw = .544;
bpsil = .544;
bpsiw = .544;
```

```
%  Altitude limits

vmin_l = 304;
vmax_l = 422;
vmin_w = 304;
vmax_w = 422;

%  Rate limits

velocity_lower_l = -5;
velocity_upper_l = 2.5;
heading_lower_l = -3;
heading_upper_l = 3;
altitude_lower_l = -42;
altitude_upper_l = 8;


velocity_lower_w = -5;
velocity_upper_w = 2.5;
heading_lower_w = -3;
heading_upper_w = 3;
altitude_lower_w = -42;
altitude_upper_w = 8;
```

The Formation Flight Control System Block Diagram
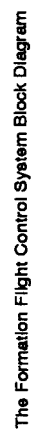
A.3 Formation Change Variables

For each different formation change, the command input variables are initialized in order to simulate the formation flight system performance. The procedure for simulating single and dual formation changes is different. For the single formation changes, the command inputs are only initialized and ramped in at the beginning of the simulation. However, dual formation changes require a predetermined matrix of command inputs with respect to simulation time.

A.3.1 Single Maneuver.   The single formation changes require a Matlab file which initializes the command inputs. An example of a single maneuver Matlab file is:

```
%  45 degree left heading change
%
%  Initial conditions

nom_velocity_1 = 350;
nom_heading_1 = 0;
nom_altitude_1 = 5000;


nom_velocity_w = 350;
nom_heading_w = 0;
nom_altitude_w = 5000;


x_initial = 500;
y_initial = 500;


velocity_command = 350;
heading_command = -45;
altitude_command = 5000;


x_command = 500;
y_command = 500;


cmd_name = ['45 deg left'];
```

A.3.2 Dual Maneuver.   Dual formation changes require a MATLAB file which establishes the time history for the command inputs. An example of a dual maneuver MATLAB file is:

```
%  45 degree left heading change then back to original heading
%
%  Initial conditions
integ = 0;


nom_velocity_1 = 350;
nom_heading_1 = 0;
nom_altitude_1 = 5000;


nom_velocity_w = 350;
nom_heading_w = 0;
nom_altitude_w = 5000;


x_initial = 500;
y_initial = 500;


time = [0; 20; 150; 170; 300];


%velocity_command = 350;
man1 = [350; 350; 350; 350; 350];
manvr1 = [time man1];


%heading_command = -45 then back to 0;
man2 = [0; -45; -45; 0; 0];
manvr2 = [time man2];


%altitude_command = 5000;
man3 = [5000; 5000; 5000; 5000; 5000];
manvr3 = [time man3];
```

```
%x_command = 500;
man4 = [500; 500; 500; 500; 500];
manvr4 = [time man4];


%y_command = 500;
man5 = [500; 500; 500; 500; 500];
manvr5 = [time man5];
cmd_name = ['45 deg left then back to Original'];
```

A.4   MATLAB Constrained Optimization

The MATLAB file which executes the constrained optimization algorithm must be have access to all the system variables. A sample code for calling the optimization routine is:

```
% Optimization of formation flight control system
clear
format compact
global kx ky kyi


% Define parameters for constrained optimization
vub=[100; 1000; 1000]; % upper bound
vlb=[0; 0; 0]; % lower bound
blkdiag='opt_ramp'; % blkdiag='the name of the simulink system'
options=foptions;
grad=[];
options(14) = 10e7; % max number of iterations
%options(16) = 0.00001; % min perturb
%options(17) = 0.1; % max perturb


% Run duration:
sim_time=150;


% C-130 A/C Model [rate (a) / non-rate limited (anr)]:
c130a
```

```
% Energy (ecomp equals 1 or 0):
ecomp=1;


% Type of Test (include nominal conditions and commanded separations):
fortyfiveleft


% Information to Ramp:
Differ;


% Starting point of Gains:
kxi = 0;
KO = [0.03; 0.02; 0.01];


% Start the optimization
[K,options]=constr('optfun', KO, options, vlb, vub, grad, blkdiag, sim_time, ecomp, kxi)
% optfun is the function being optimized
% KO is the initial starting point


quit
```

A.5   MATLAB Optimization Function

The MATLAB file, which calls the constrained optimization algorithm, must refer to a MATLAB Function that determines conditions for optimization. An example of a MATLAB Function which establishes the cost function and constraints for the optimization routine is:

```
function [f,g]=optfun(x,blkdiag,sim_time,ecomp,kxi)
% slight saturation of limits may be allowed
global kx ky kyi


kx = x(1,1)
ky = x(2,1)
kyi = x(3,1)
```

```
% C-130 A/C Model [rate (a) / non-rate limited (anr)]:
c130a


% Type of Test (include nominal conditions and commanded separations):
fortyfiveleft


% Information to ramp:
Differ;


[t,x,y] = rk45(blkdiag,sim_time,[],[1e-3,5e-2,5e-2]);


% weighting of f function:
grav = 32.2; % gravity
alpha = 1; % weighting of x channel
beta = 1; % weighting of y channel
gamma = 32.2; % weighting of energy channel


% f is the function to be minimized:
den = size(t);
numx = (alpha) * (sum ( abs (x_command - y(:,7)) ) / den(1,1) )
numy = (beta) * (sum ( abs (y_command - y(:,8)) ) / den(1,1) )
nume = (gamma) * (sum( abs (y(:,9) - y(:,10)) ) / den(1,1) )
f = numx + numy + nume


% Avoid saturation of a simulation: (g must be less than or equal to zero)
% set variable limits for the constraints
c130a
sat=0; % saturation percentage allowed for this opt simulation


g(:,1) = (vmin_1 - (350-304)*(sat)) - y(:,1);
g(:,2) =-(vmax_1 + (420-350)*(sat)) + y(:,1);
g(:,3) = (vmin_w - (350-304)*(sat)) - y(:,2);
g(:,4) =-(vmax_w + (420-350)*(sat)) + y(:,2);
```

```
g(:,5) = (velocity_lower_l + (-5.0)*(sat)) - y(:,11);
g(:,6) =-(velocity_upper_l + ( 2.5)*(sat)) + y(:,11);
g(:,7) = (velocity_lower_w + (-5.0)*(sat)) - y(:,16);
g(:,8) =-(velocity_upper_w + ( 2.5)*(sat)) + y(:,16);


g(:,9) = (heading_lower_l + (-3.0)*(sat)) - y(:,12);
g(:,10)=-(heading_upper_l + ( 3.0)*(sat)) + y(:,12);
g(:,11)= (heading_lower_w + (-3.0)*(sat)) - y(:,14);
g(:,12)=-(heading_upper_w + ( 3.0)*(sat)) + y(:,14);


g(:,13)= (altitude_lower_l + (-42)*(sat)) - y(:,13);
g(:,14)=-(altitude_upper_l + (8.0)*(sat)) + y(:,13);
g(:,15)= (altitude_lower_w + (-42)*(sat)) - y(:,15);
g(:,16)=-(altitude_upper_w + (8.0)*(sat)) + y(:,15);


[loc,i]=max(max(g)) % running check of constraints


return
```

Bibliography

1. Blakelock, John H., *Automatic Control of Aircraft and Missiles* (Second Edition), John Wiley & Sons, Inc., 1991.

2. Buzogany, Louis E., *Automated Control of Aircraft in Formation Flight*, MS thesis, AFIT/GE/ENG/92D-07, Graduate of Engineering, Air Force Institute of Technology (AU), Wright-Patterson AFB, OH, December 1992.

3. Buzogany, Louis E., M. Pachter and J.J. D'Azzo, *Automated Control of Aircraft in Formation Flight*, Proceedings of the 1993 AIAA Guidance, Navigation, and Control Conference, AIAA paper No. 93-3852, pp 1349-1369, Monterey, CA, August 1993.

4. Dargan, John L., *Proportional Plus Integral Control of Aircraft for Automated Maneuvering Formation Flight*, MS thesis, AFIT/GE/ENG/91D-14, Graduate School of Engineering, Air Force Institute of Technology (AU), Wright-Patterson AFB, OH, December 1991.

5. Dargan, John L., M. Pachter and J.J. D'Azzo, *Automatic Formation Flight Control*, Proceedings of the 1992 AIAA Guidance, Navigation, and Control Conference, AIAA paper No. 92-4473, pp 838-857, Hilton Head, SC, June 1992.

6. Grace, Andrew, *Optimization Toolbox For Use with MATLAB*, The Mathworks, Inc., 1992.

7. D'Azzo, John J., Personal Interviews, Summer Quarter, 1995.

8. D'Azzo, John J. and Constantine H. Houpis, *Linear Control System Analysis and Design* (Fourth Edition), McGraw-Hill Book Company, 1995.

9. *Intraformation Positioning System (IFPS): Baseline Design Study*, Flight Dynamics Directorate, Wright Laboratory, Air Force Materiel Command, WL-TR-92-3068, Wright-Patterson AFB, OH, May 1992.

10. *Test Report For The Quick-Look Flight Demonstration On The Intraformation Positioning System*, Flight Dynamics Directorate, Wright Laboratory, Air Force Materiel Command, WL-TR-92-3068, Wright-Patterson AFB, OH, May 1992.

11. Krishnakumar, K., and David E. Goldberg, *Control System Optimization Using Genetic Algorithms*, Journal of Guidance, Control and Dynamics, Vol. 15, No. 3, pp 735-740, May-June 1992.

12. *MATLAB Reference Guide*, The Mathworks, Inc., 1992.

13. Maybeck, Peter S., *Stochastic Models, Estimation, and Control, Volume 3*, New York: Academic Press, Inc., 1982.

14. Pachter, Meir, Personal Interviews, Summer Quarter, 1995.

15. Porter, Brian, *Genetic Design of Control Systems*, SCIE, Vol. 34, No. 5, 1995.

16. Porter, Brian, and M. Boriari, *Genetic Design Of Linear Multivariable Feedback Control Systems Using Eigenstructure Assignments*, International Journal of Systems Science, Vol. 23, No. 8, pp 1387-1390, 1994.

17. Porter, B., and A. H. Jones, *Genetic Tuning Of Digital PID Controllers*, Electronic Letters, Vol. 28, No. 9, pp 843-844, April 1992.

18. Porter, B., and D. L. Hicks, *Genetic Robustification of Digital Model-Following Flight-Control Systems*, NAECON, pp 556-563, Dayton, OH, May 1994.

19. Porter, B., and D. L. Hicks, *Performance Measures In The Genetic Design Of Digital Model-Following Flight-Control Systems*, NAECON, pp 564-570, Dayton, OH, May 1994.

20. Reyna, Vincent P., *Automation of Formation Flight Control*, MS thesis, AFIT/GE/ENG/94M-01, Graduate School of Engineering, Air Force Institute of Technology (AU), Wright-Patterson AFB, OH, March 1994.

21. Reyna, Vincent P., *Formation Flight Control Automation*, Proceedings of the 1994 AIAA Guidance, Navigation, and Control Conference, AIAA paper No. 94-3557, pp 1379-1404, Scottsdale, AZ, August 1994.

22. Rohs, Paul R., *A Fully Coupled, Automated Formation Control System for Dissimilar Aircraft in Maneuvering, Formation Flight*, MS thesis, AFIT/GE/ENG/91M-03, Graduate School of Engineering, Air Force Institute of Technology (AU), Wright-Patterson AFB, OH, March 1991.

23. Veth, Michael J., *Advanced Formation Flight Control*, MS thesis, AFIT/GE/ENG/94M-30, Graduate School of Engineering, Air Force Institute of Technology (AU), Wright-Patterson AFB, OH, December 1994.

24. Veth, Michael J., M. Pachter and J.J. D'Azzo, *Autopilots for Flying Circular Paths*, Proceedings of the 1995 AIAA Guidance, Navigation, and Control Conference, AIAA paper No. 95-3177, pp 1446-1458, Baltimore, MD, August 1995.

25. Veth, Michael J., M. Pachter and J.J. D'Azzo, *Proportional and Integral Control of Nonlinear Systems*, To appear in the International Journal of Control.

26. Veth, Michael J., M. Pachter and J.J. D'Azzo, *Energy Preserving Formation Flight Control*, 33rd Aerospace Sciences Meeting, AIAA paper No. 95-0335, Reno, NV, January 1995.

REPORT DOCUMENTATION PAGE

1. AGENCY USE ONLY *(Leave blank)*	2. REPORT DATE December 1995	3. REPORT TYPE AND DATES COVERED Master's Thesis

4. TITLE AND SUBTITLE
OPTIMAL FORMATION FLIGHT CONTROL

5. FUNDING NUMBERS

6. AUTHOR(S)

Shawn B. McCamish
Second Lieutenant, USAF

7. PERFORMING ORGANIZATION NAME(S) AND ADDRESS(ES)

Air Force Institute of Technology
WPAFB OH 45433-6583

8. PERFORMING ORGANIZATION REPORT NUMBER

AFIT/GE/ENG/95D-16

9. SPONSORING/MONITORING AGENCY NAME(S) AND ADDRESS(ES)

Capt Peter K. Eide
WL/FIGS
2210 Eighth Street Suite 11
Wright-Patterson AFB, OH 45433

10. SPONSORING/MONITORING AGENCY REPORT NUMBER

11. SUPPLEMENTARY NOTES

12a. DISTRIBUTION/AVAILABILITY STATEMENT

Approved for public release; distribution unlimited

12b. DISTRIBUTION CODE

13. ABSTRACT *(Maximum 200 words)*

Automatic formation flight involves controlling multiple wing aircraft equipped with standard Mach-hold, altitude-hold, and heading-hold autopilots in order to maintain a desired position relative to a lead aircraft throughout formation maneuvers. Changes in the lead aircraft's states, including formation heading, velocity, altitude, and geometry changes, are treated as disturbance and are rejected by the formation flight control system. The work in this thesis is a continuation of five previous theses, dealing with the design of formation flight control systems. The goal of the optimal formation flight control design is to achieve robust formation maintenance in the face of formation maneuvers and the presence of full system nonlinearities. Second-order aircraft/autopilot models are included in the design and a new control law is employed. A constrained optimization for determining the optimal controller gains of fixed structure controllers is employed. The two controllers considered are a Proportional plus FeedForward (PFF) controller, previously developed at AFIT, and a new Proportional plus Integral and FeedForward (PIFF) controller, which uses less feedforward information. Finally, the constrained optimization is applied to a wide variety of formation maneuvers and geometry changes initiated from both the *tight*, closely spaced, and *loose*, more widely dispersed, types of formations.

14. SUBJECT TERMS

Formation Flight Control, Optimization, C-130, Energy Tracking Maneuvers, Energy Swing Minimizing Maneuvers

15. NUMBER OF PAGES
180

16. PRICE CODE

17. SECURITY CLASSIFICATION OF REPORT UNCLASSIFIED	18. SECURITY CLASSIFICATION OF THIS PAGE UNCLASSIFIED	19. SECURITY CLASSIFICATION OF ABSTRACT UNCLASSIFIED	20. LIMITATION OF ABSTRACT UL

GENERAL INSTRUCTIONS FOR COMPLETING SF 298

The Report Documentation Page (RDP) is used in announcing and cataloging reports. It is important that this information be consistent with the rest of the report, particularly the cover and title page. Instructions for filling in each block of the form follow. It is important to *stay within the lines* to meet *optical scanning requirements*.

Block 1. Agency Use Only *(Leave blank)*.

Block 2. Report Date. Full publication date including day, month, and year, if available (e.g. 1 Jan 88). Must cite at least the year.

Block 3. Type of Report and Dates Covered. State whether report is interim, final, etc. If applicable, enter inclusive report dates (e.g. 10 Jun 87 - 30 Jun 88).

Block 4. Title and Subtitle. A title is taken from the part of the report that provides the most meaningful and complete information. When a report is prepared in more than one volume, repeat the primary title, add volume number, and include subtitle for the specific volume. On classified documents enter the title classification in parentheses.

Block 5. Funding Numbers. To include contract and grant numbers; may include program element number(s), project number(s), task number(s), and work unit number(s). Use the following labels:

C	-	Contract	PR	- Project
G	-	Grant	TA	- Task
PE	-	Program Element	WU	- Work Unit Accession No.

Block 6. Author(s). Name(s) of person(s) responsible for writing the report, performing the research, or credited with the content of the report. If editor or compiler, this should follow the name(s).

Block 7. Performing Organization Name(s) and Address(es). Self-explanatory.

Block 8. Performing Organization Report Number. Enter the unique alphanumeric report number(s) assigned by the organization performing the report.

Block 9. Sponsoring/Monitoring Agency Name(s) and Address(es). Self-explanatory.

Block 10. Sponsoring/Monitoring Agency Report Number. *(If known)*

Block 11. Supplementary Notes. Enter information not included elsewhere such as: Prepared in cooperation with...; Trans. of...; To be published in.... When a report is revised, include a statement whether the new report supersedes or supplements the older report.

Block 12a. Distribution/Availability Statement. Denotes public availability or limitations. Cite any availability to the public. Enter additional limitations or special markings in all capitals (e.g. NOFORN, REL, ITAR).

DOD - See DoDD 5230.24, "Distribution Statements on Technical Documents."
DOE - See authorities.
NASA - See Handbook NHB 2200.2.
NTIS - Leave blank.

Block 12b. Distribution Code.

DOD - Leave blank.
DOE - Enter DOE distribution categories from the Standard Distribution for Unclassified Scientific and Technical Reports.
NASA - Leave blank.
NTIS - Leave blank.

Block 13. Abstract. Include a brief *(Maximum 200 words)* factual summary of the most significant information contained in the report.

Block 14. Subject Terms. Keywords or phrases identifying major subjects in the report.

Block 15. Number of Pages. Enter the total number of pages.

Block 16. Price Code. Enter appropriate price code *(NTIS only)*.

Blocks 17. - 19. Security Classifications. Self-explanatory. Enter U.S. Security Classification in accordance with U.S. Security Regulations (i.e., UNCLASSIFIED). If form contains classified information, stamp classification on the top and bottom of the page.

Block 20. Limitation of Abstract. This block must be completed to assign a limitation to the abstract. Enter either UL (unlimited) or SAR (same as report). An entry in this block is necessary if the abstract is to be limited. If blank, the abstract is assumed to be unlimited.